Introduction to Climate
~ Part II ~

Shuhei MAEDA (MRI/JMA)

Climate Research Department
Meteorological Research Institute (MRI/JMA)

2. Climate Variability

Outline of the lecture

1. Climate System (90 min. + α)
   1.1 Introduction
   1.2 Radiative Balance
   1.3 Horizontal Radiative Imbalance and Circulations
   1.4 Seasonal Change
   1.5 Role of Orography on Climate
2. Climate Variability (120 min. + α)
   2.1 Introduction
   2.2 Intraseasonal Variability: Quasi-stationary Rossby wave, MJO and equatorial waves
   2.3 Interannual Variability: ENSO, El Nino Modoki, IOD
   2.4 Decadal Variability: PDO, ENSO-Monsoon relation
3. JMA's latest one-month prediction

2.1 Introduction

Causes of Climate Variability

- **Natural origin**

  external: land-sea distribution, orography

  solar constant, orbital variations

  volcano

  internal variability of the climate system

  (e.g., air-sea interaction,,,)

- **Anthropogenic origin**

  emission of greenhouse gases, destruction of ozone layer, land surface modification,,, (= climate change)

Various time scales of climate variability

- glacial and interglacial
- ocean thermohaline circulation
- decadal to interdecadal climate variability
- seasonal to interannual climate variability
  - El Nino/Southern Oscillation (ENSO)
  - monsoon variability
  - modes of variability (NAO, PNA, WP patterns)
- days to intraseasonal variability
  - Quasi-stationary Rossby wave
  - Madden-Julian Oscillation (MJO)

N.B. climate system is not in equilibrium

2.2 Intraseasonal Variability:

Quasi-stationary Rossby wave, MJO and equatorial waves

Quasi-stationary Rossby waves

Rossby waves:

are large scale (synoptic and planetary scale) waves in the atmosphere and ocean.

obey the conservation law of potential vorticity.

are dispersive and propagate westward (longer wave is faster).

are stationary if phase speed is the same as westerly wind which advect the waves.

Group velocity of stationary Rossby wave packet is eastward.

Stationary Rossby wave packet tends to propagate trapped by Jet streams.

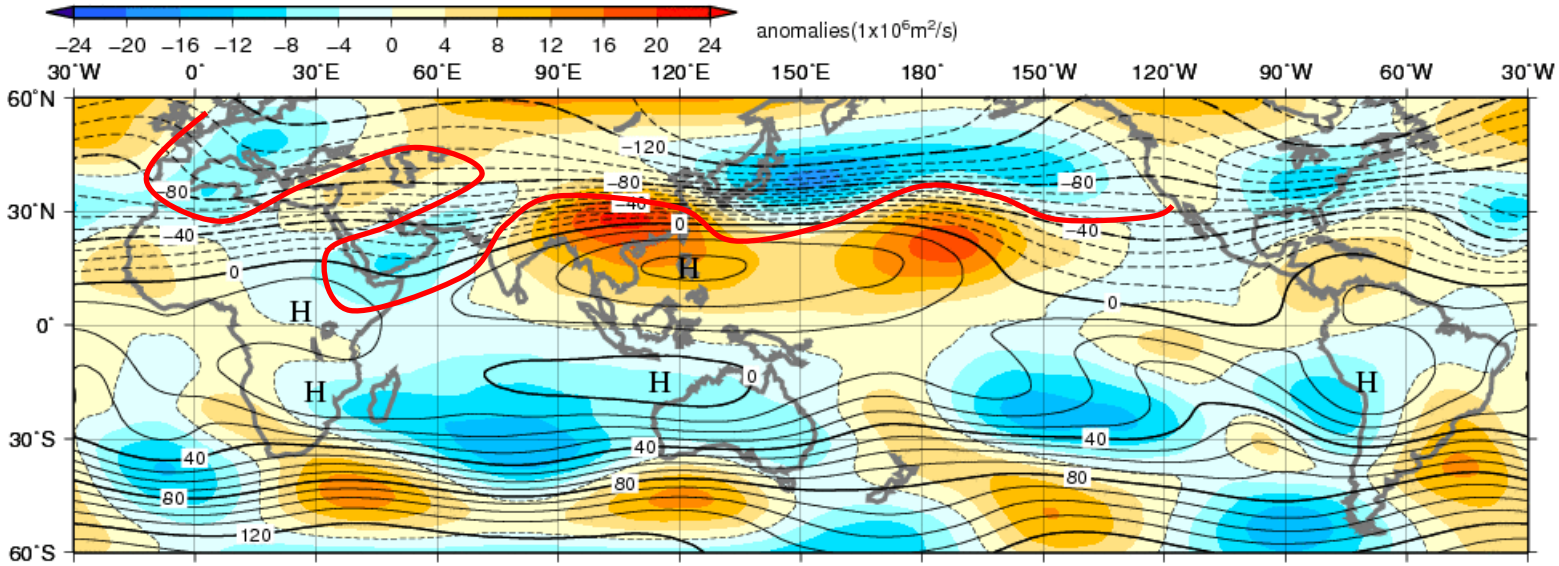

Examples of Quasi-stationary Rossby waves: 2002/1, 2005/2

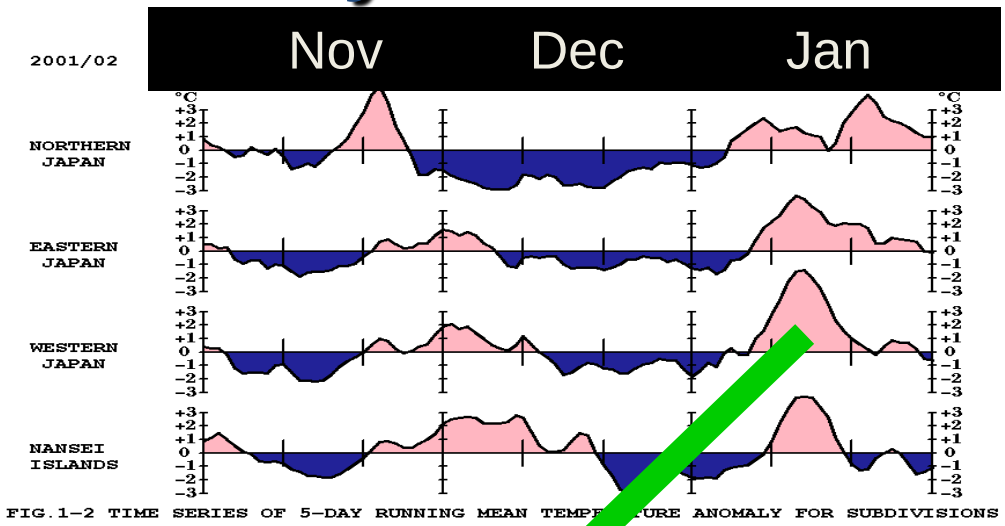

FIG.1−2 TIME SERIES OF 5−DAY RUNNING MEAN TEMPE URE ANOMALY FOR SUBDIVISIONS

Time sequences of temperature anomalies in Japan (5 day running mean)

2001.11-2002.2

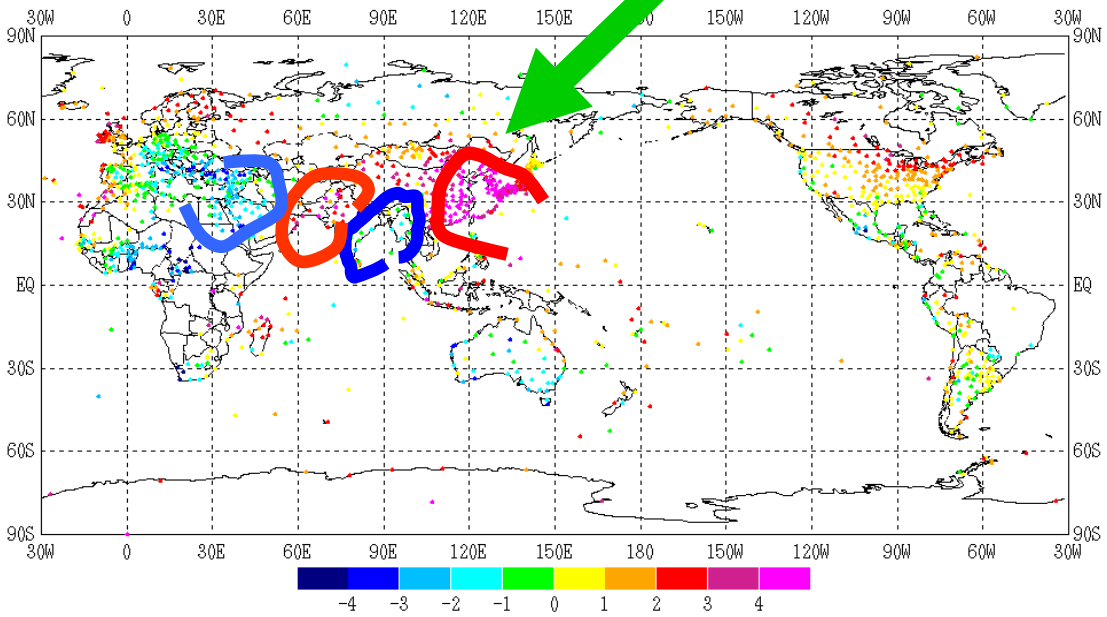

Observed normalized temperature anomalies

2002.1.11-15

Wave train along the Asian jet

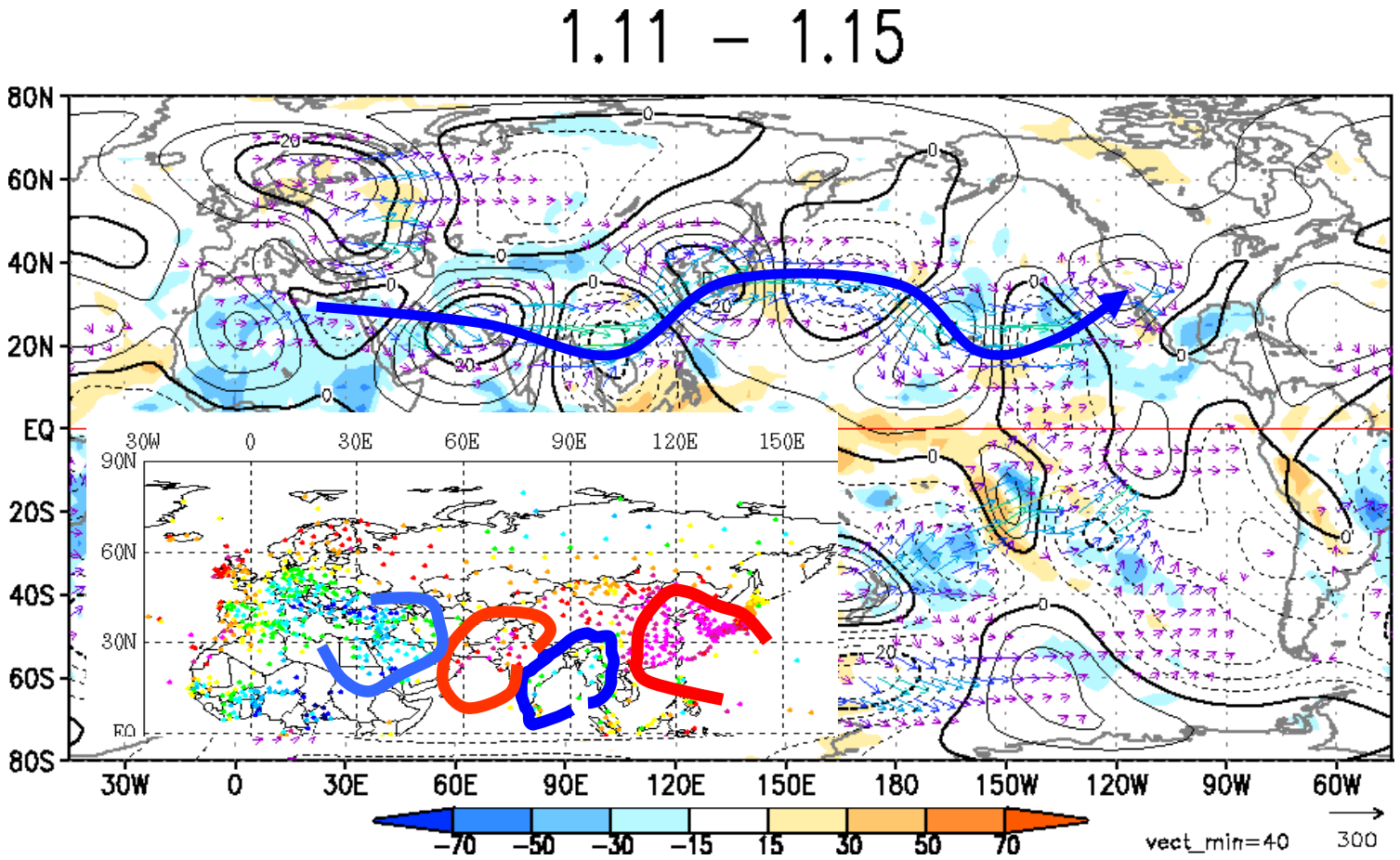

Observed 5-day mean stream function anomalies at 200hPa (contours) 2002.1.11-1.15

Structure of the wave train

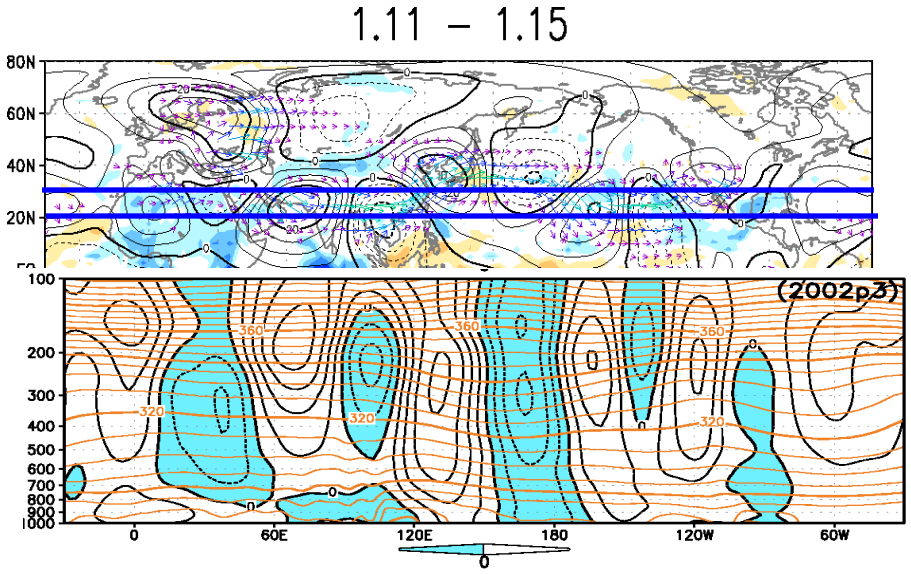

Observed Longitude-height cross section of 20N-30N mean stream function anomalies

2002.1.11-1.15

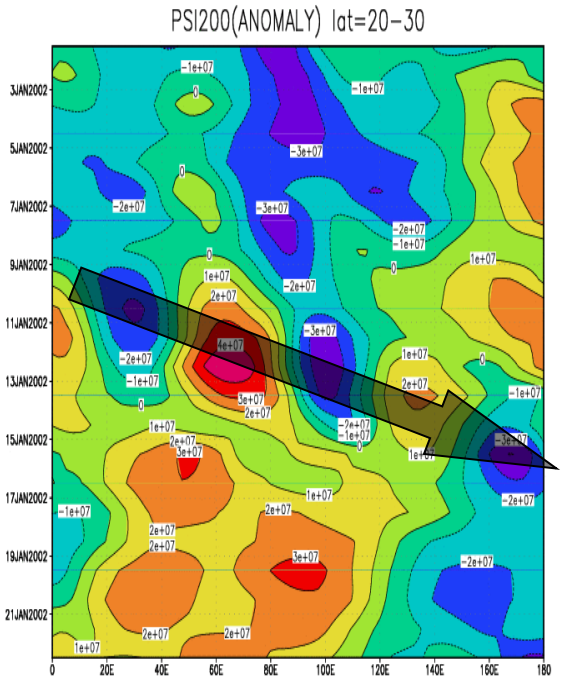

Observed Longitude-time cross section of 20N-30N mean stream function anomalies at 200hPa

2002.1.1-1.23

Equivalent barotropic stationary Rossby wave.
Wave length: 70 ˚ Group velocity 30˚/day

Statistical relationship between 10-day mean temperature in western Japan and wave trains along the Asian jet

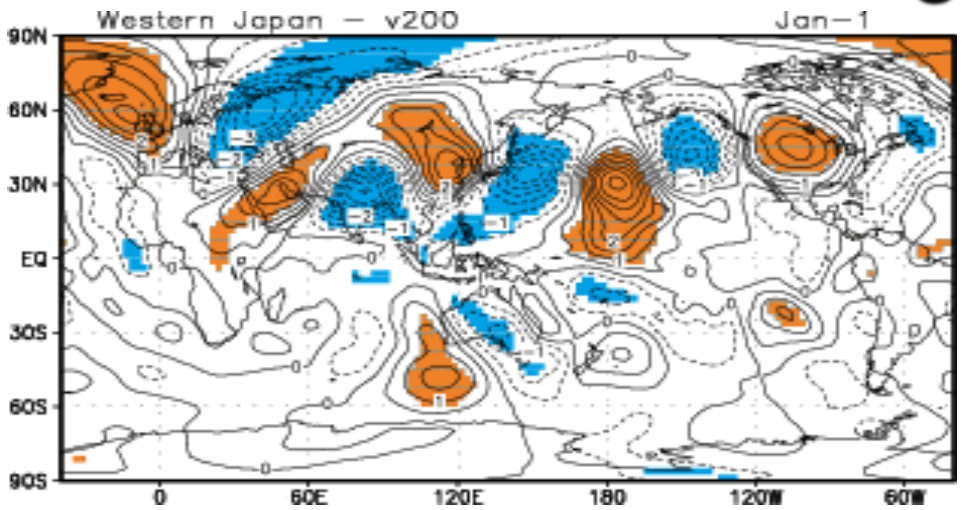

Regression of meridional wind v at 200hPa on 10-day mean temperature in western Japan . 1 Jan.-10 Jan.

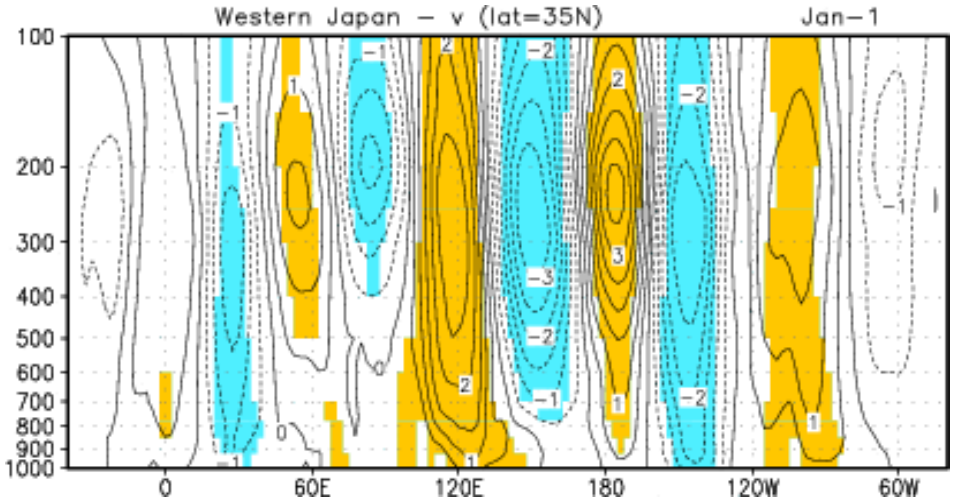

Longitude-height cross section of regression of meridional wind v at 35N

Climatology of stationary Rossby wave packets propagation (1-10 JAN,1971-2000)

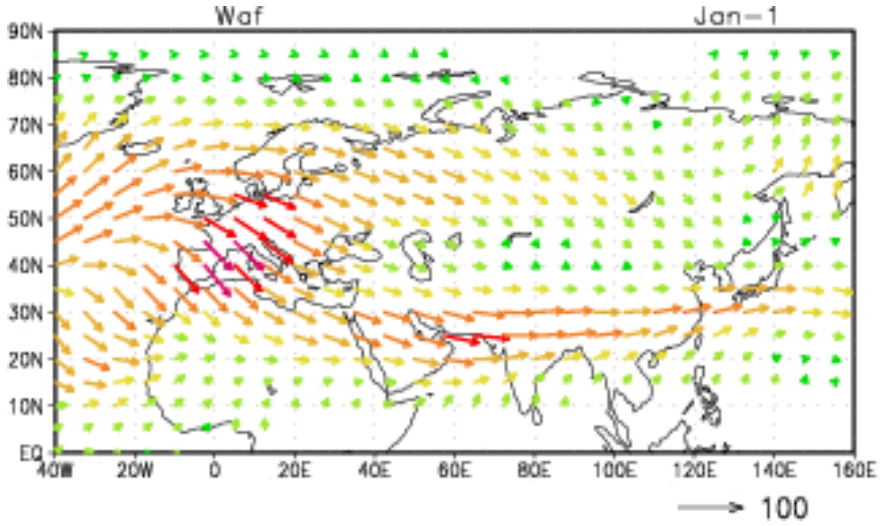

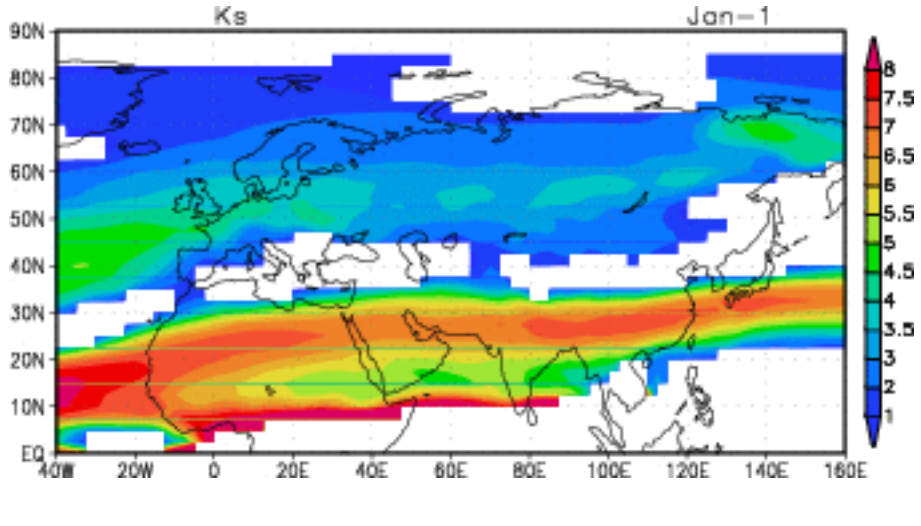

Wave activity flux (Takaya and Nakamura,2001,JAS,608-) at 200hPa

Stationary Rossby wave number Ks (Hoskins and Ambrizzi,1993,JAS,1661-) at 200hPa

Source of Rossby wave train along the Asian jet ?

Blocking over the North Atlantic and Rossby wave trains along the Asian jet

5-day mean stream function anomalies at 200hPa 2005.1.18-2.2 – 2.6

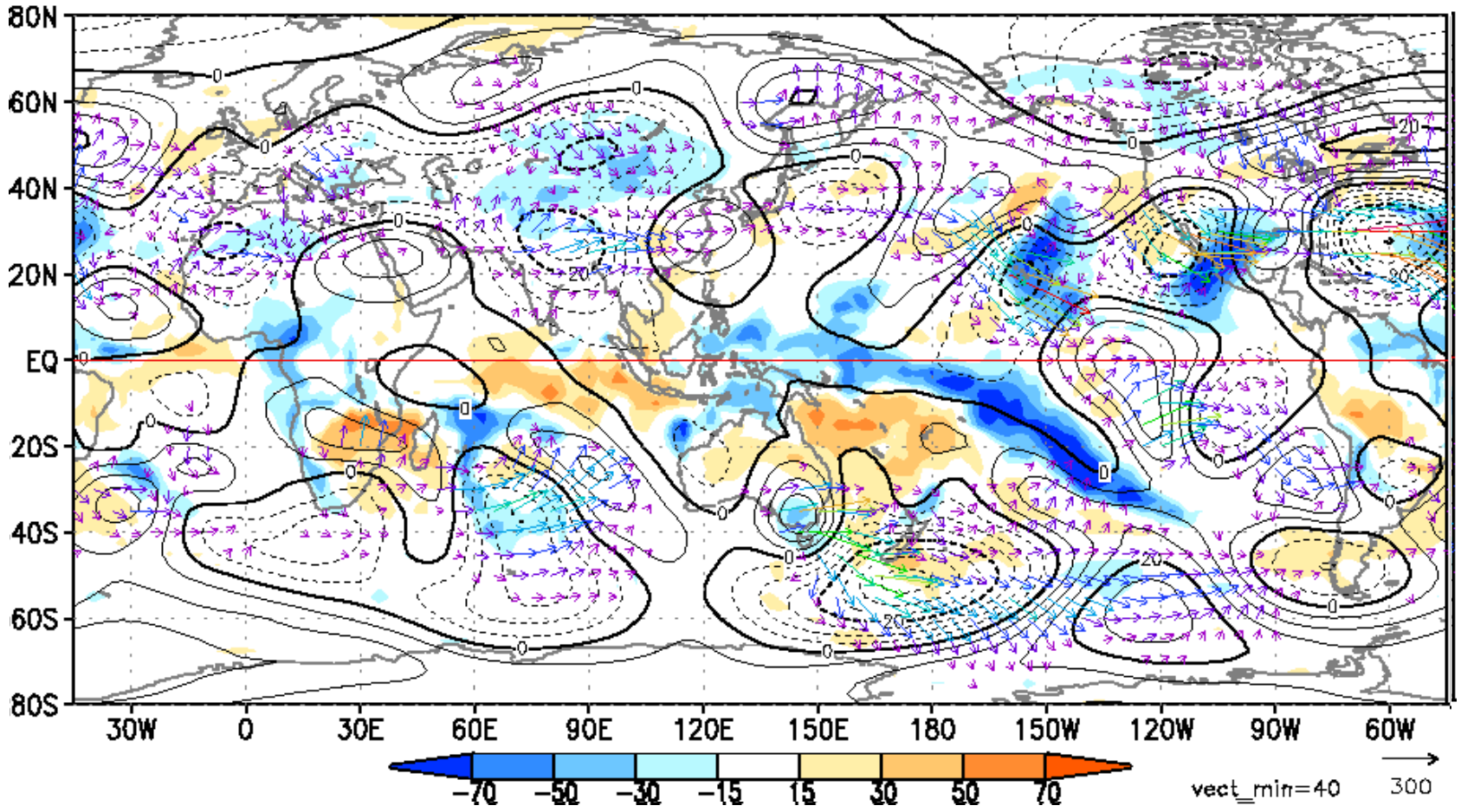

Time cross section of stream function anomalies at 200hPa x-axis : distance along the red line from a base point (60W,60N)

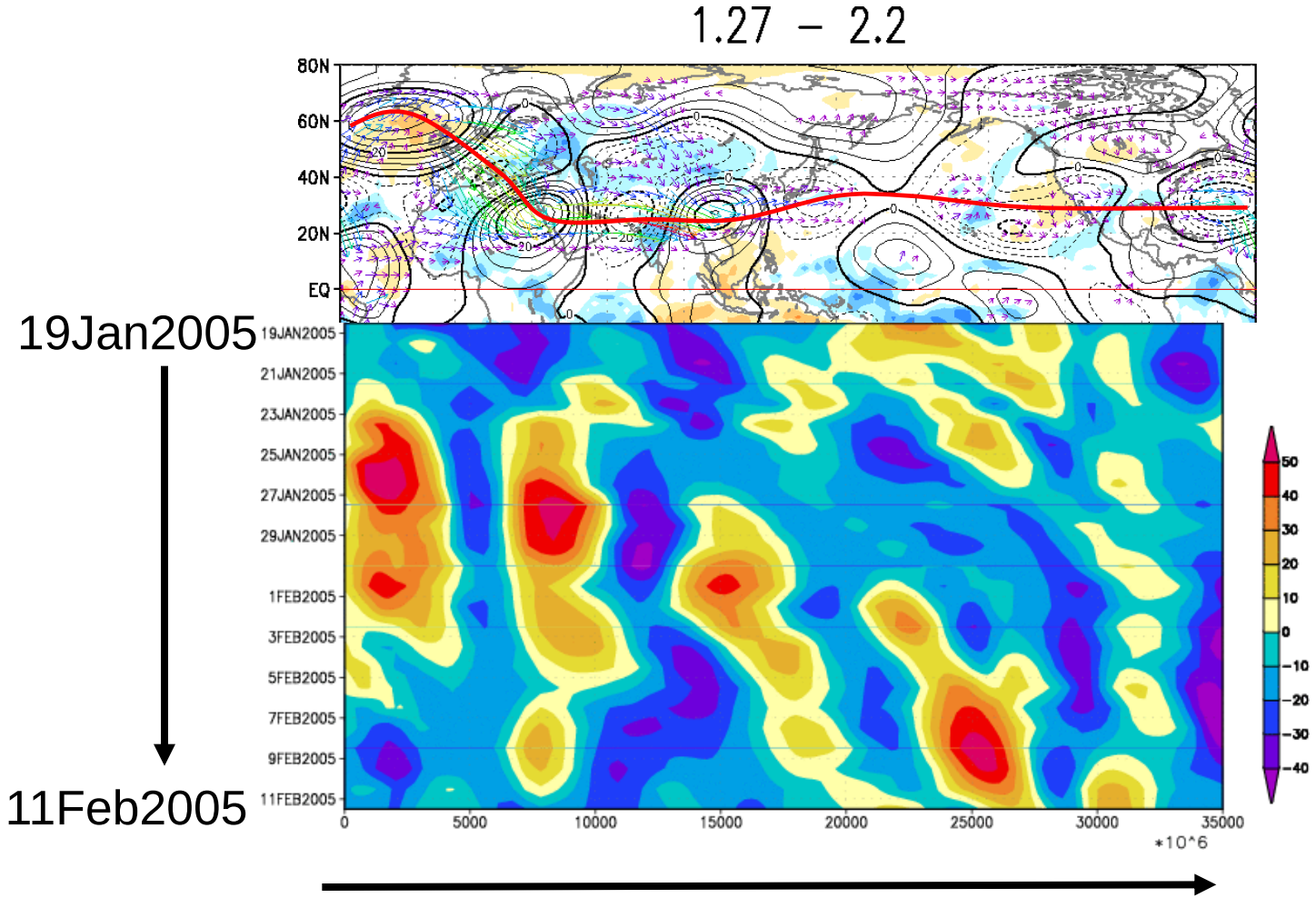

Decay of Blocking due to Rossby wave radiation

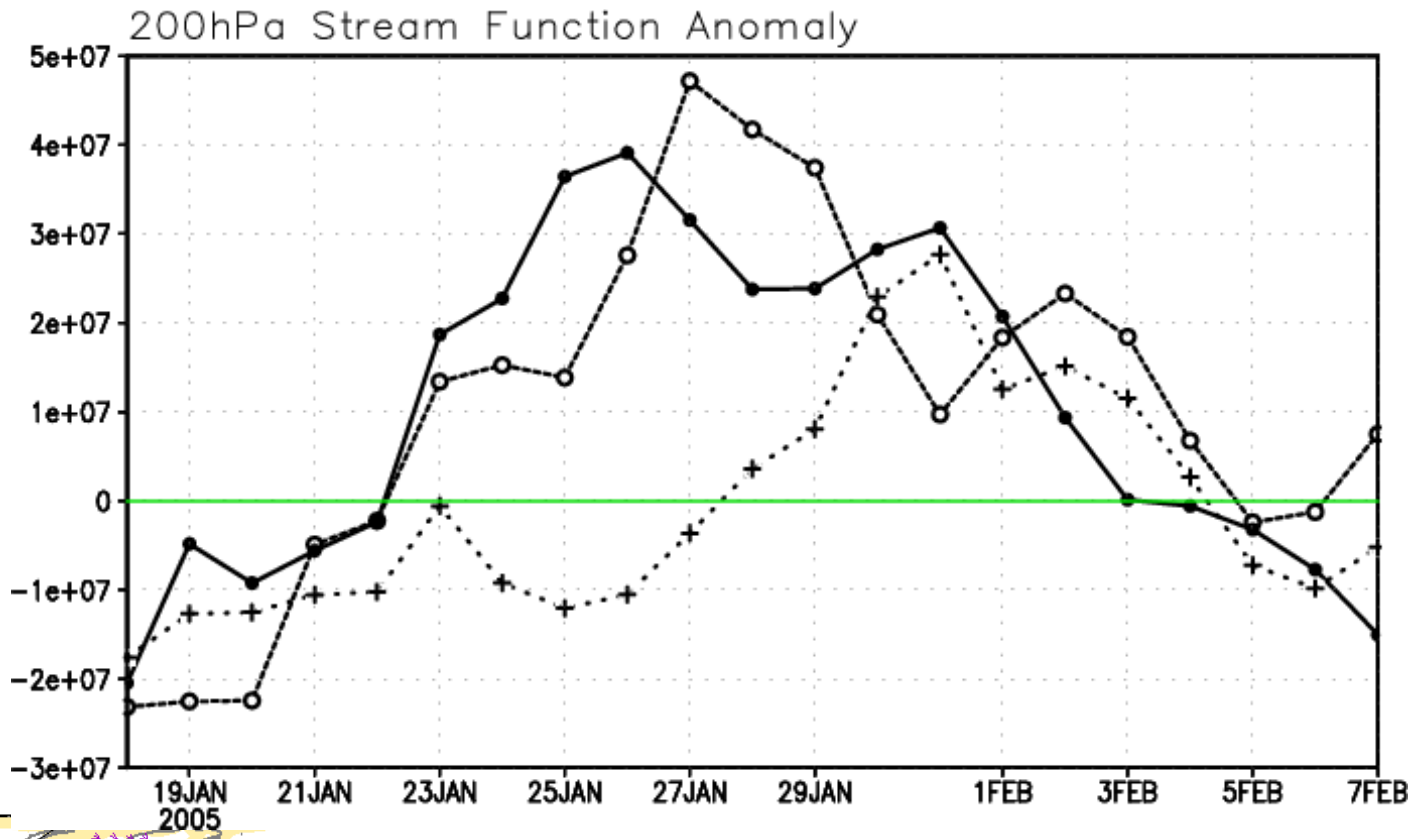

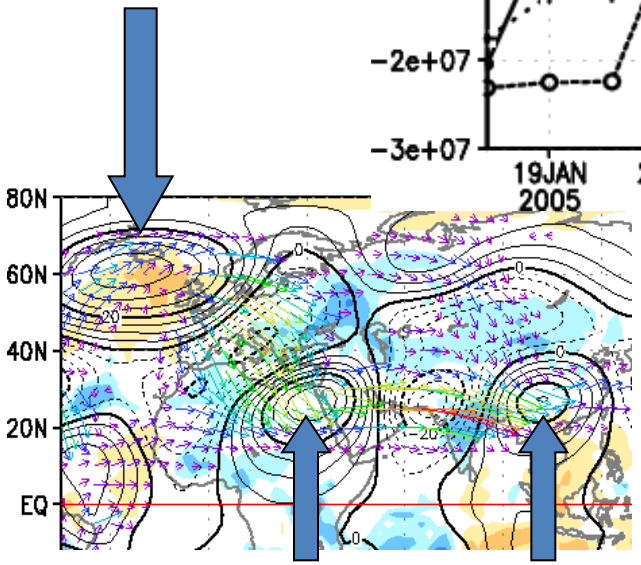

Prediction of development of Blocking

Initial : 20th JAN 2005

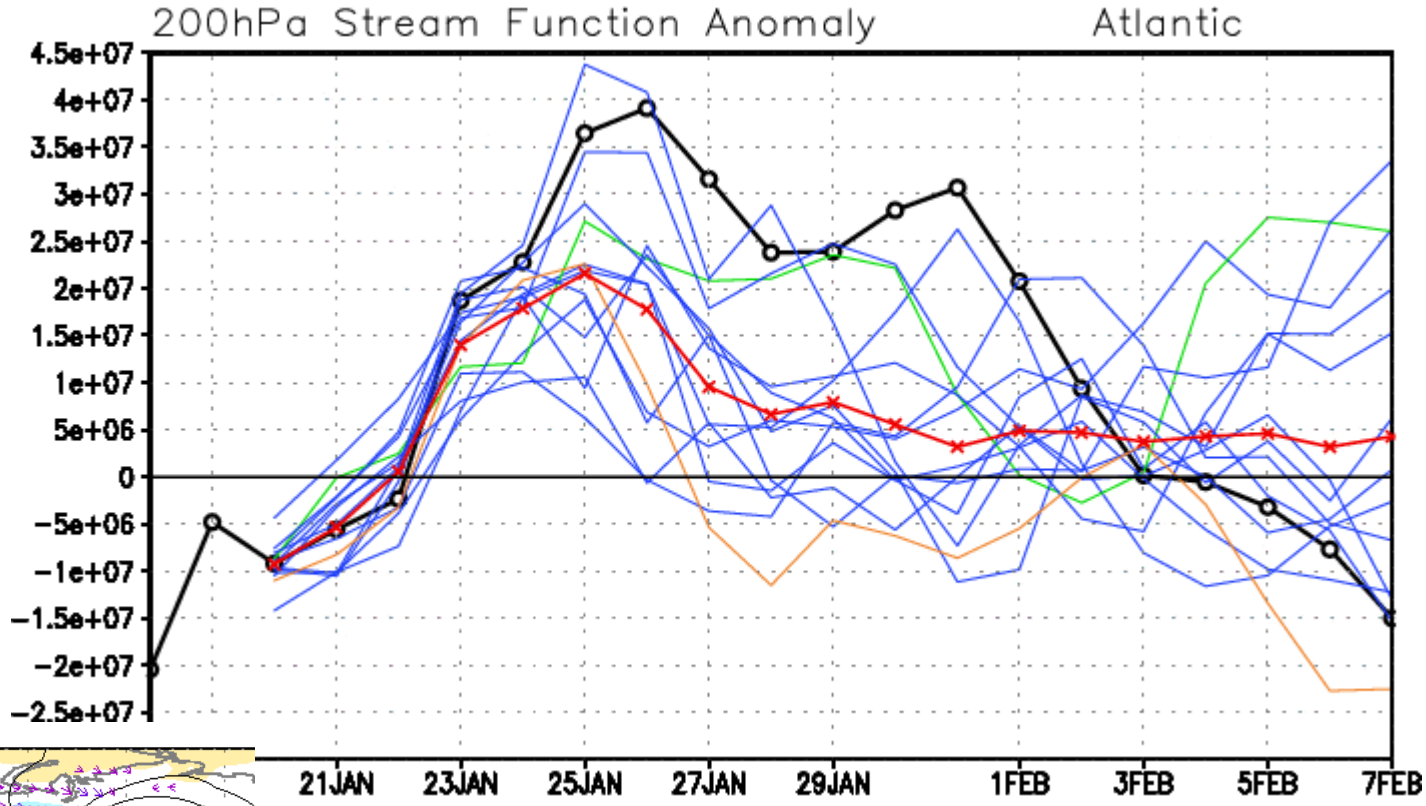

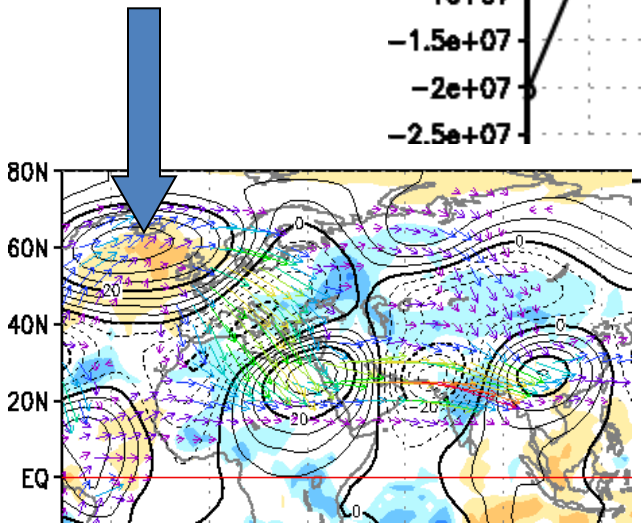

Prediction of decay of Blocking

Initial : 26th JAN 2005

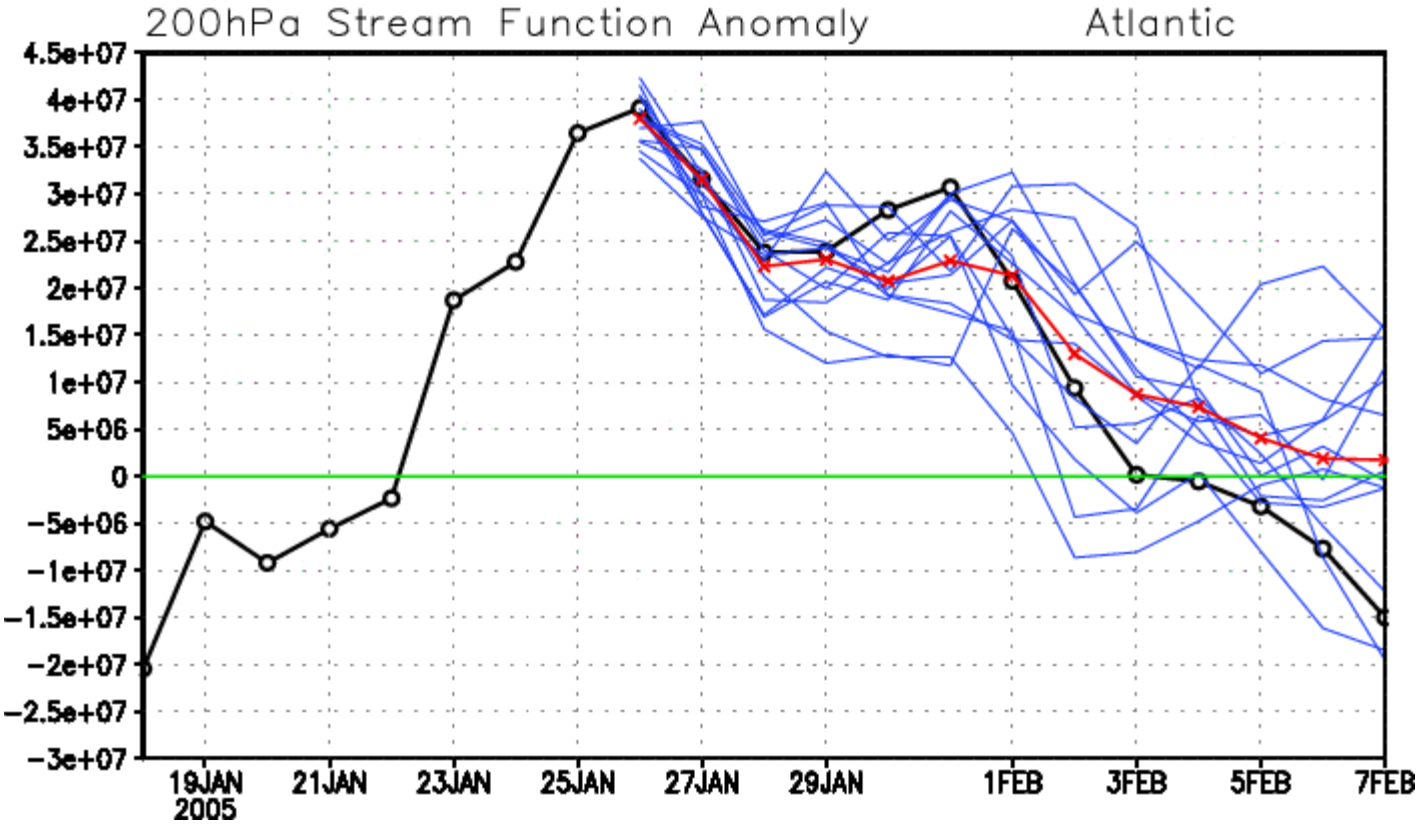

Prediction of decay of Blocking due to Rossby wave radiation

Initial : 26th JAN 2005

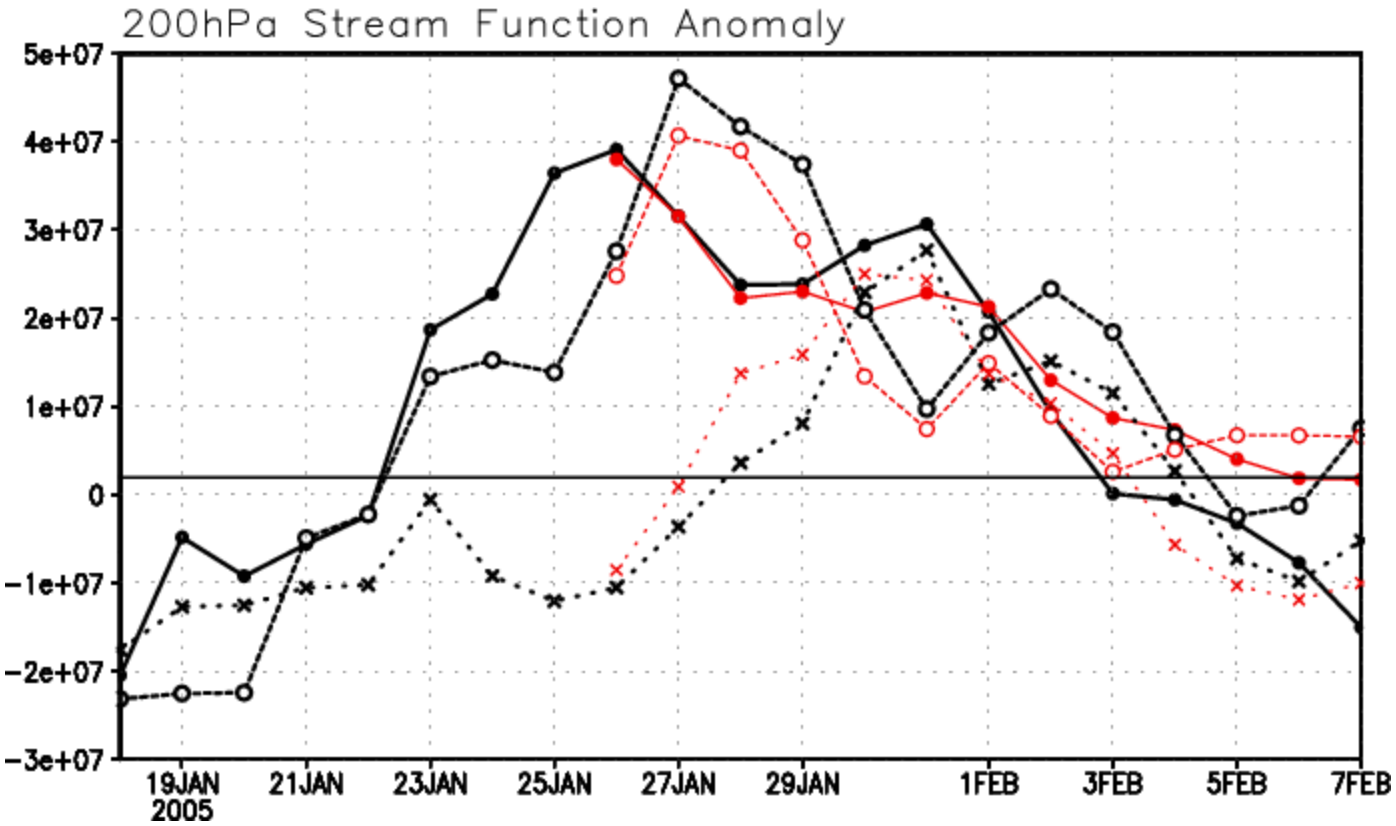

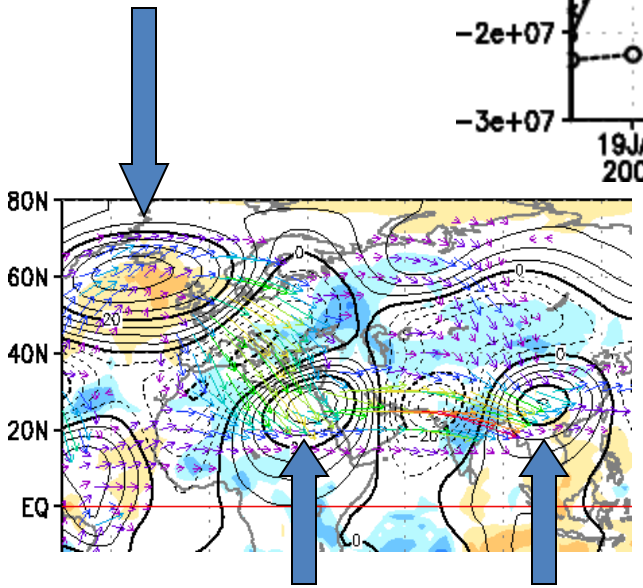

Madden-Julian Oscillation (MJO) and equatorial waves

Multi-scale clouds in the tropics

In the tropics, Heavy precipitation -> Deep cloud -> Low cloud-top temperature -> Low OLR

- Outgoing Longwave Radiation (OLR) from MTSAT JMA at 00 UTC Nov. 14, 2015

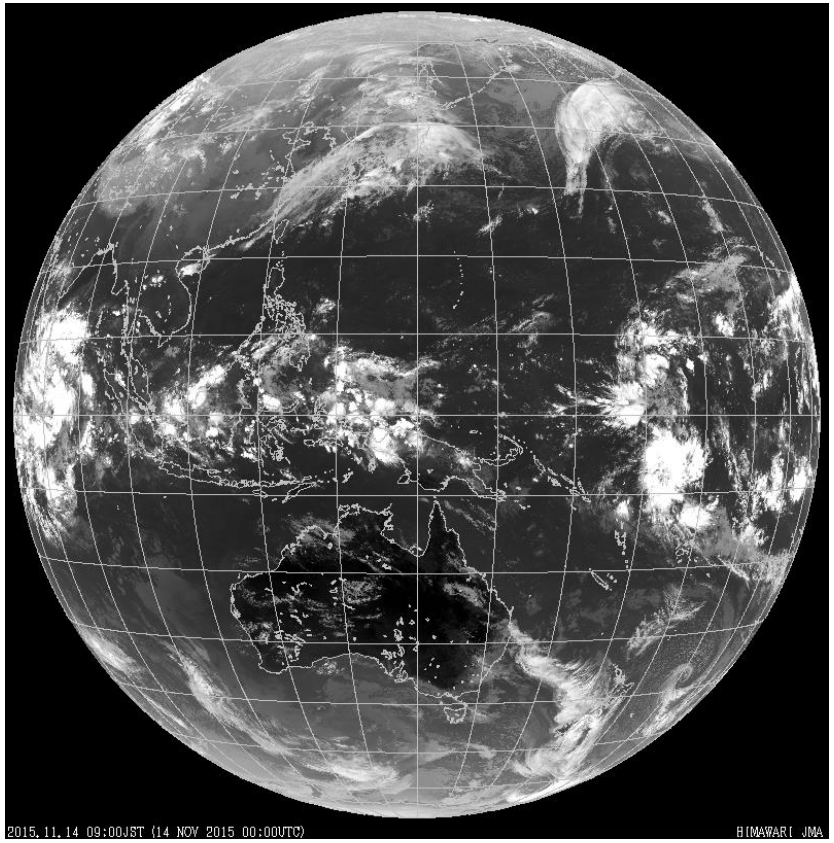

OLR variance of all from planetary scales to synoptic scales

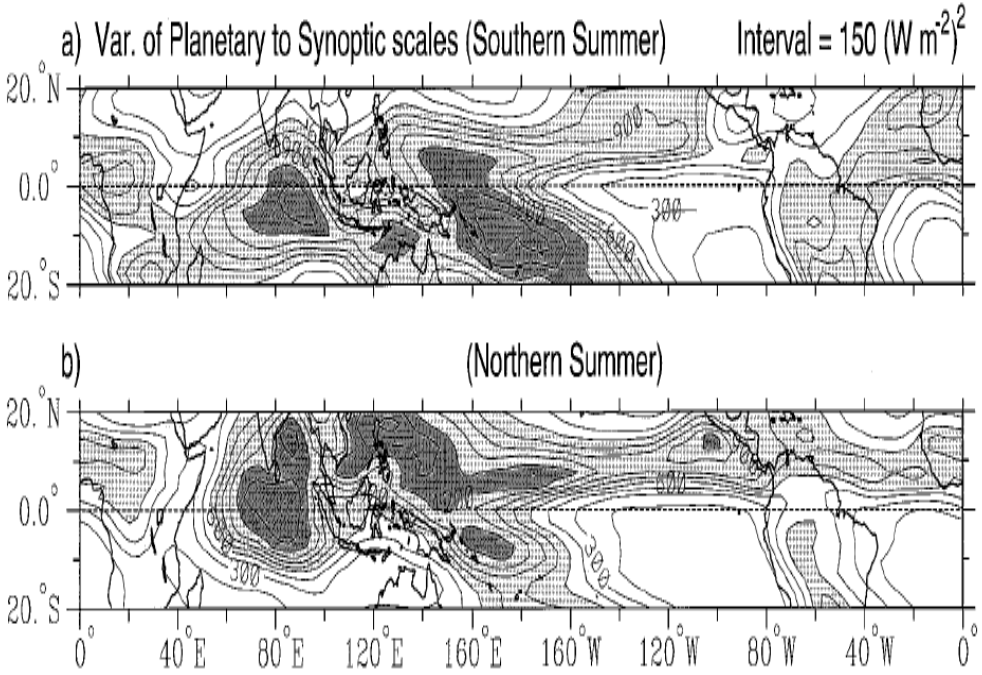

From Wheeler, M., and G. N. Kiladis, 1999

Matsuno, T., 1966: Quasi-geostrophic motions in the equatorial area. *J. Meteor. Soc. Japan,* **44,** 25–43.

Equatorial Waves

Kelvin wave

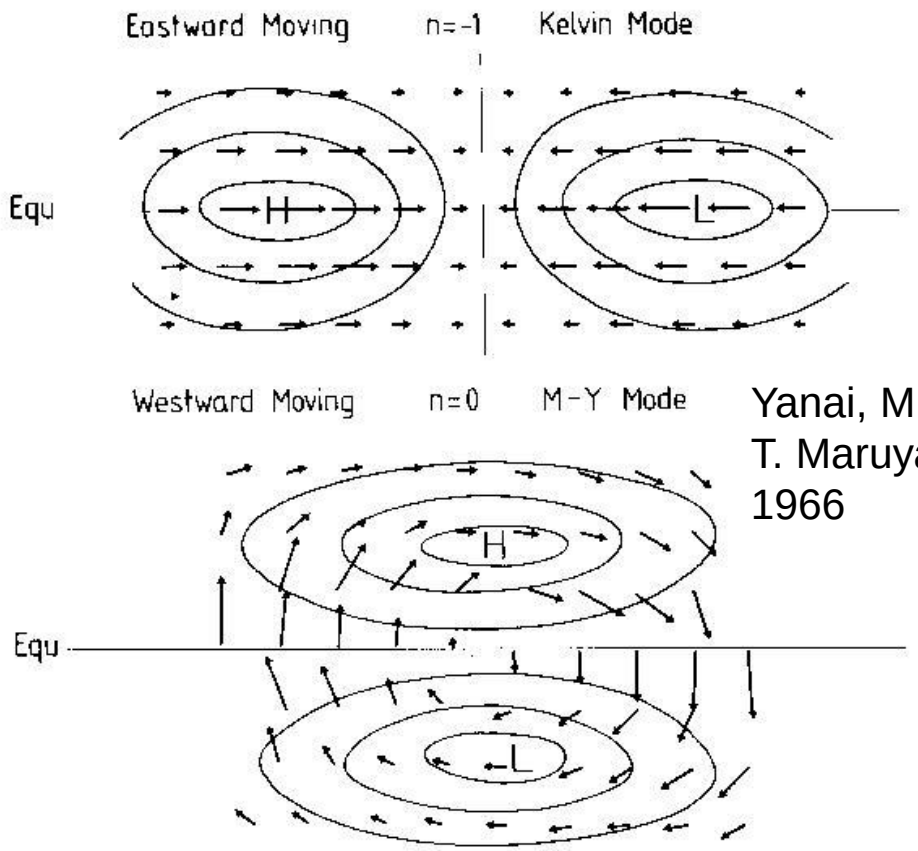

Yanai, M. and T. Maruyama, 1966

ER: Rossby wave (n=1)

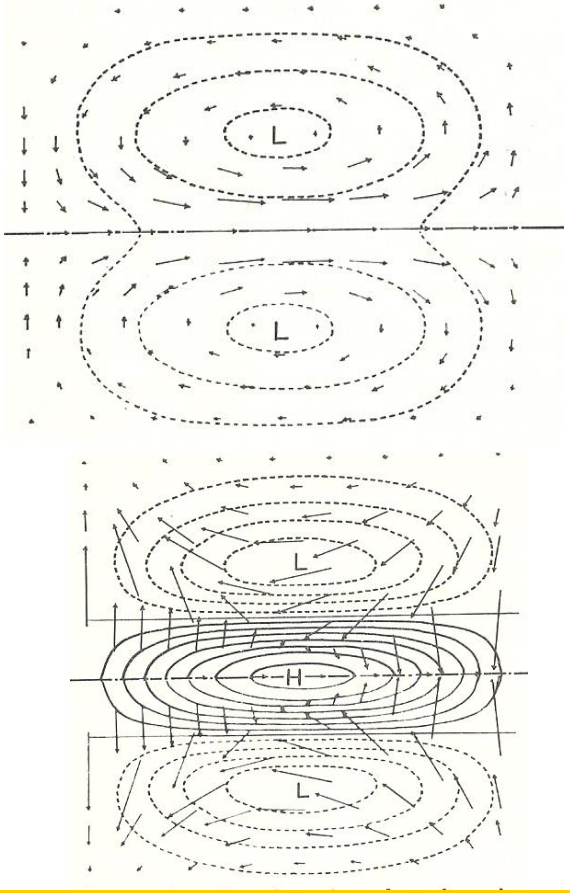

MRG : mixed Rossy-Gravity wave

EIG: eastward propagating inertio-gravity wave (n=1)

Convectively coupled equatorial waves

Wave number–frequency power spectrum of the (a) symmetric and (b) antisymmetric component of Cloud Archive User Services (CLAUS) T_b

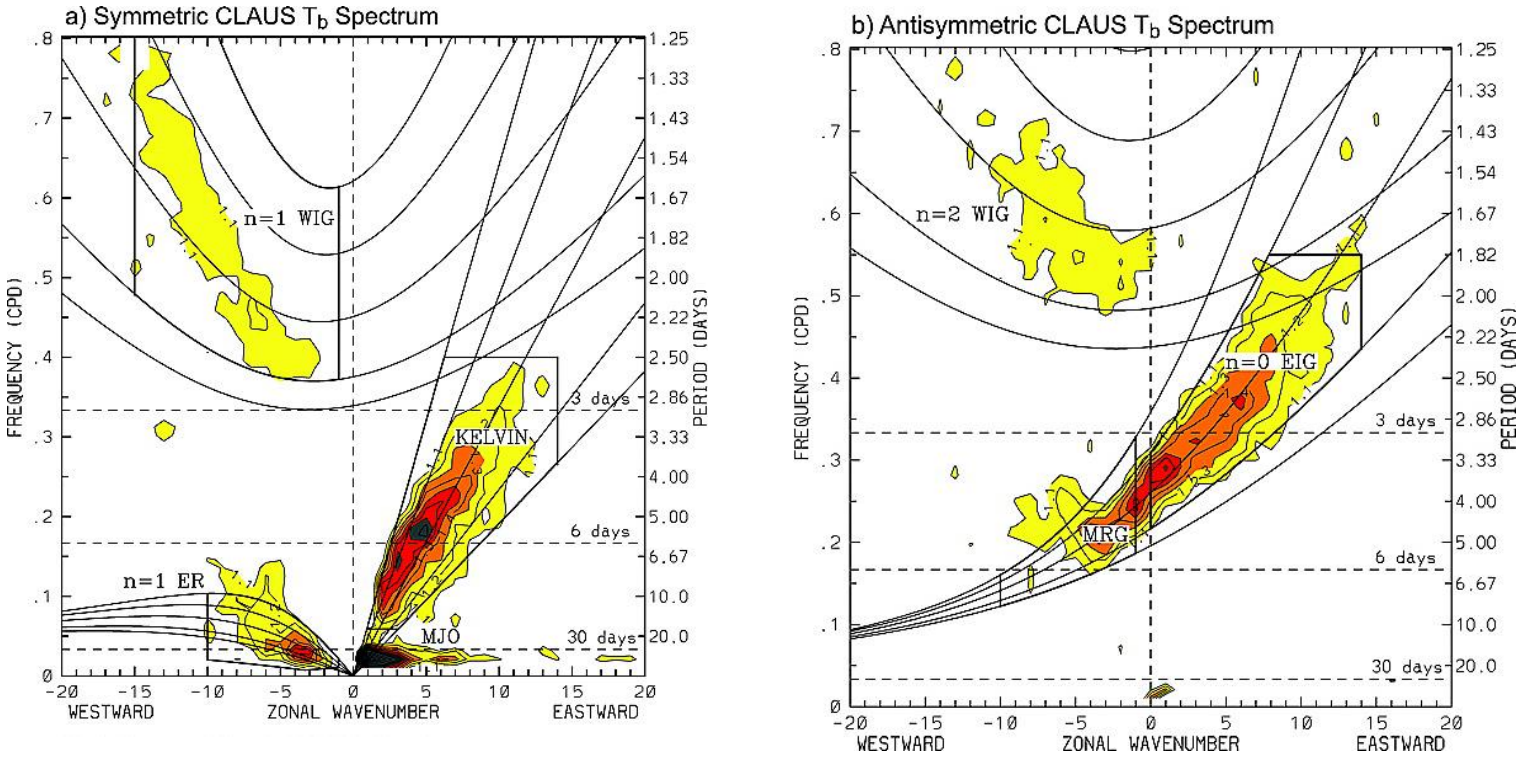

Wave number–frequency power spectrum of the (a) symmetric and (b) antisymmetric component of Cloud Archive User Services (CLAUS) T_b for July 1983 to June 2005, summed from 15° N to 15° S, plotted as the ratio between raw T_b power and the power in a smoothed red noise background spectrum (see WK99 for details). Contour interval is 0.1, and contours and shading begin at 1.1, where the signal is significant at greater than the 95% level. Dispersion curves for the Kelvin, n = 1 equatorial Rossby (ER), n = 1 and n = 2 westward inertio-gravity (WIG), n = 0 eastward inertio-gravity (EIG), and mixed Rossby-gravity (MRG) waves are plotted for equivalent depths of 8, 12, 25, 50, and 90 m. Heavy solid boxes represents regions of wave number–frequency filtering

Kiladis et. al.(2009)

Reviews of Geophysics
Volume 47, Issue 2, RG2003, 10 APR 2009 DOI: 10.1029/2008RG000266
http://onlinelibrary.wiley.com/doi/10.1029/2008RG000266/full#rog1687-fig-0001

Decomposition of the equatorial OLR anomalies

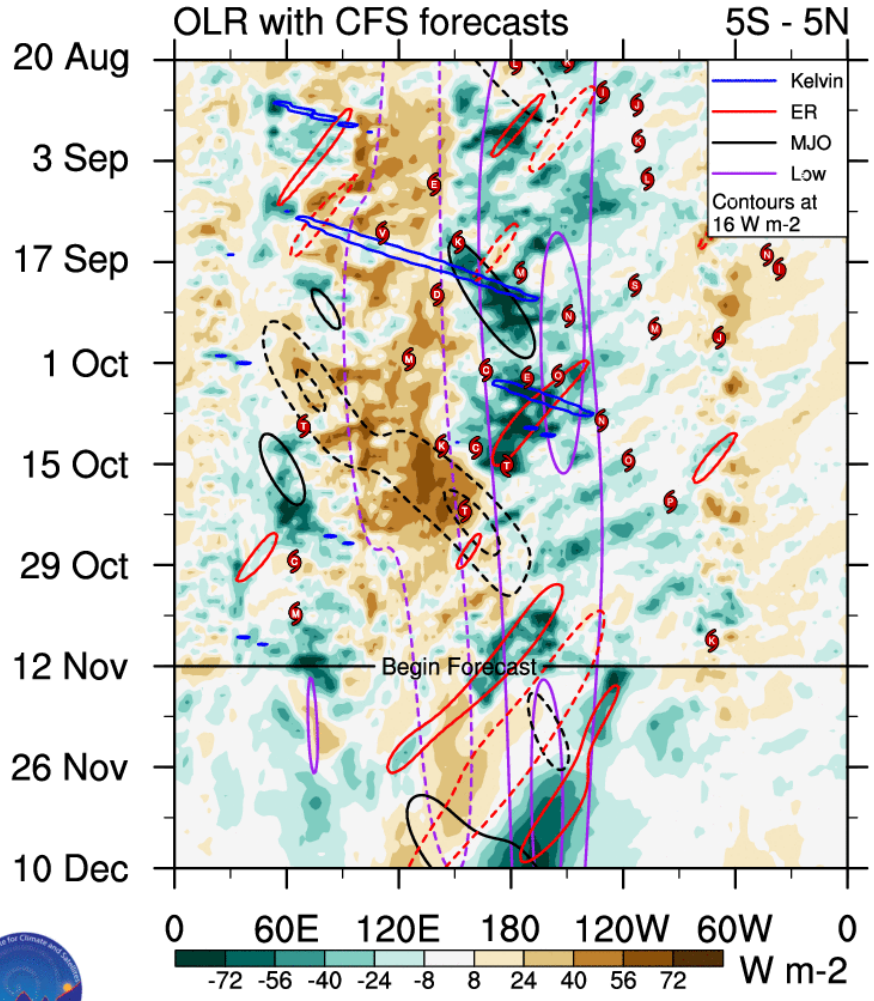

https://monitor.cicsnc.org/mjo/v2/images/spectra.png

Equatorial Rossby wave

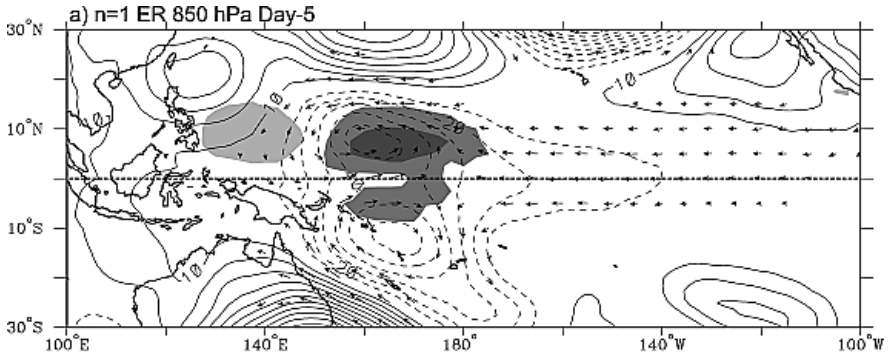

850hPa day= -5

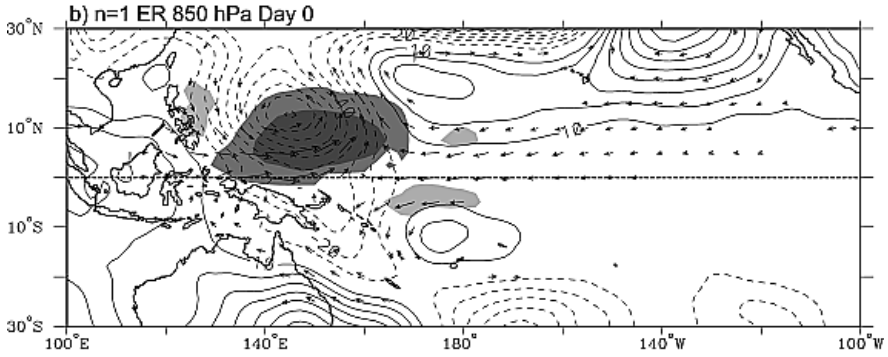

850hPa day= 0

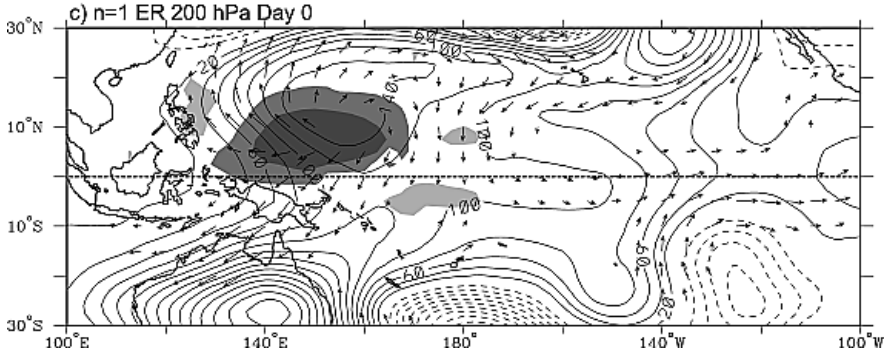

200hPa day= 0

Maps of anomalous T_b (shading), geopotential height (contours), and wind (vectors) associated with a −20 K perturbation in n = 1 ER wave T_b at the base point 7.5° N, 152.0° E, for (a) day −5 at 850 hPa, (b) day 0 at 850 hPa, and (c) day 0 at 200 hPa. The contour interval is 10 m in Figures 17a and 17b and 20 m in Figure 17c, with negative contours dashed. Dark (light) shading is for negative (positive) T_b perturbations of ±10 K and 3 K. T_b and wind vectors are locally significant at the 95% level, with the largest vectors around 2 m s^{-1}.

Kiladis et. al.(2009)

Madden-Julian Oscillation (MJO)

Surface pressure at Canton Iceland (3S, 172W)

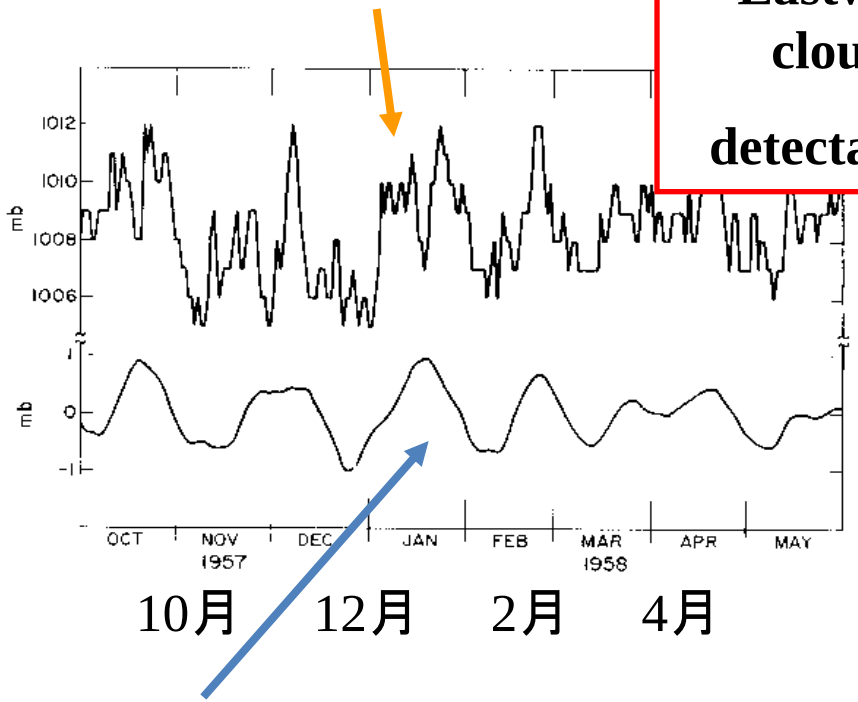

10月 12月 2月 4月

After applying band-pass filter around 45 days

Eastward super cloud cluster

detectable by OLR

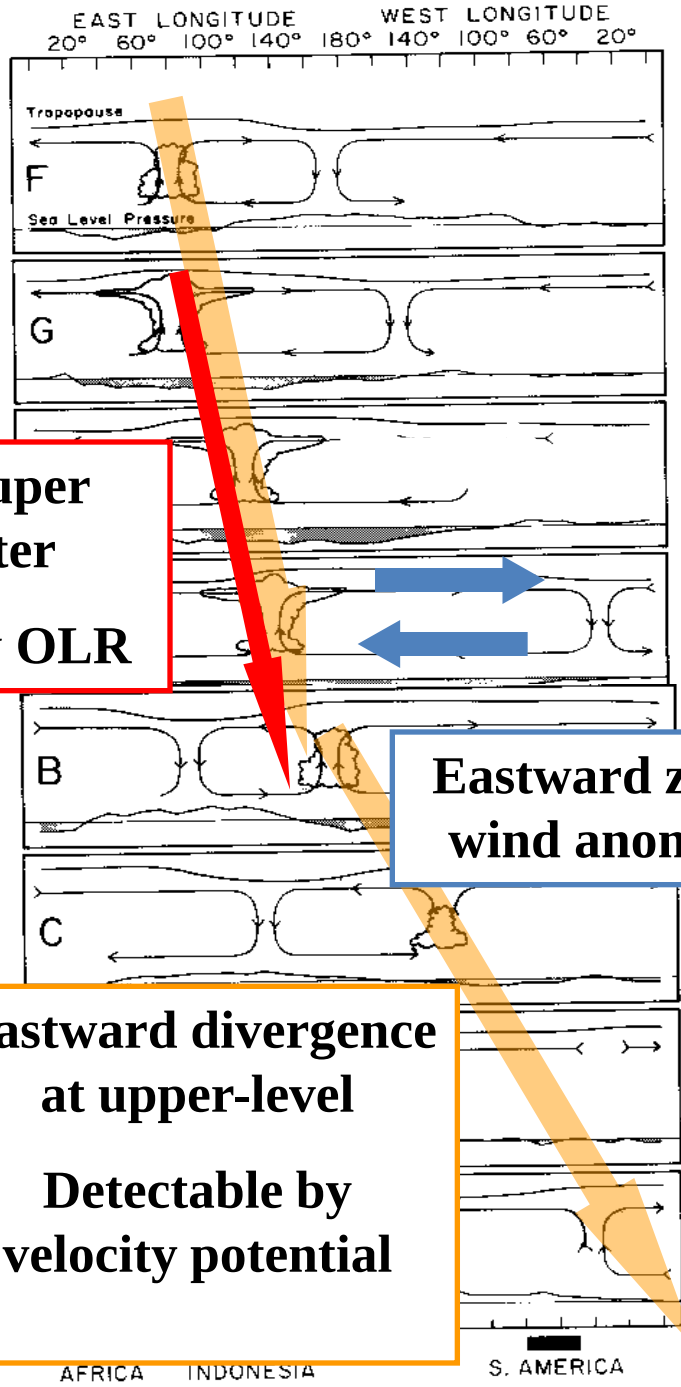

Eastward zonal wind anomaly

Eastward divergence at upper-level

Detectable by velocity potential

30-60 day Period

Schematic structure of MJO

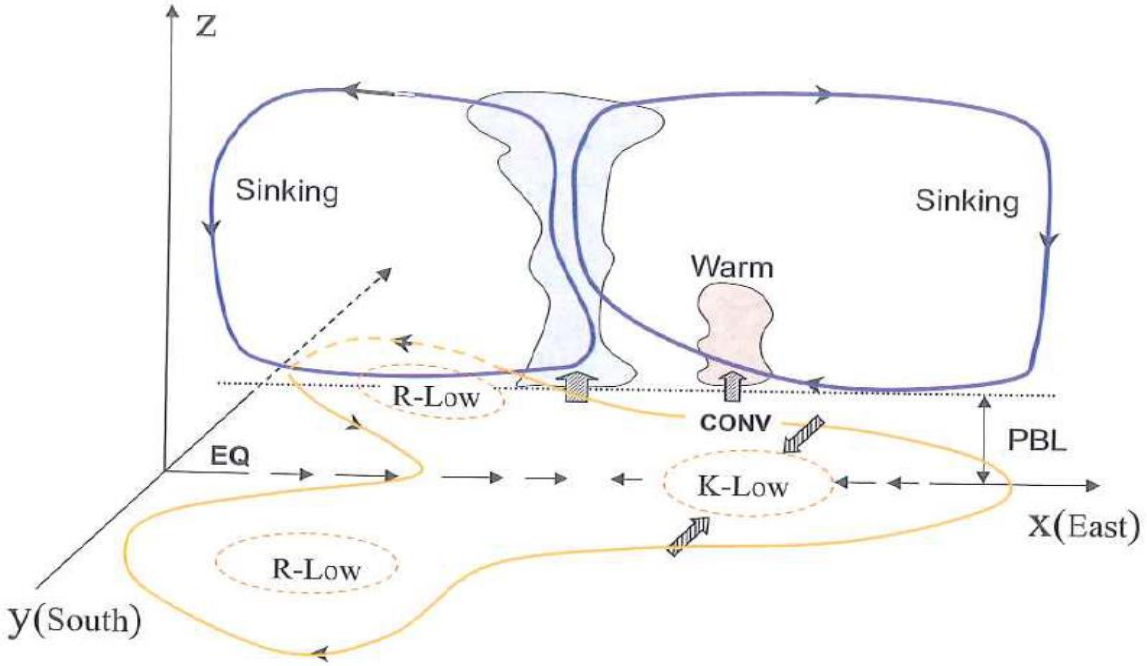

Figure 10.13. Schematic structure of the frictional CID mode, which is the counterpart of observed MJO mode. In the horizontal plane the "K-low" and "R-low" represents the low-pressure anomalies associated with the moist equatorial Kelvin and Rossby waves, respectively. Arrows indicate the wind directions. In the equatorial vertical plane the free-tropospheric wave circulation is highlighted. The wave-induced convergence is in phase with the major convection, whereas the frictional moisture convergence in the "K-low" region is ahead of the major convection due primarily to meridional wind convergence.

From Wang (2005)

Composition maps of stream function at 200hPa and OLR at each phase (1-12) of MJO in winter (DJF)

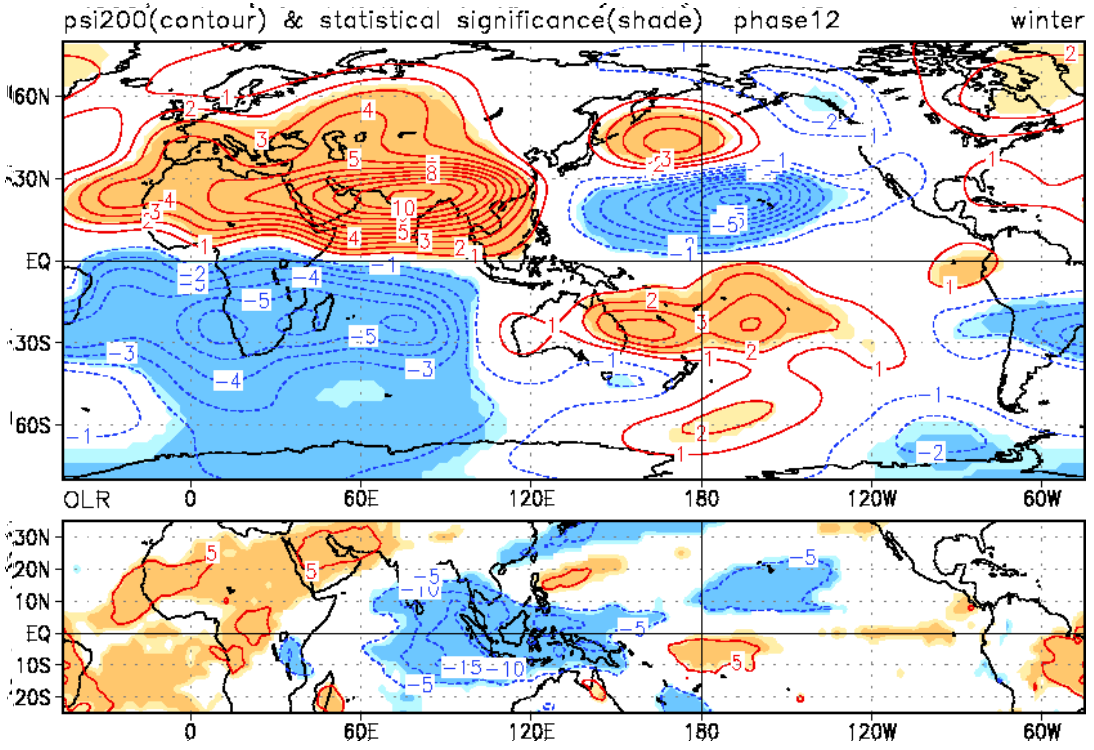

Stream function at 200hPa

OLR

Endoh and Harada (2005)

Impact of MJO (Example for Japan)

DJF Temperature Anomaly over Japan

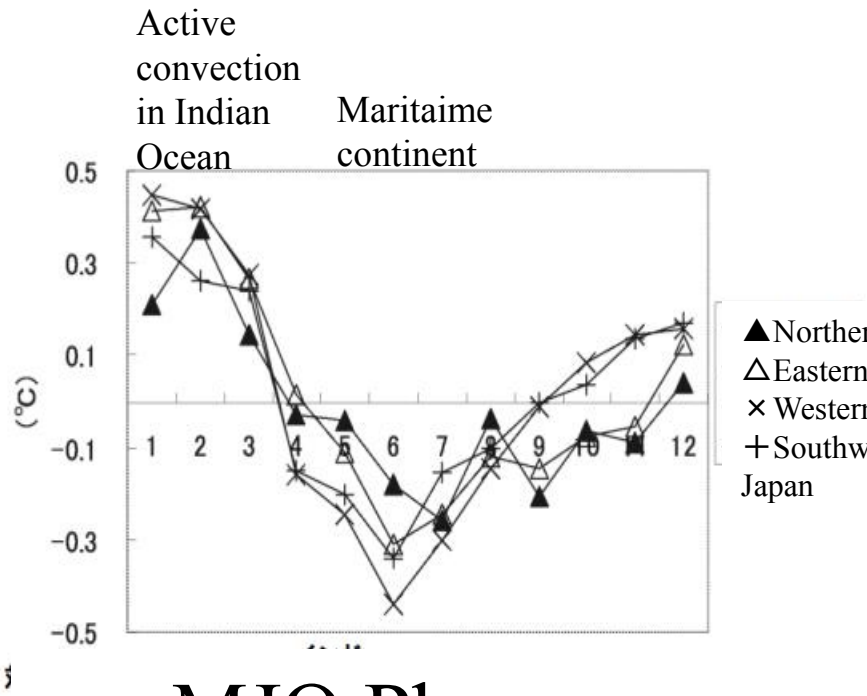

MJO Phase

Endo and Harada (2008)

Composition maps of MJO in DJF

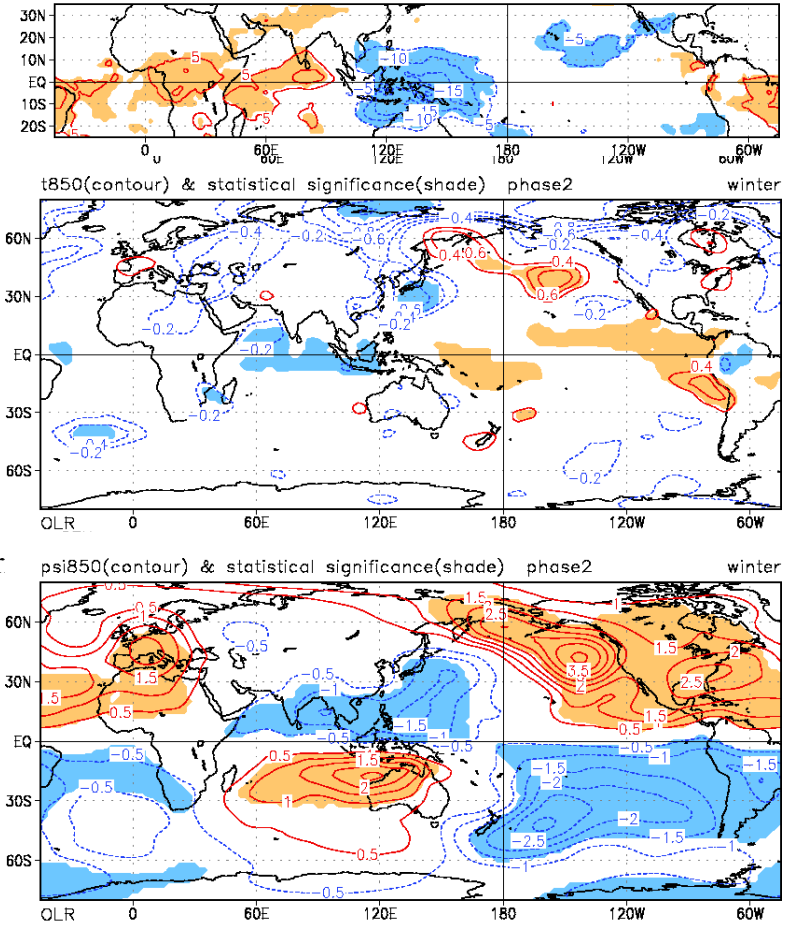

OLR

T850

Stream function at 850

Endoh and Harada (2005)

Example: extreme event caused by Rossby waves and MJO

Extreme warm event in early Nov. 2011

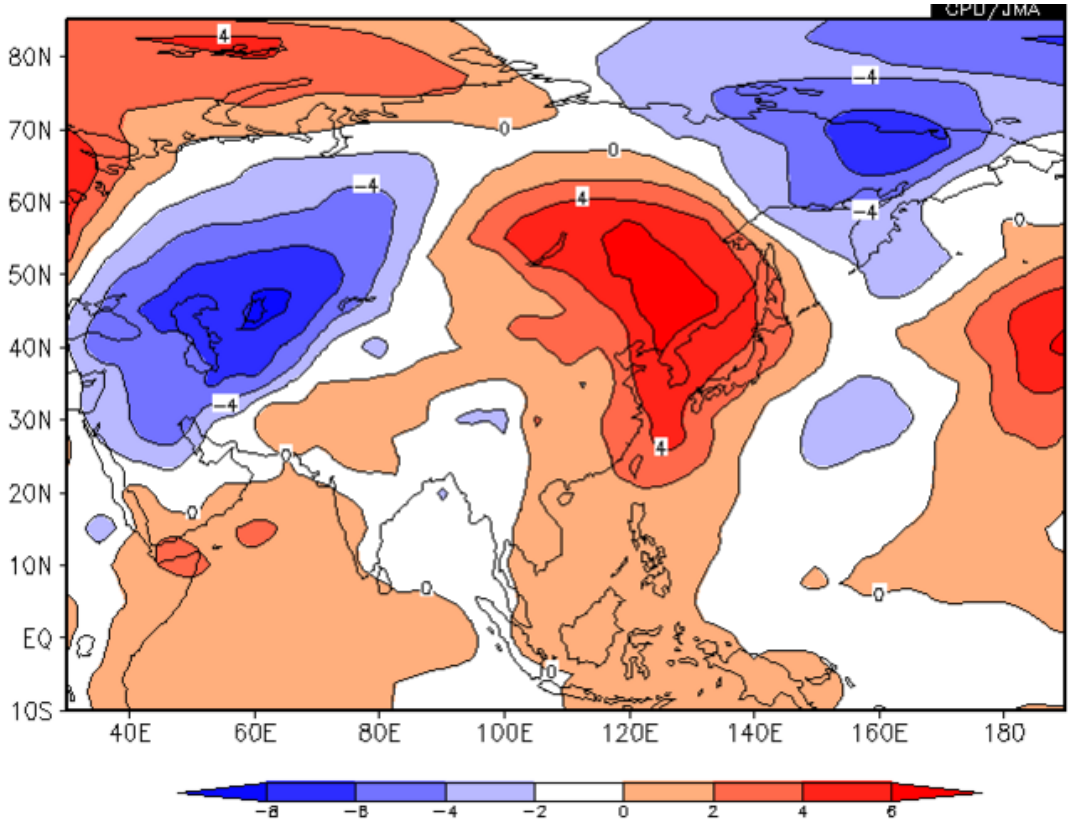

Western Japan experienced the warmest first ten days of Nov. since 1961.

10 day mean temperature anomalies at 850hPa in 1-10th Nov. 2011

Propagation of Stationary Rossby wave packet along the Polar front jet

10 day mean Stream function anomalies at 200hPa,2011.11.1-10

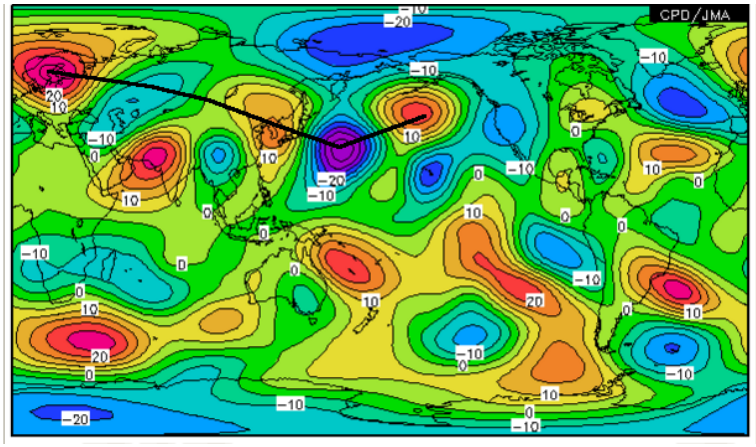

Wave length ≒8000km
Group velocity ≒25m/s

Stream function anomalies at 200hPa along the black line in the right figure,2011/10/25-11/15

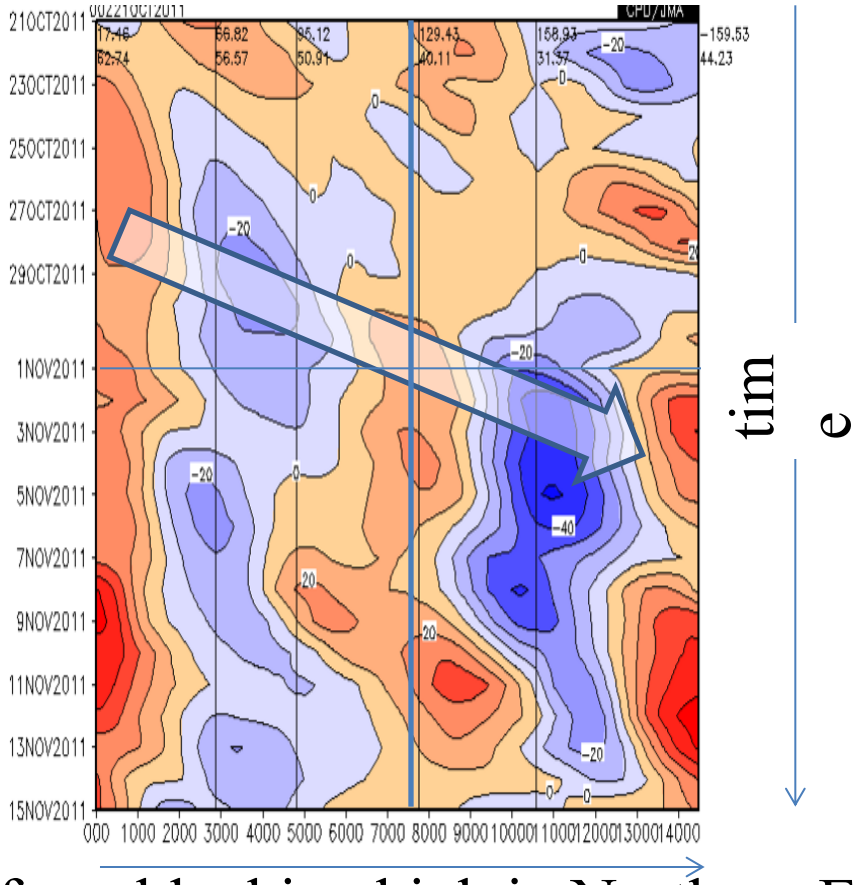

Propagation of Stationary Rossby wave packet along the Sub tropical jet

10 day mean Stream function anomalies at 200hPa,2011.11.1-10

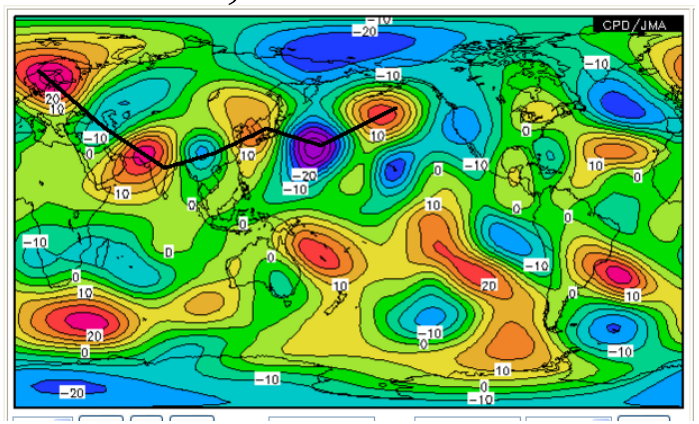

Stream function anomalies at 200hPa along the black line in the right figure,2011/10/25-11/15

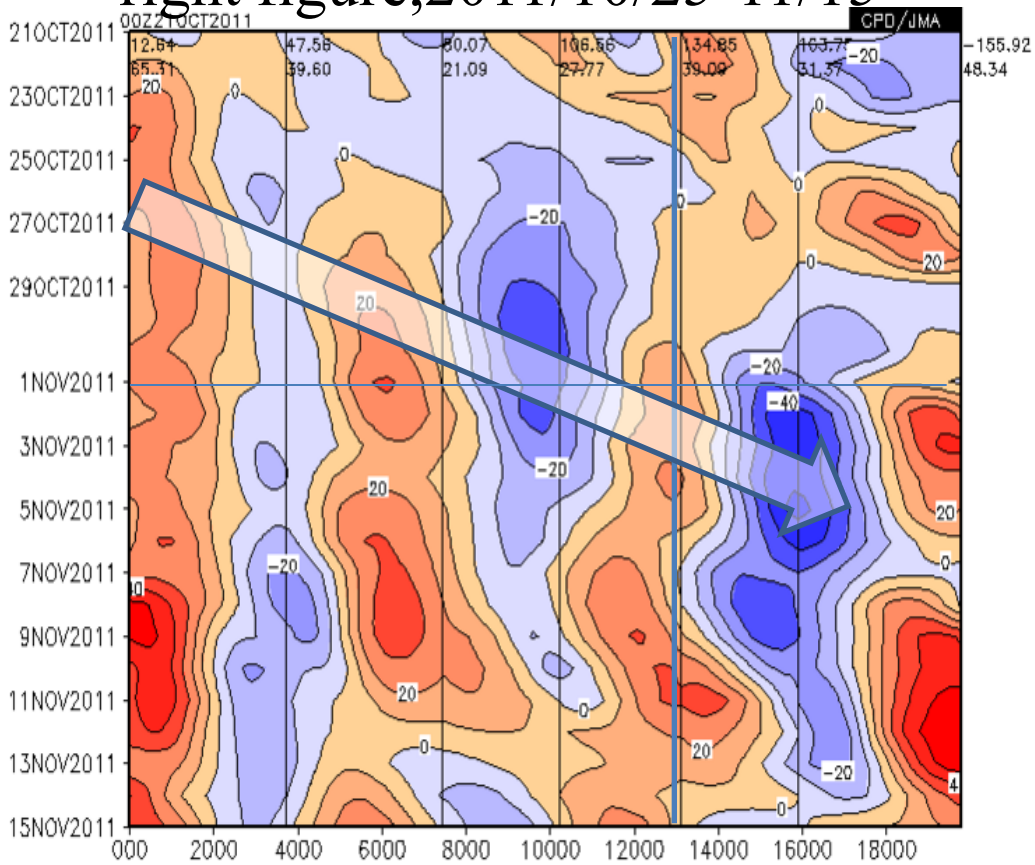

Wave length ≒ 6000km
Group velocity ≒ 25m/s
Enhanced near Pakistan in the end of Oct.

Distance from blocking high in Northern Europe(km)

Enhancement of the Rossby wave packet by convection over east north Indian Ocean in the end of Oct. 2011

Stream function and OLR anomalies

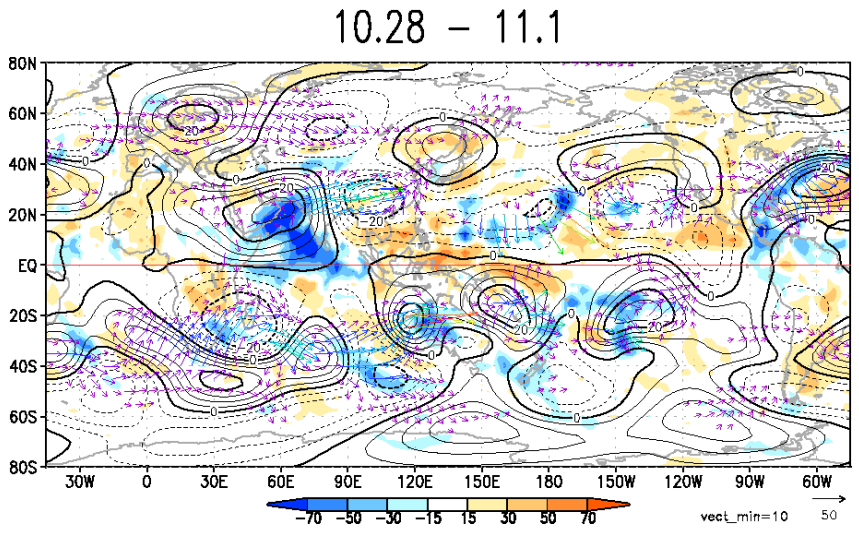

Rossby wave source anomalies

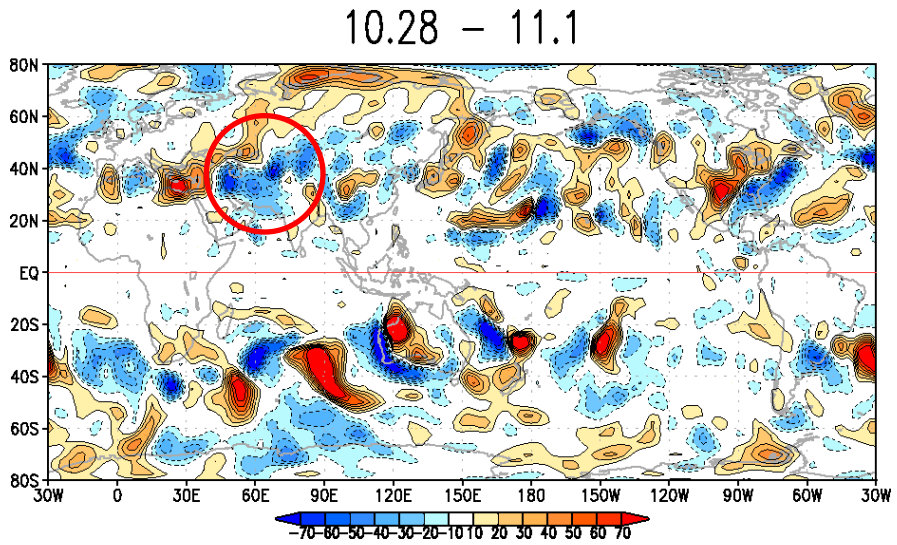

Contour : 5day mean Stream function anomalies at 200hPa

Shade : 5day mean OLR anomalies

Arrows : Wave activity flux (Takaya and Nakamura, 2000) at 200hPa

Shade: Rossby wave source anomalies at 200hPa. 10^{-6} /s /day

Origin of active convection over western Indian Ocean

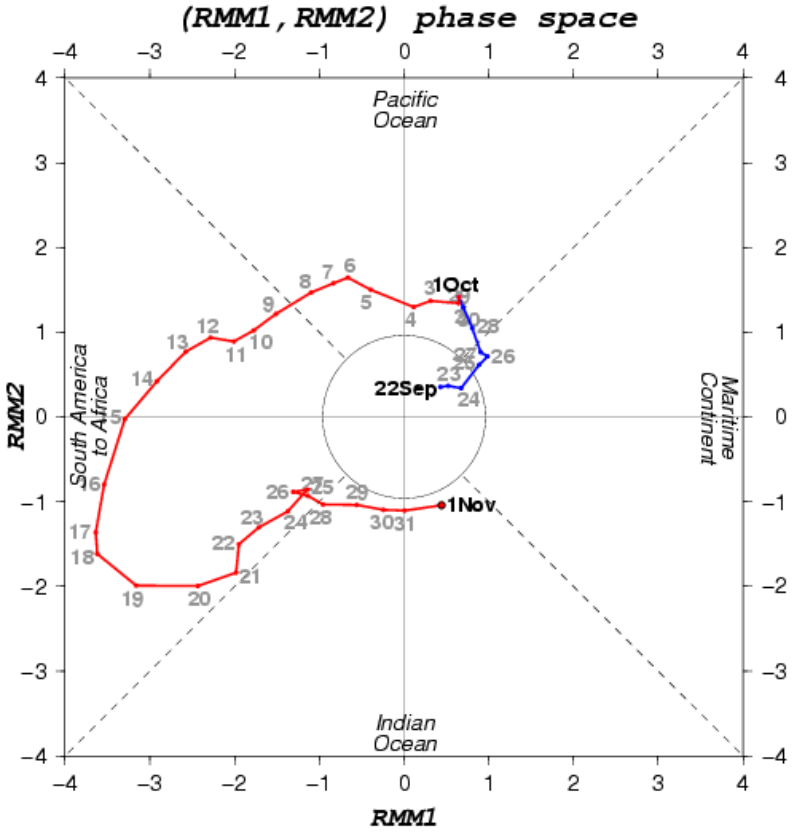

Fig. MJO phase monitor based on multivariate EOF analysis (OLR+U200+U850,) Data period for the normal is from 1981 to 2010. Seasonal, interannual and ENSO variations were subtracted from the tropical variations (Wheeler and Hendon, 2004). JRA-55 is used for the atmospheric data. OLR data are provided by NOAA. NINO.3 index was used for calculating ENSO variation instead of COBE-SST because of the difficulty to extract ENSO variation. Each figures show the last 40 days trajectory from the final day of each month.

- Strong MJO (at peak, the second strongest since 1979) propagated from the Atlantic to the Indian Ocean in the end of Oct.
- The MJO weekend over Indian Ocean
- So, active convection over western Indian Ocean is triggered by the MJO.

http://ds.data.jma.go.jp/tcc/tcc/products/clisys/mjo/monitor.html

Could we predict the event? Intial: 2011.10.24

7day mean temperature anomaly at 850hPa in Western Japan850.
Red: Obs. Others:FCST

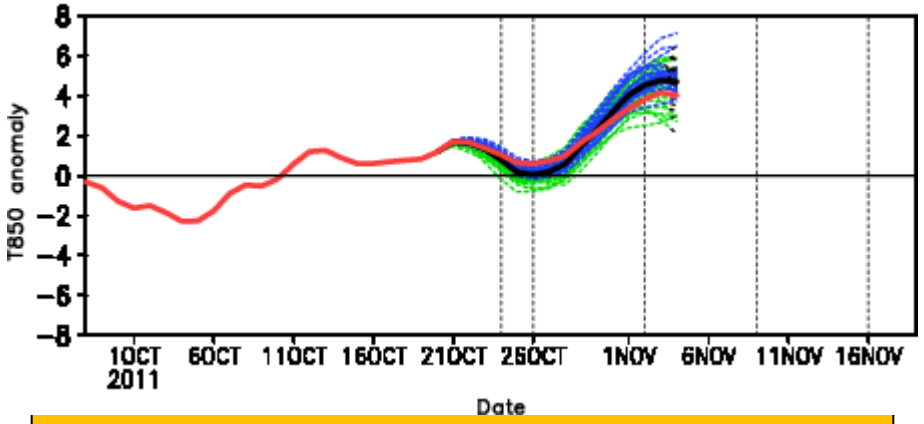

7day day mean Stream function anomalies and wave activity flux at 200hPa from 11/3-11/9 . a) Obs. b) FCST

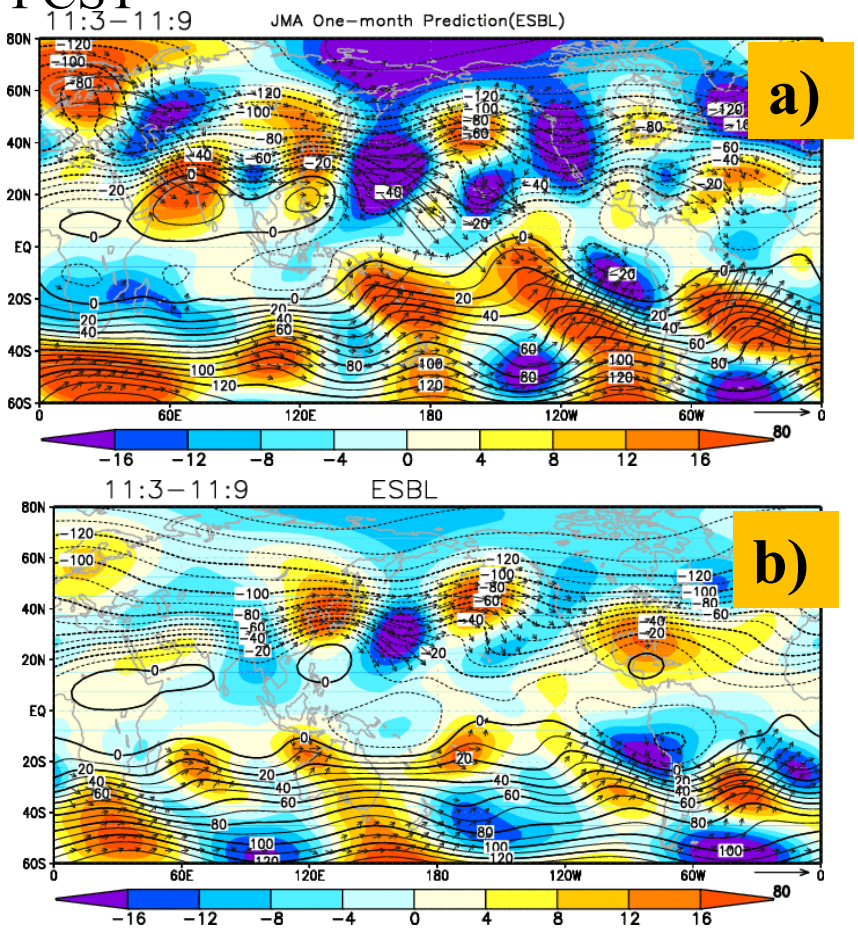

▪ The event was well predicted from 2011.10.24 initial (Rossby wave packets along PFJ and STJ which was enhanced by MJO related convection, and extremely high Temperature)

2.3 Interannual Variability: ENSO, El Niño Modoki, IOD

El Niño and Southern Oscillation (ENSO)

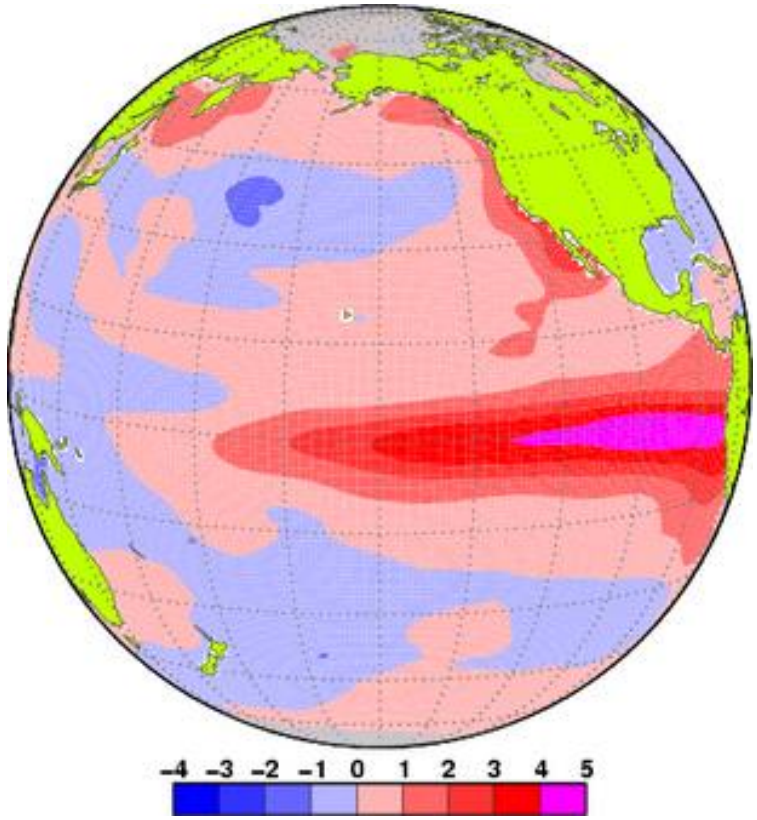

Why is El Niño/La Niña important ?

1. Predominant inter-annual climate variability
2. Big Impact on the world climate
3. Predictable with one or two seasons lead time

The prediction of El Niño or La Niña is a base of our long range forecast. First, we check the ENSO conditions and then discuss our long range forecast.

Normal condition in the equatorial Pacific Ocean

Trade wind, a persistent easterly atmospheric flow blowing over the equatorial Pacific Ocean, sustains warmer-western, cooler-eastern sea surface condition.

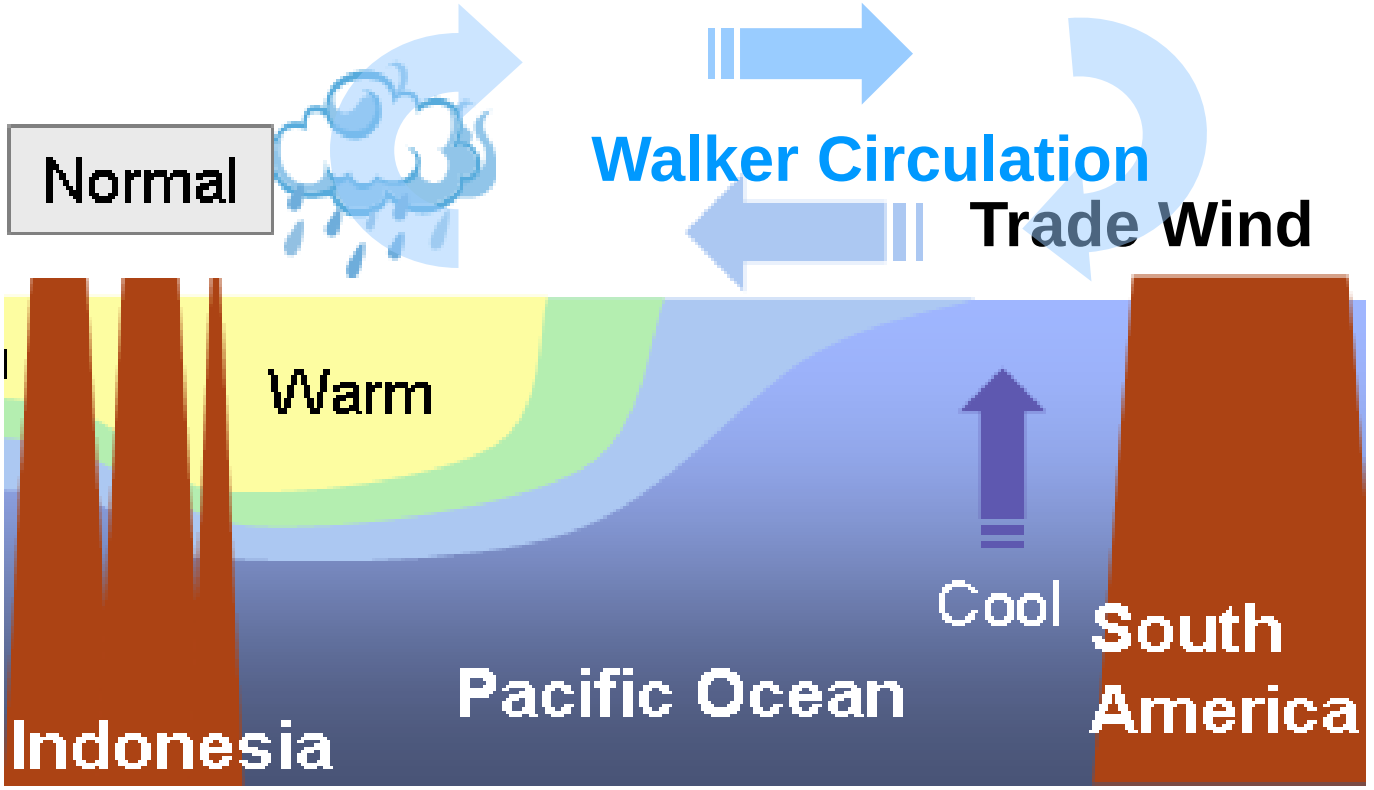

Sea surface temperature (SST)

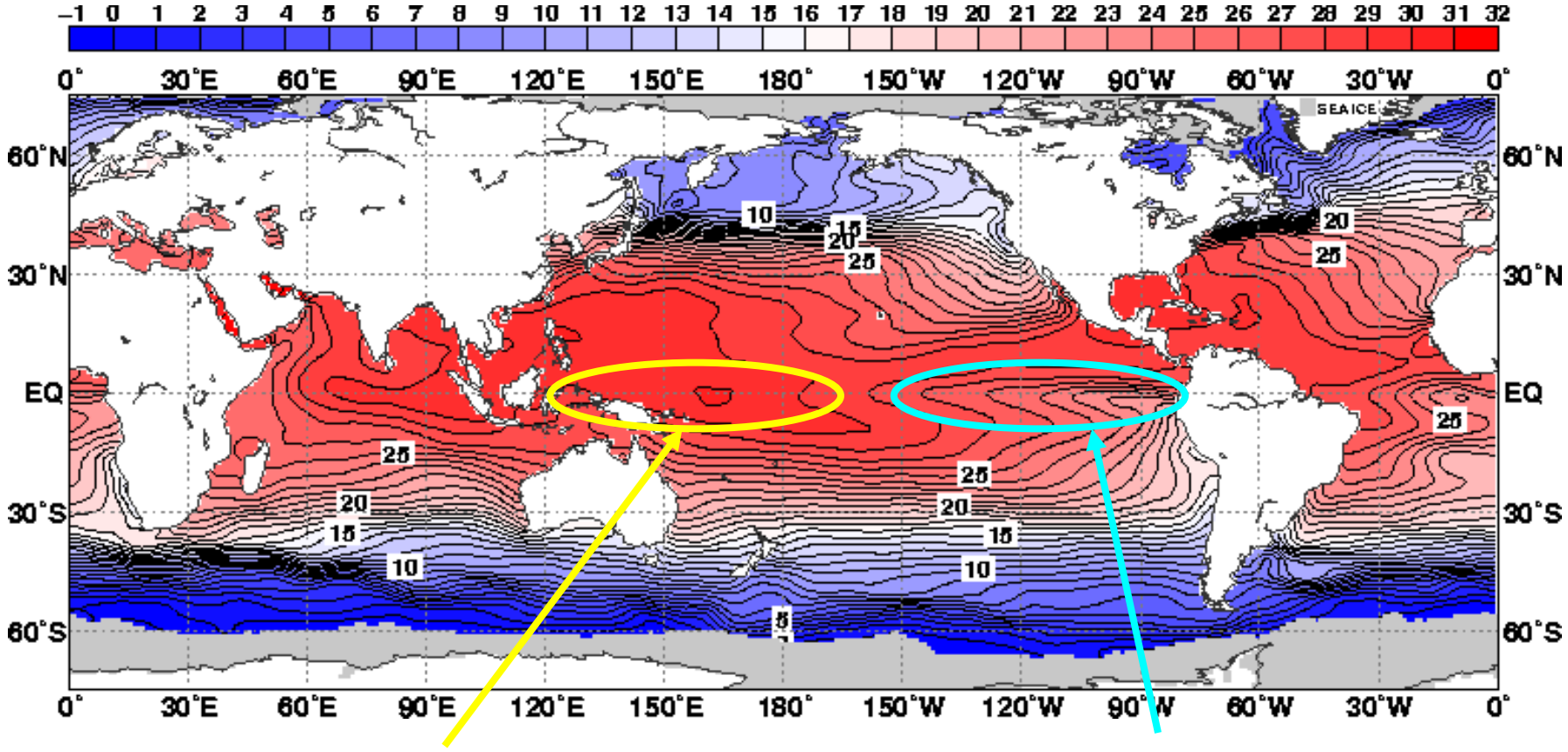

1-month mean sea surface temperature observed in July 2005 when the conditions in the equatorial Pacific Ocean stayed close to normal.

Atmosphere-ocean interaction during El Niño

Normal condition

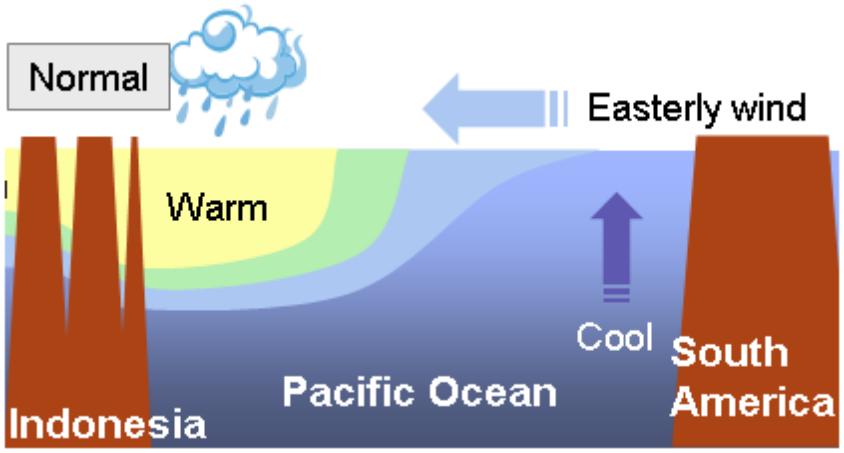

El Niño condition

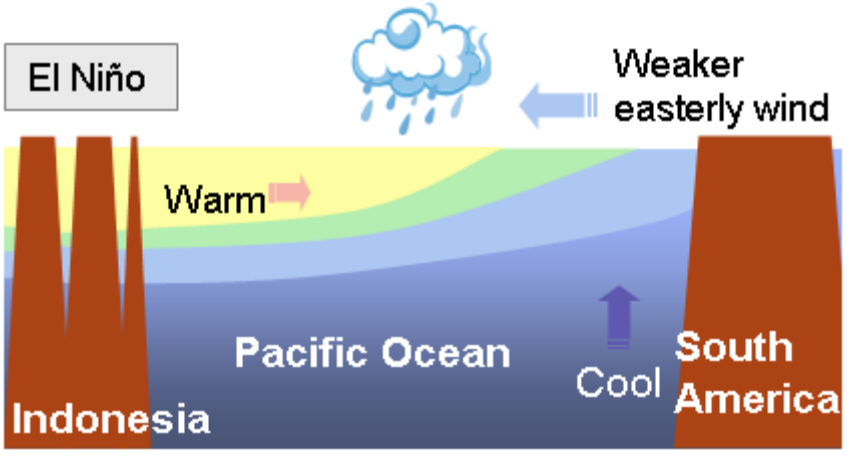

Warmer SST in the eastern Pacific → Eastward shift of active convection → Weaker easterly trade wind → Eastward shift of warm water → Warmer SST in the eastern Pacific

El Niño + Southern Oscillation = ENSO

Atmosphere-ocean interaction during La Niña

Normal condition

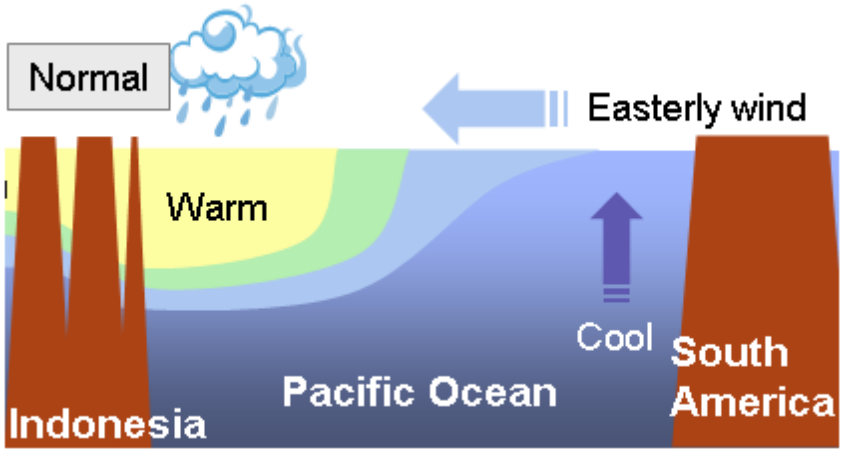

La Niña condition

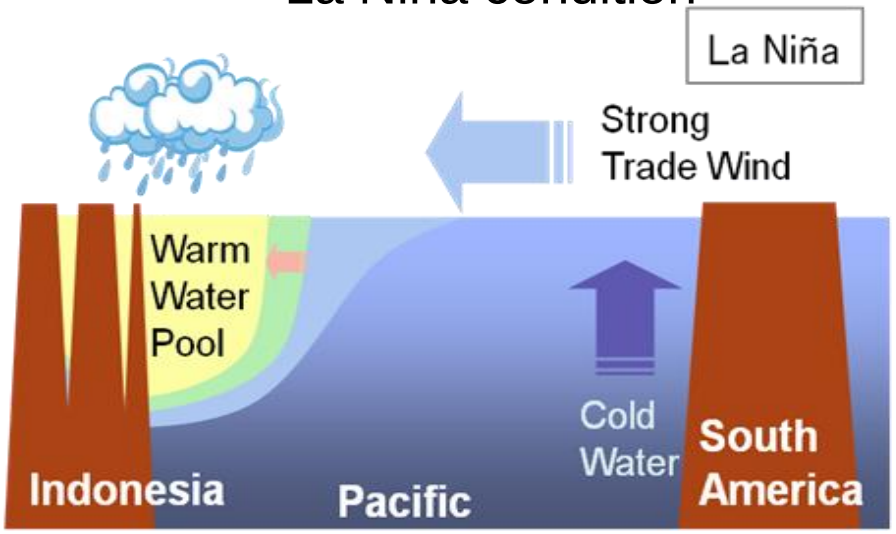

Colder SST in the eastern Pacific → Westward shift of active convection

↓

Stronger easterly trade wind → Westward shift of warm water

↑

Colder SST in the eastern Pacific

“El Niño”(“La Niña”) refers to:

気象庁
Japan Meteorological Agency

A large-scale ocean climate phenomenon linked to a periodic rise (fall) in sea surface temperatures across the central to east equatorial Pacific

El Niño (NOV1997)

La Niña (NOV1988)

sea surface temperature

departure from normal

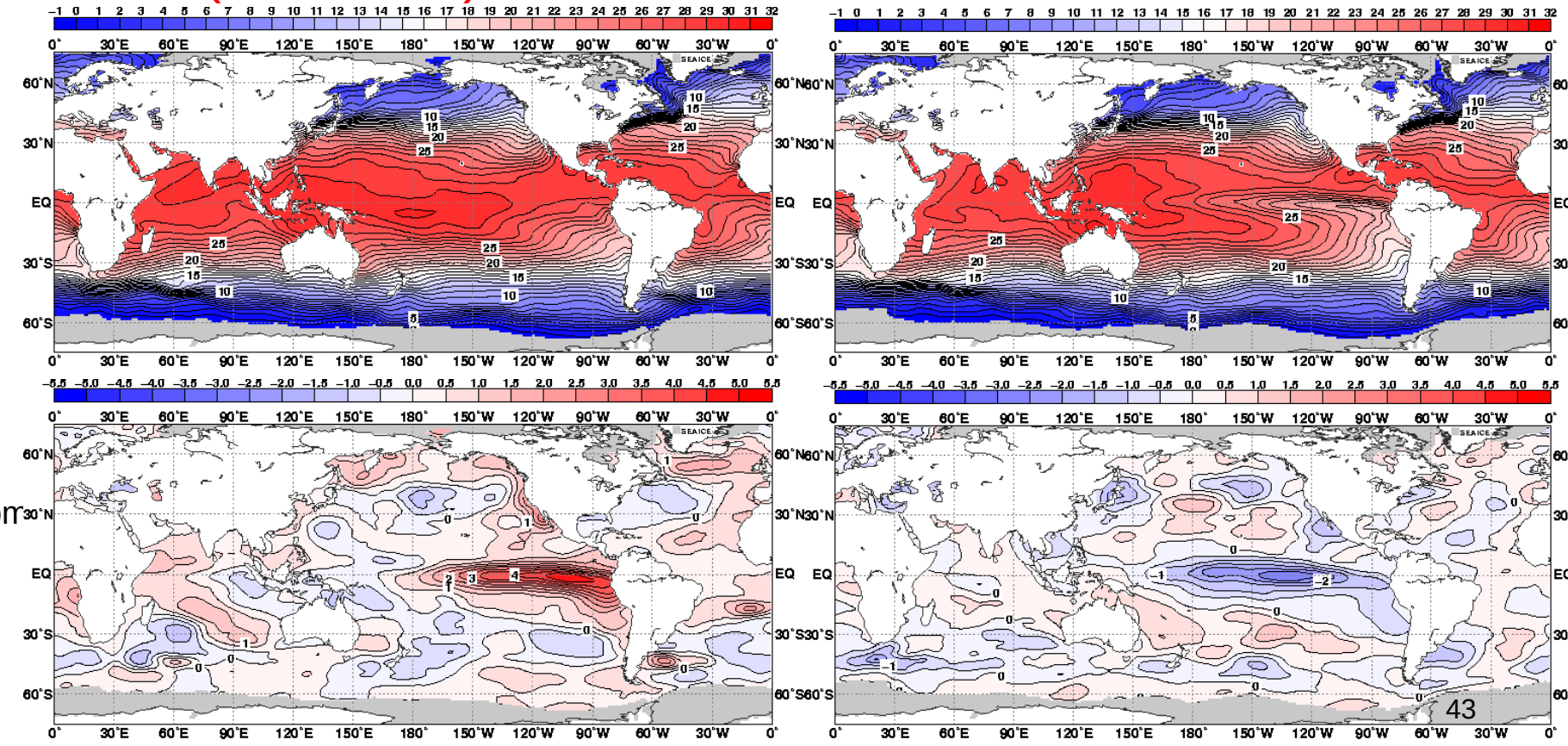

Look deep into the sea

SST anomaly in 27OCT1997

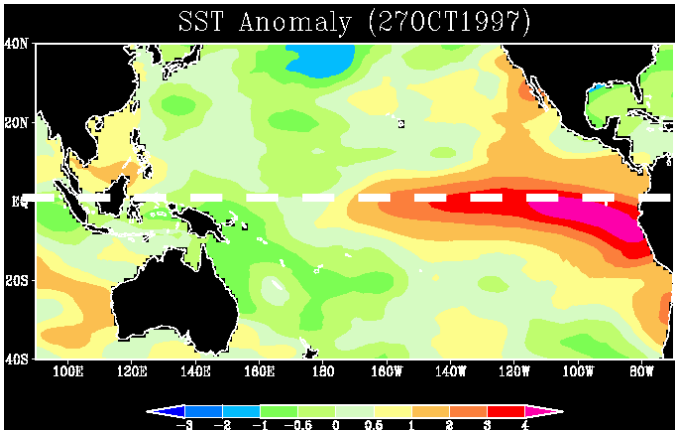

Subsurface temperatures in the equatorial Pacific in 1996/12-98/12

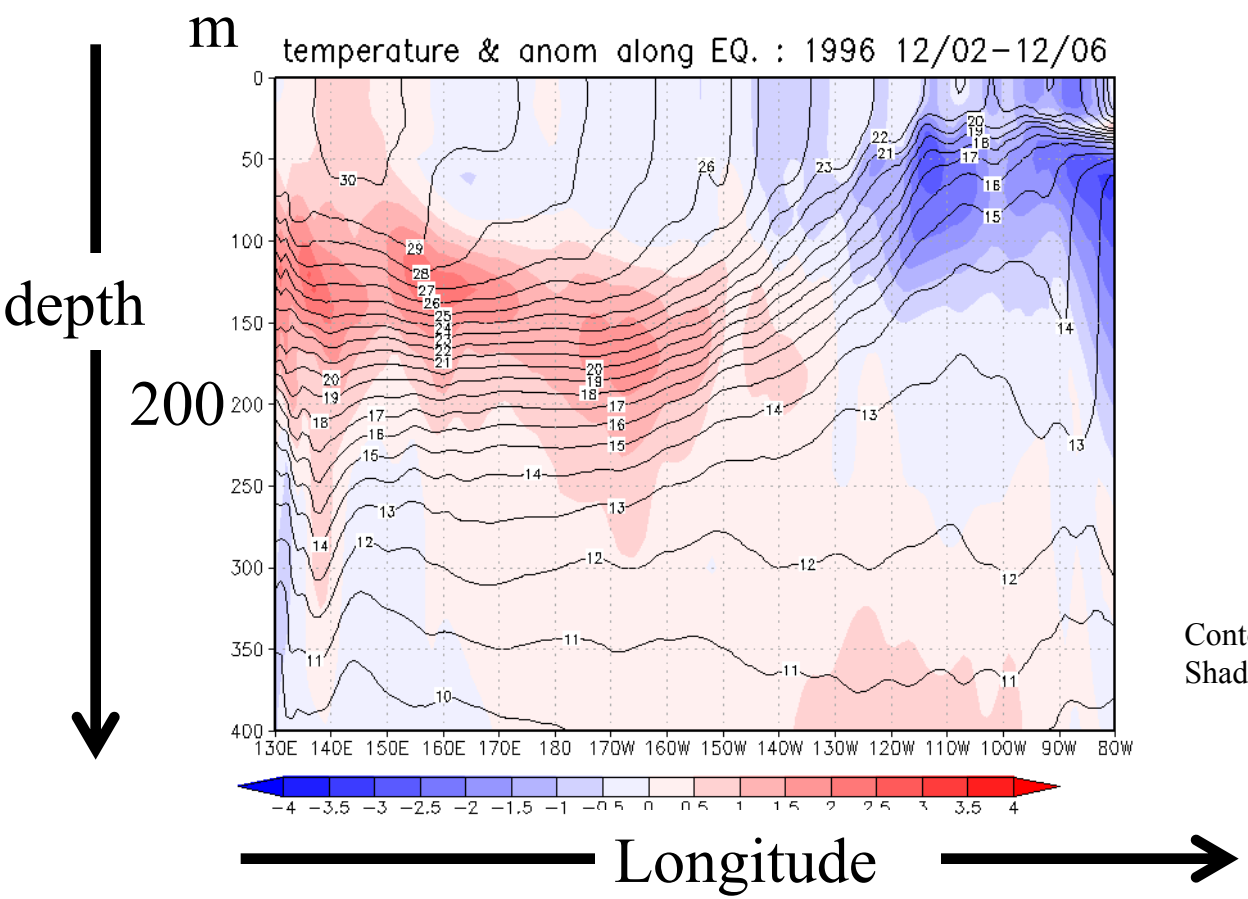

Contour: sea temperature(℃)
Shade:anomaly(℃)

1997/98 El Niño development and decay – hovmoeller plots

SST anomaly

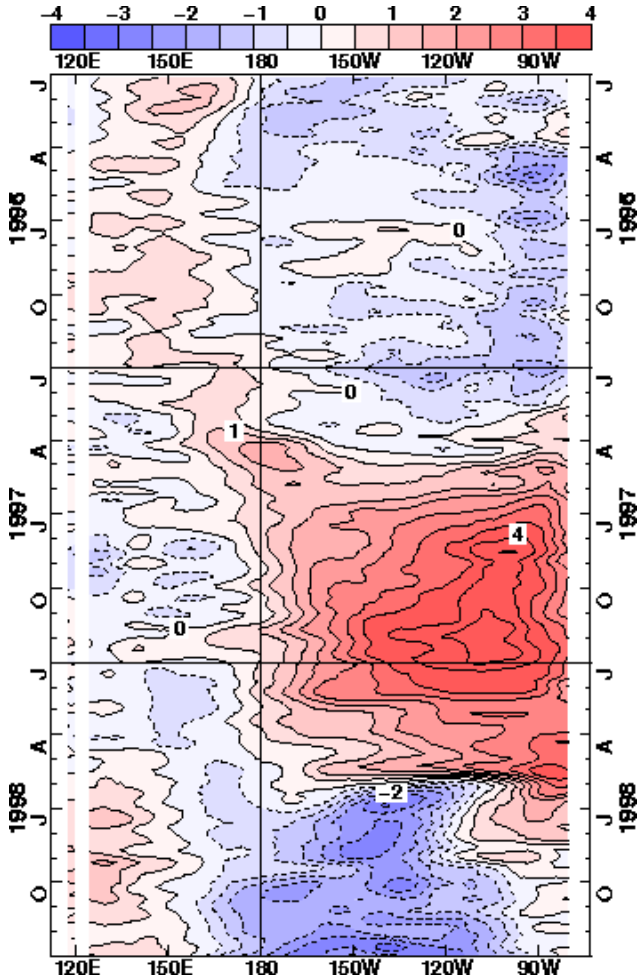

OHC anomaly

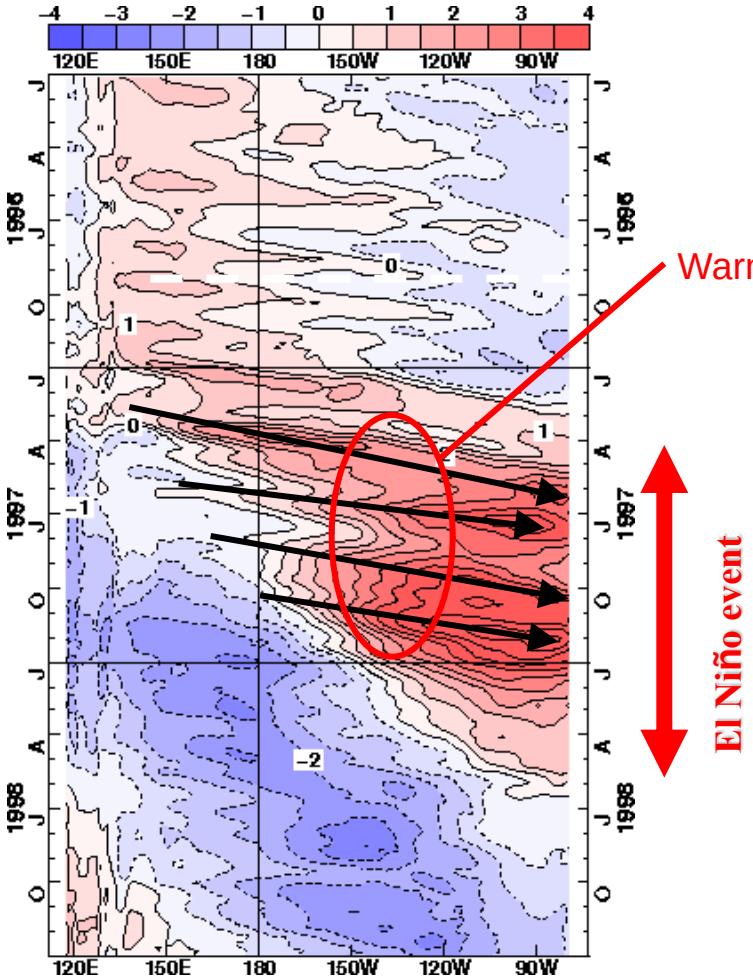

OHCs are defined as vertically averaged temperatures of top 300m.

Positive feedback

Hövmoeller (Longitude-time section) in equatorial Pacific

SST

OHC (Ocean Heat Content) anomalies

Wind stress

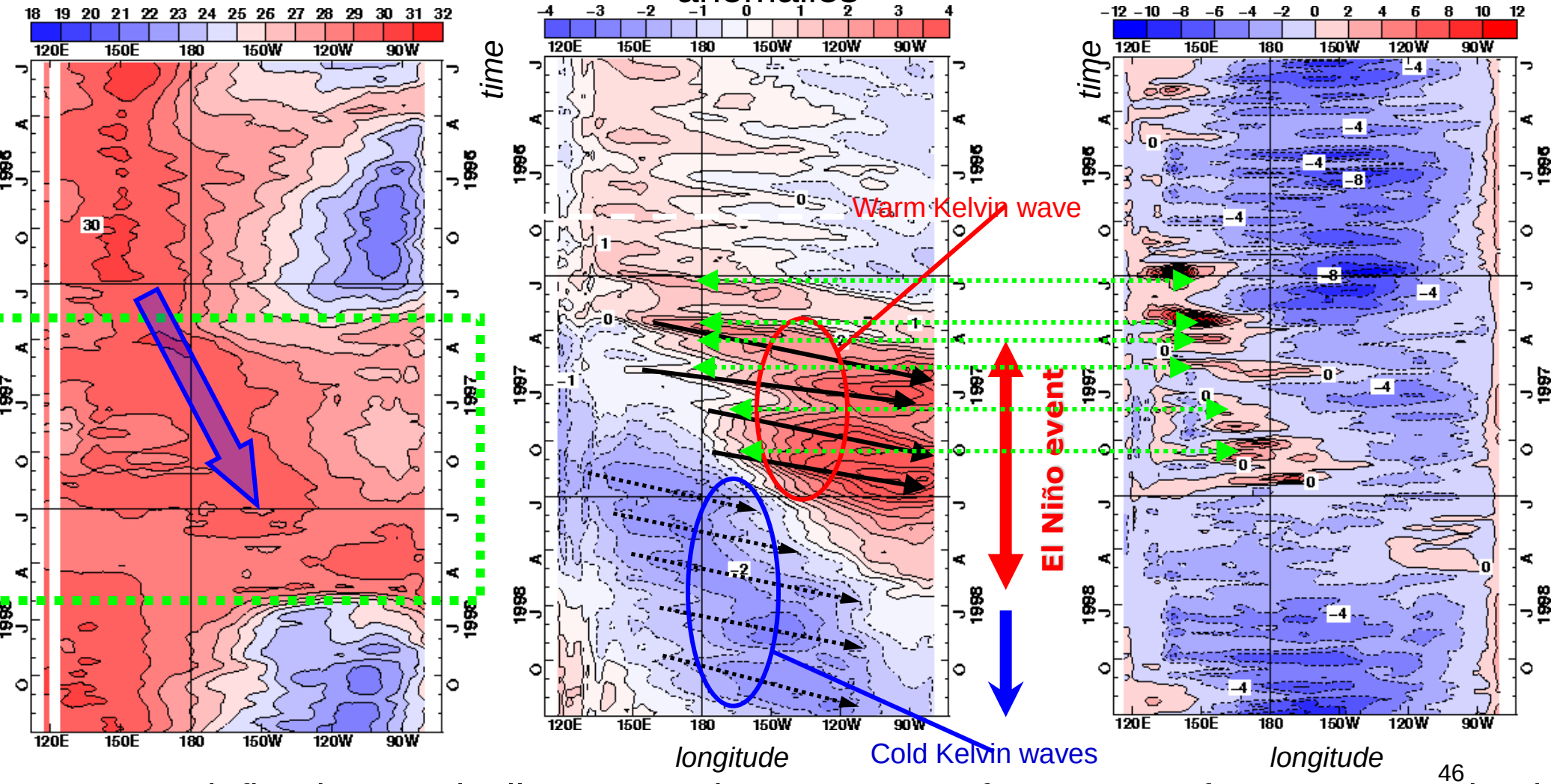

OHCs are defined as vertically averaged temperatures from sea surface to 300-m depth

ENSO is huge heat variation in the climate system

	Atmosphere	Ocean
Density	1.2-1.3kgm^{-3}	10^3kgm^{-3} ：atom. X 800
Mass(per 1 m^2)	（Top ～ Surface） 10^4kgm^{-2}	（Surface ～10m depth） 10^4kgm^{-2} ：Mass of the atmosphere is the same as that of ocean with 10m depth
Specific heat	10^3Jkg^{-1}K^{-1}	4×10^3Jkg^{-1}K^{-1} ：atom. X 4
Heat capacity (per 1 m^2)	（Top ～ Surface） 10^7JK^{-1}m^{-2}	（Surface ～2.5m depth） 10^7JK^{-1}m^{-2} ：Heat capacity of the atmosphere is the same as that of ocean with 2.5m depth

“1K in 250m depth ocean” is near equal to “100K in the atmosphere”

* from Gill 1982

Historical look at SST variations

5-month running mean SST departures from normal in the JMA's El Niño monitoring region for 1950-2015

red: El Niño period

blue: La Niña period

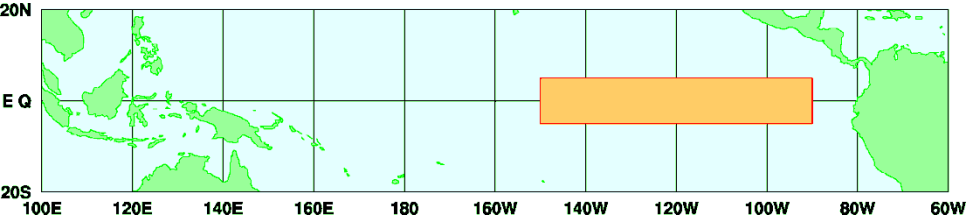

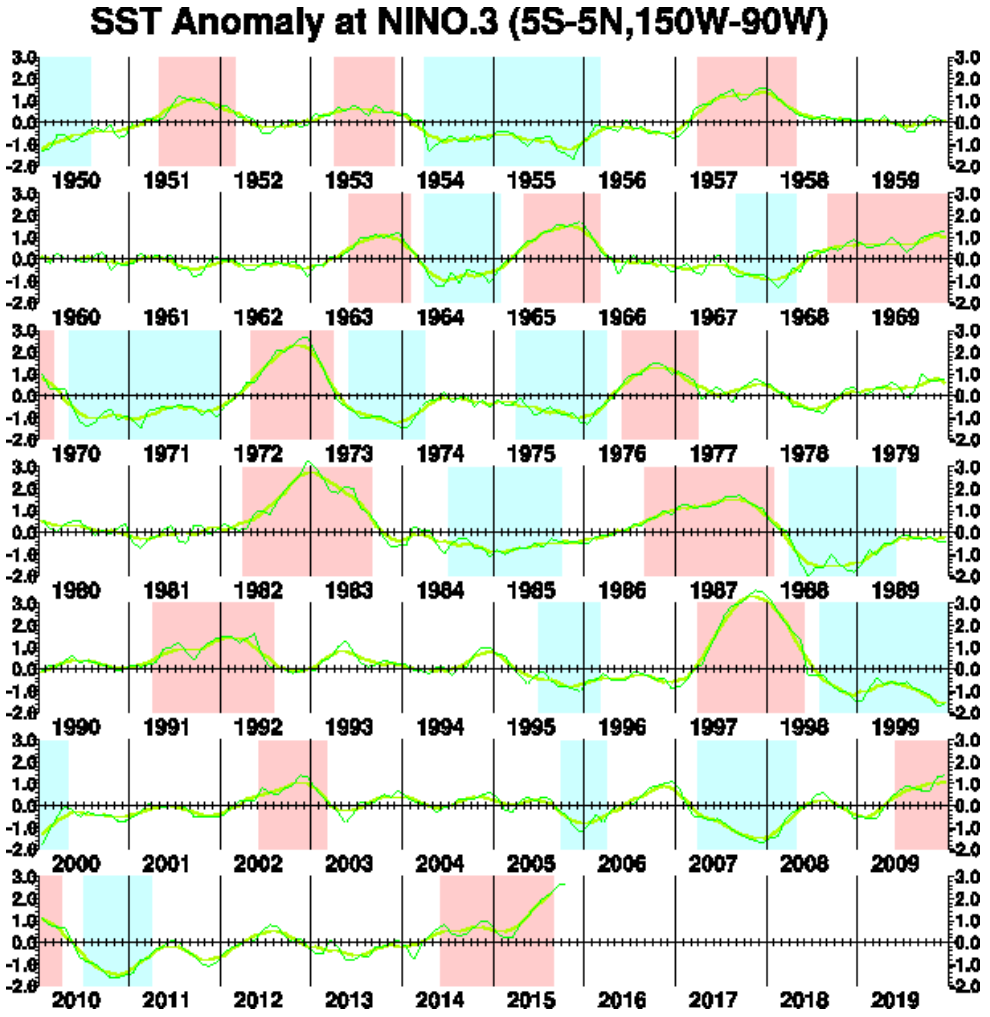

El Niño and La Niña impact on the world climate

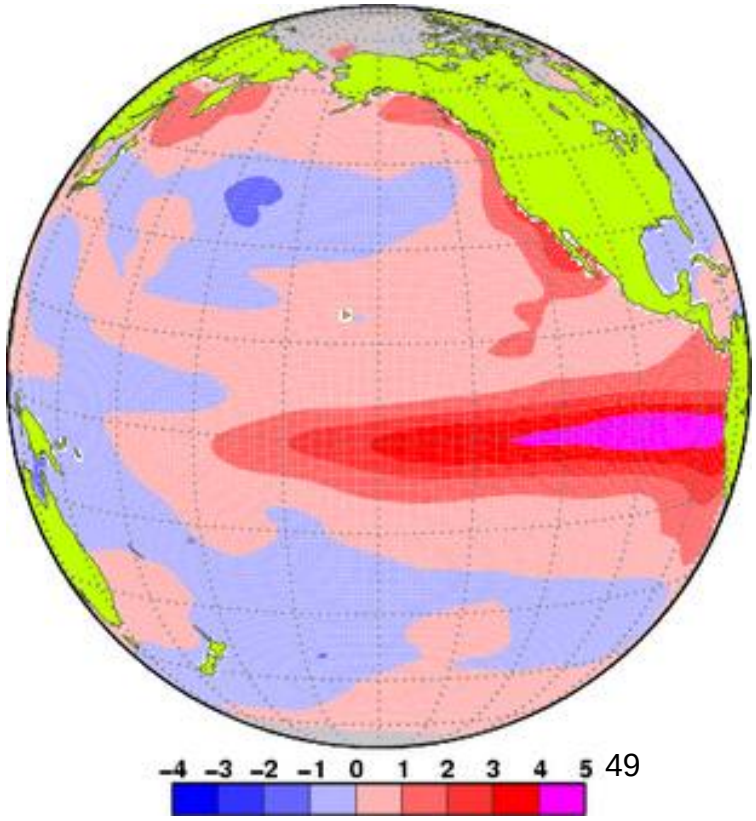

Walker Circulation along the equator during El Nino (lower panel) and La Nina (upper panel)

Webster and Chang 1988

La Nina

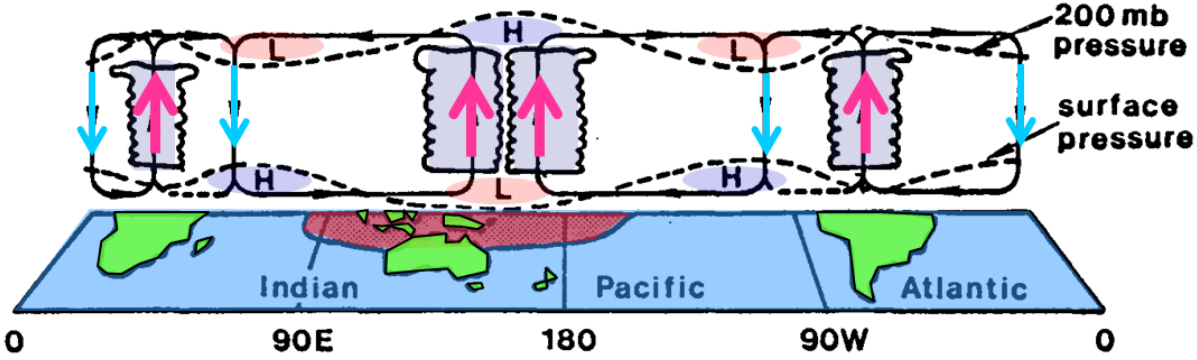

El Nino

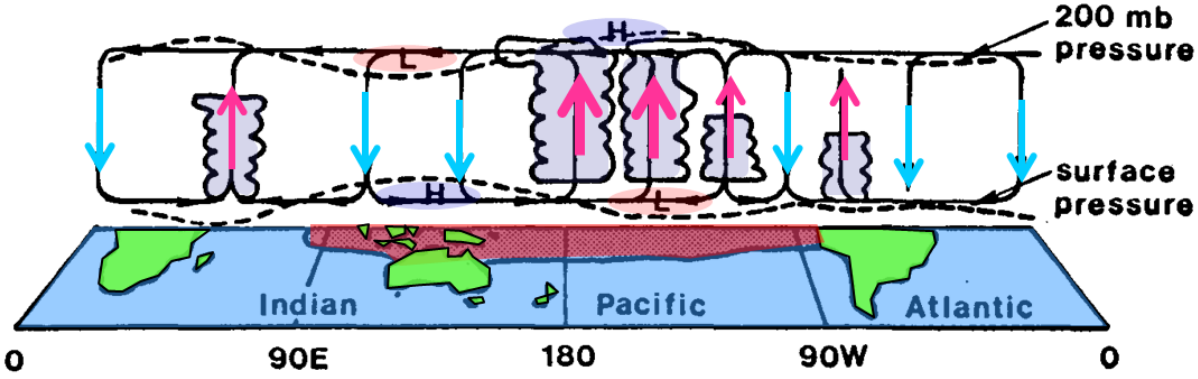

FIG. 1. Schematic view of the Walker Circulation along the equator during El Niño (lower panel) and La Niña (upper panel) periods that occur at the extremes of the Southern Oscillation. The shaded areas indicate sea surface temperatures warmer than 27°C and the dashed lines show relative horizontal pressure variations in the lower and upper troposphere. (From Webster, 1983)

Precipitation in 1997/98 winter(DJF)

Upper : 1997/98, lower : normal

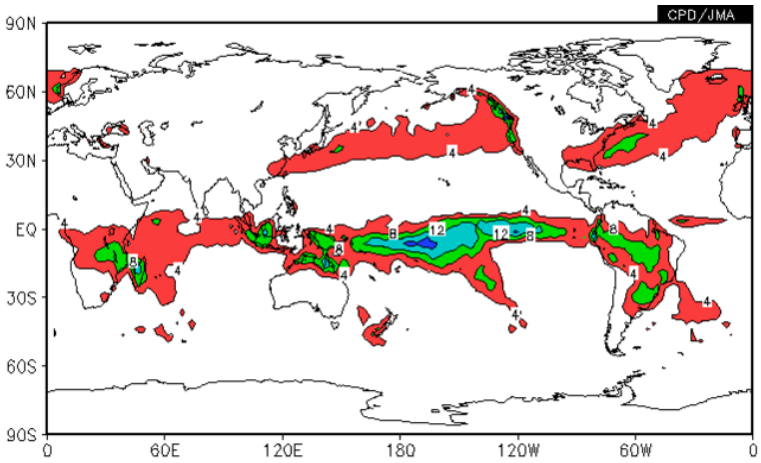

mm/day

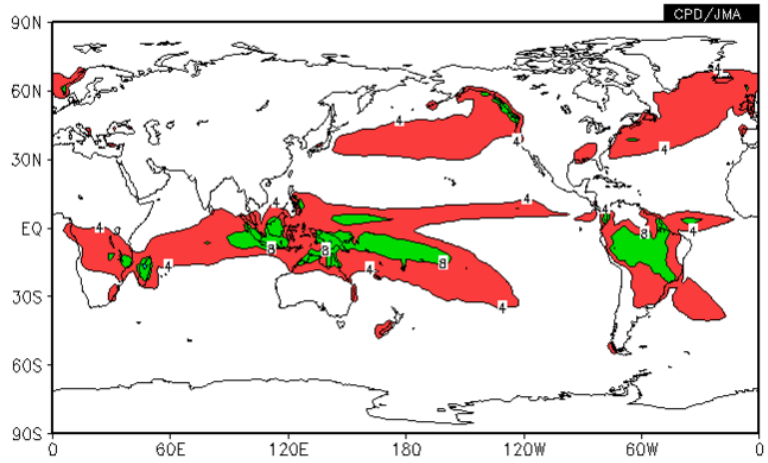

Anomalies in 1997/98

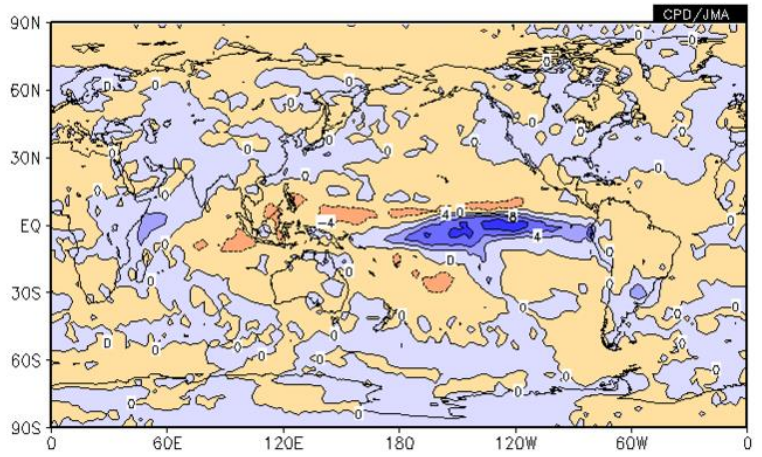

mm/day

Atmospheric heating by condensation

Latent heat

: $2.5 \times 10^6 Jkg^{-1}$

Heat capacity of the atmosphere (per $1m^2$)

: $10^7 JK^{-1}m^{-2}$

→

4kg/day(=4mm/day) condensation heats the atmosphere 1K/day

Statistical relationship between NINO.3 and atmospheric circulation fields in DJF

SST

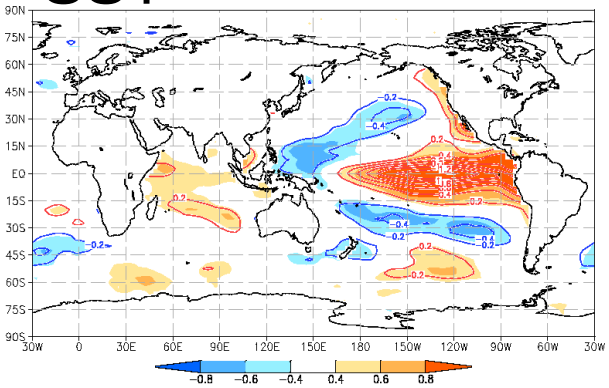

OLR

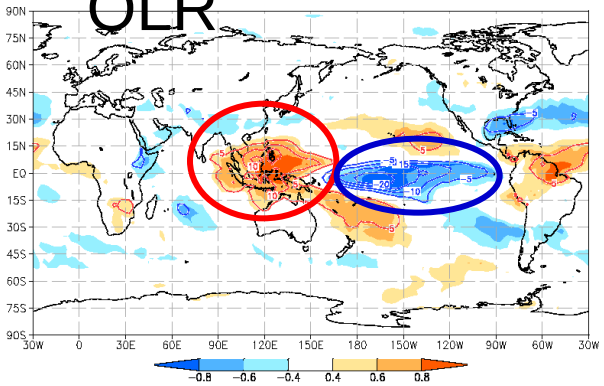

Sea Level Pressure

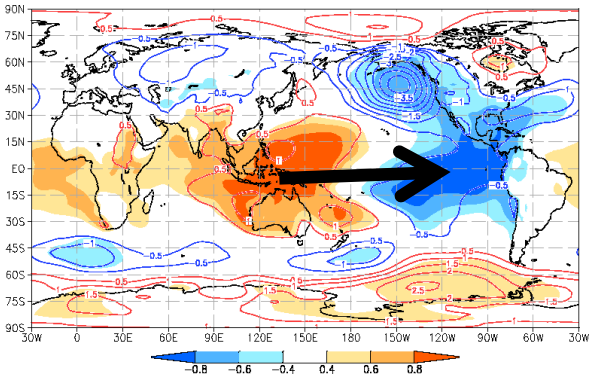

Velocity Potential at 200hPa

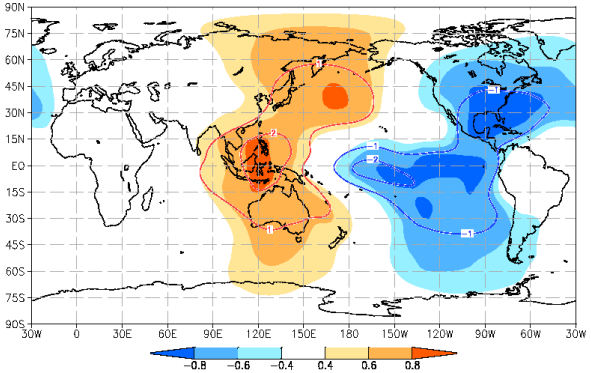

Stream Function at 850hPa

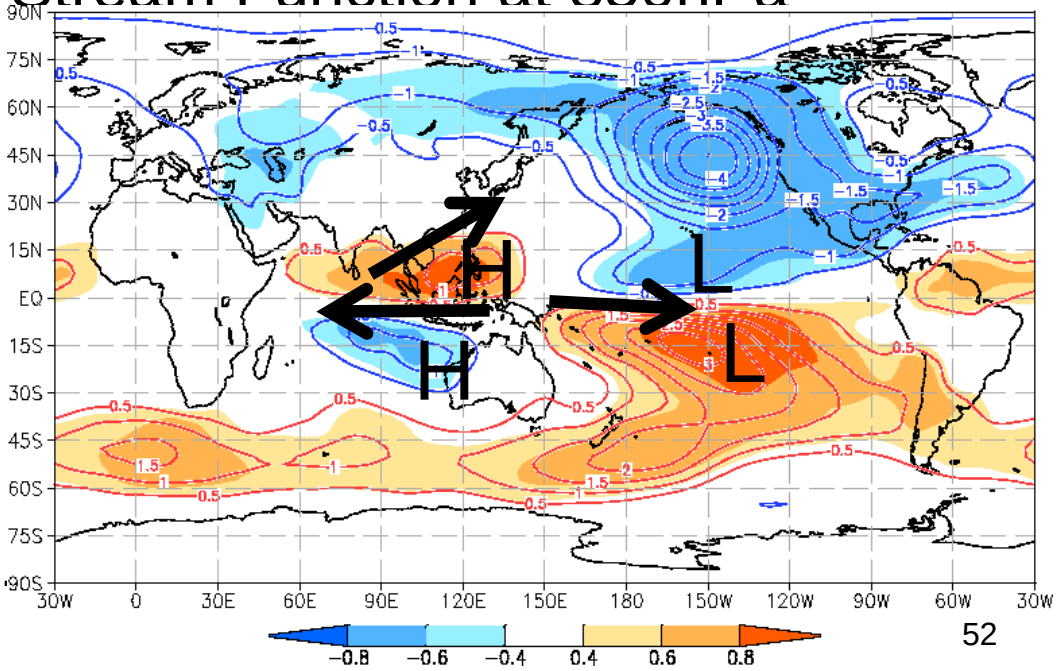

Contours show atmospheric circulation anomalies when normalized NINO.3 is+1.0
Shadings show correlation coefficients.

Some simple solutions for heat-induced tropical circulation

Quarterly Journal of the Royal Meteorological Society
Volume 106, Issue 449, July 1980, Pages: 447–462, A. E. Gill

Symmetric Heating Anomaly about the equator

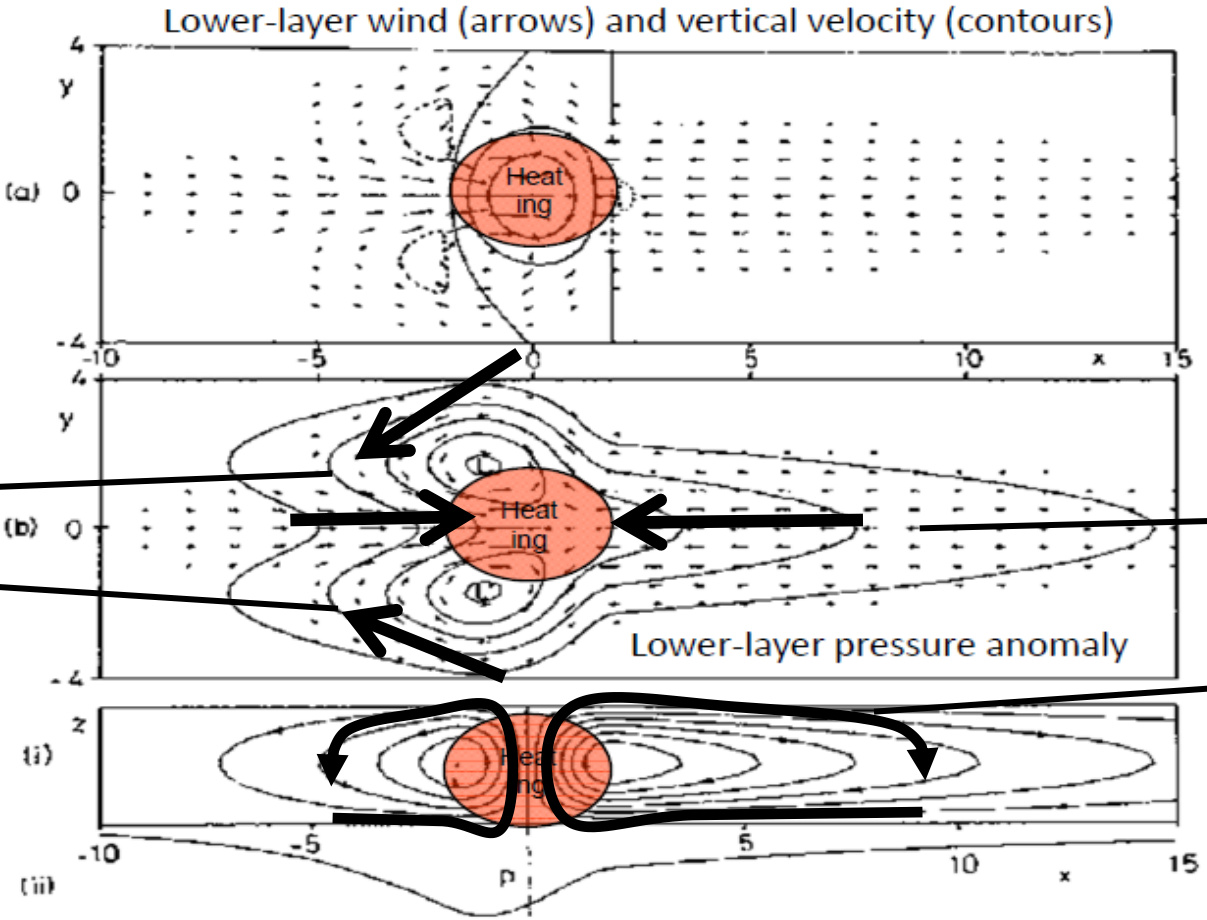

Rossby wave

Kelvin wave

Walker circulation

Global atmospheric response to condensation heating in the central equatorial Pacific

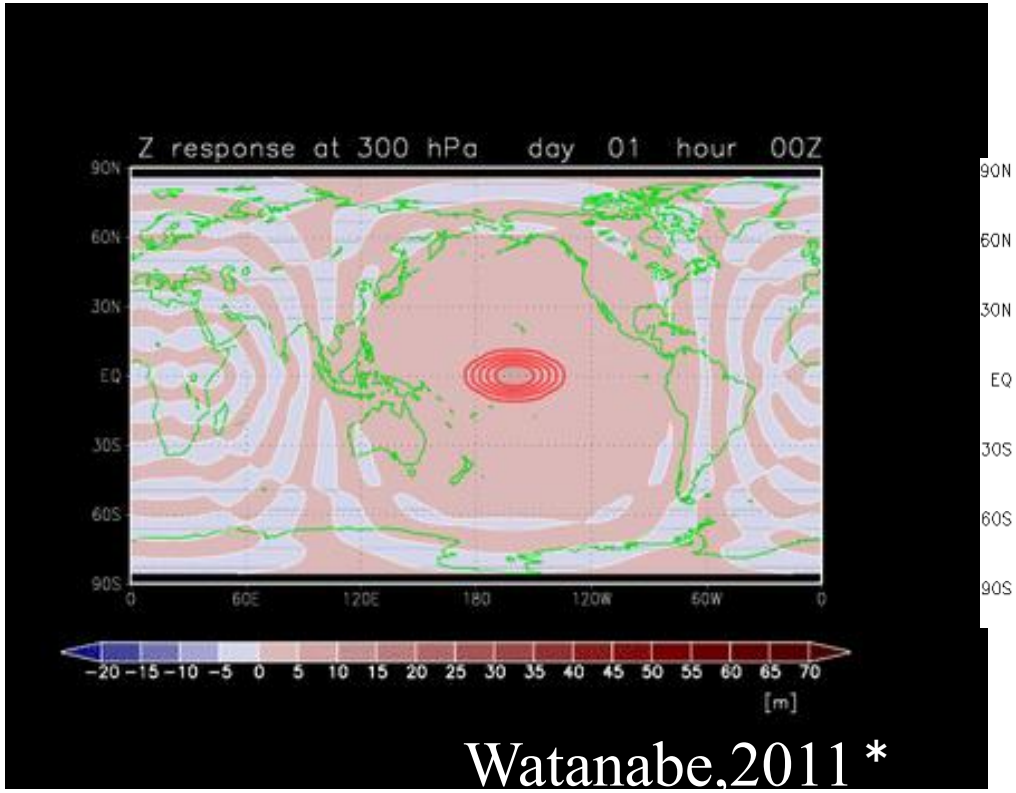

Watanabe,2011 *

LBM simulation of response to condensation heating in the central equatorial Pacific.

Geopotential height at 300hPa

* from his presentation in "Twelfth Joint Meeting for the Seasonal Prediction of the East Asian Winter Monsoon"

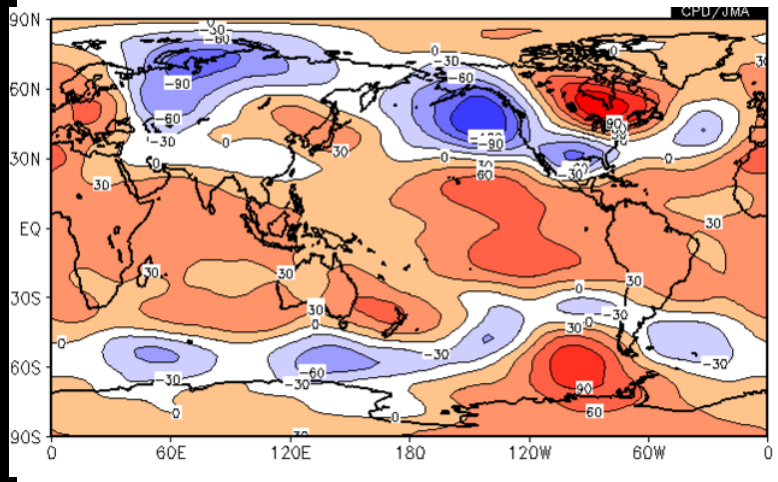

Geopotential height anomalies at 300hPa in 1997/98 winter (DJF).

Localized condensation heating in the tropics force stationary Rossby waves which propagate to the mid-high latitudes.

Climate tendencies during El Nino/La Nina

Warm Cold Wet Dry

EL in boreal summer

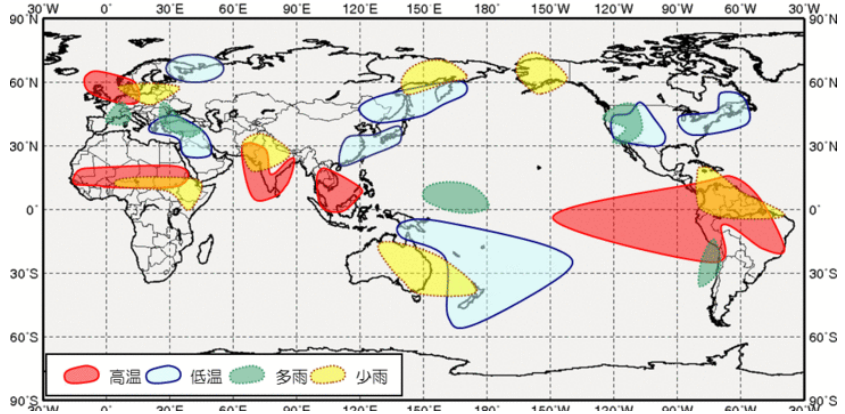

EL in boreal winter

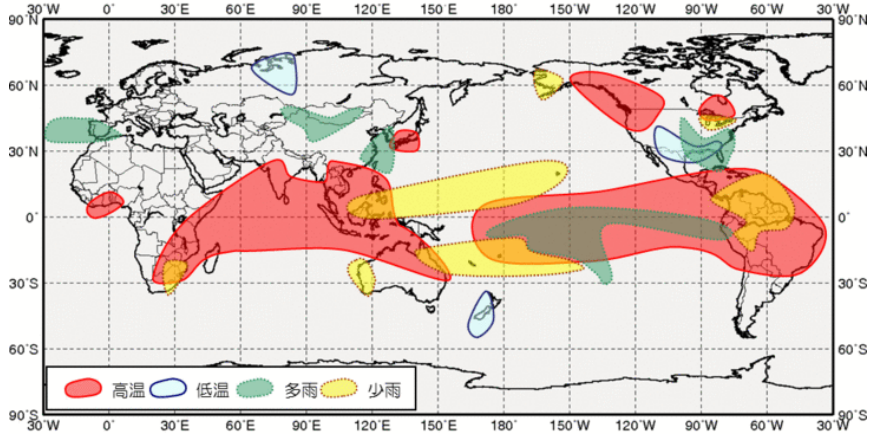

LA in boreal summer

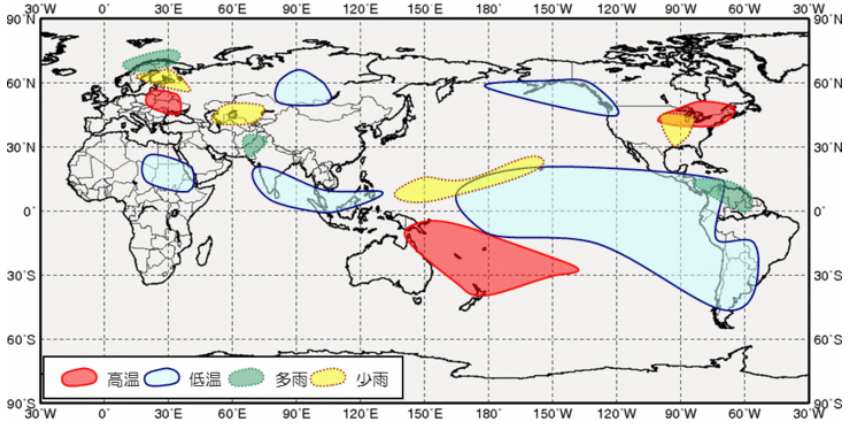

LA in boreal winter

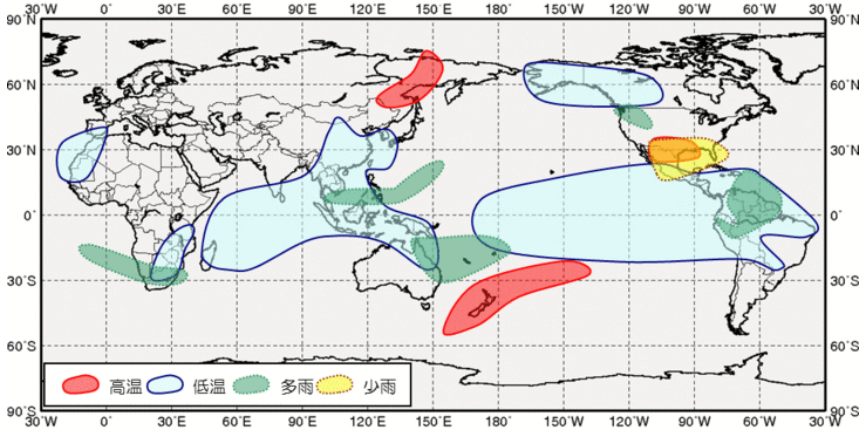

The maps show the regions where climate tendencies observed during El Niño/La niña episodes are statistically significant in boreal summer/winter.

Example of ENSO prediction

Initial :1997.8.29,　Valid time : 1997.12～1998.2

OBS.　　**Prediction**

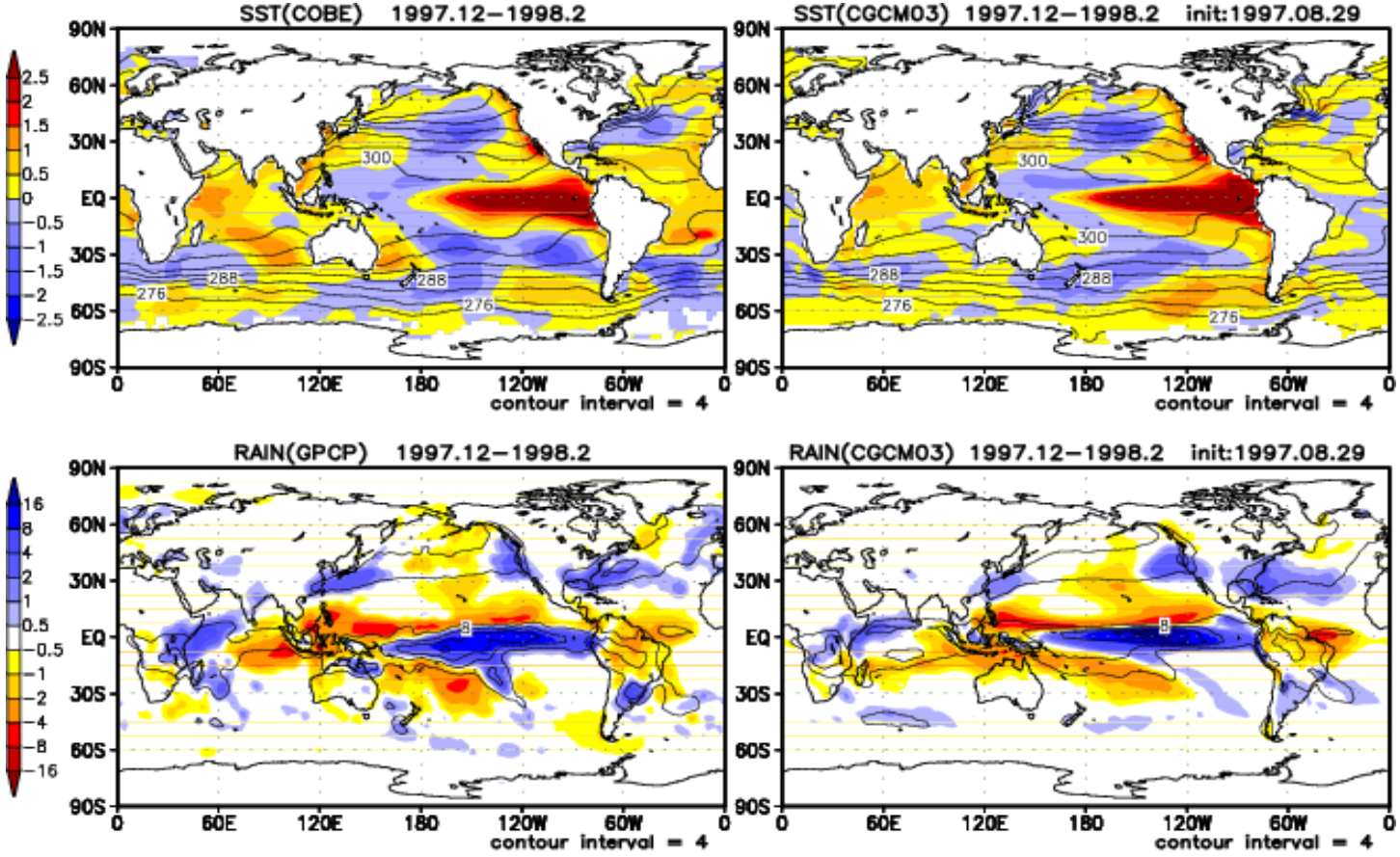

Contour : SST

Shade: SST anomaly

Contour : Precipitation

Shade: Precipitation anomaly

Current conditions and outlook

SST anomalies in 2015 ASO

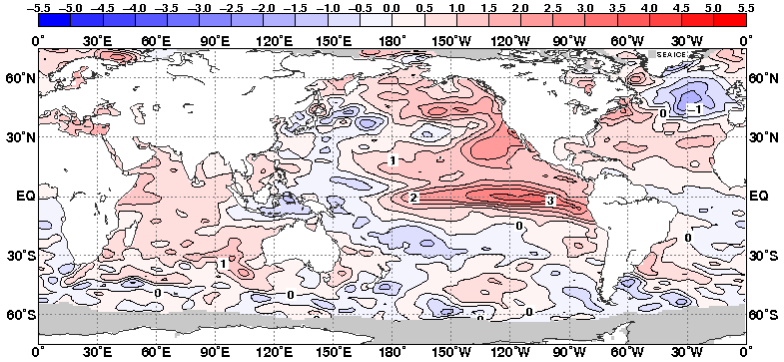

Outlook of the SST deviation for NINO.3 by the El Niño prediction model.

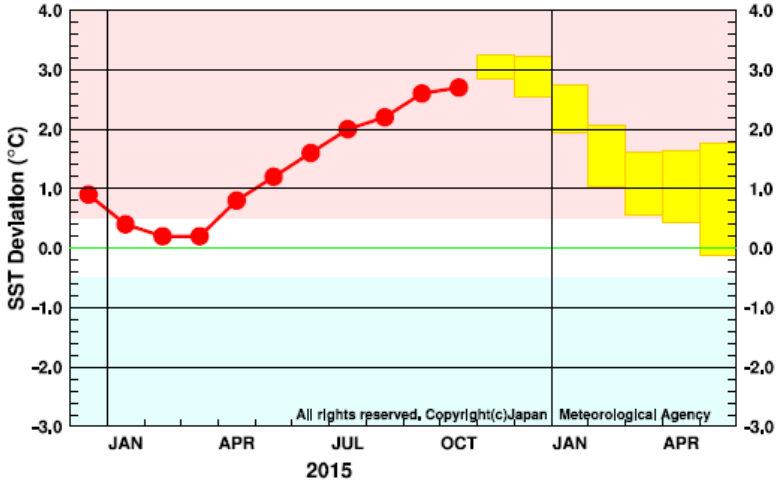

Issued on 10th NOV. 2015

2015/16 DJF Prediction by the JMA CGCM2. Init:2015.10.08

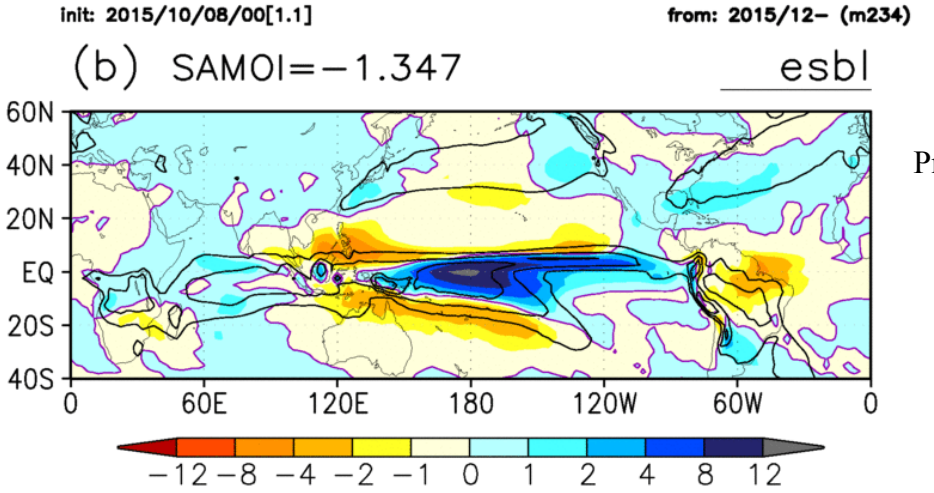

Precipitation

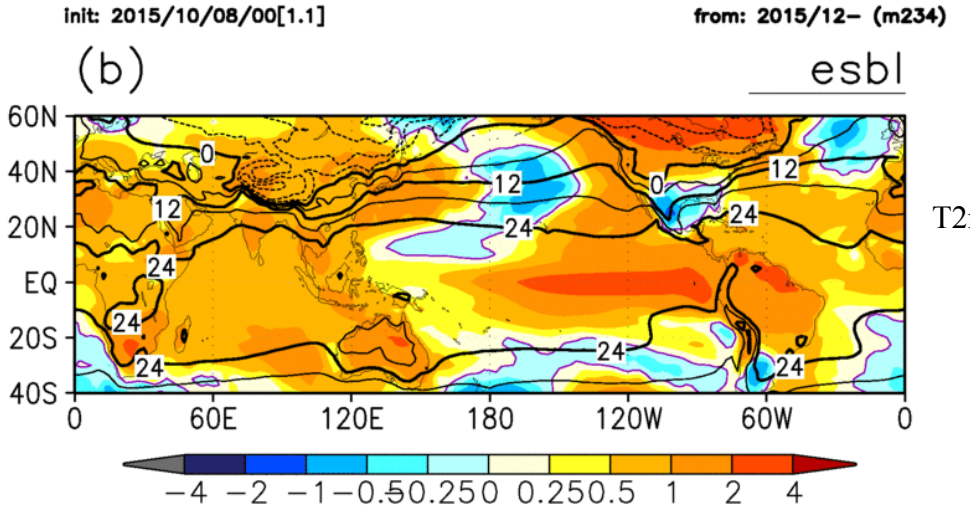

T2m

2015/16 DJF Prediction by the JMA CGCM2. Init:2015.10.08

Wind & stream function at 850hPa

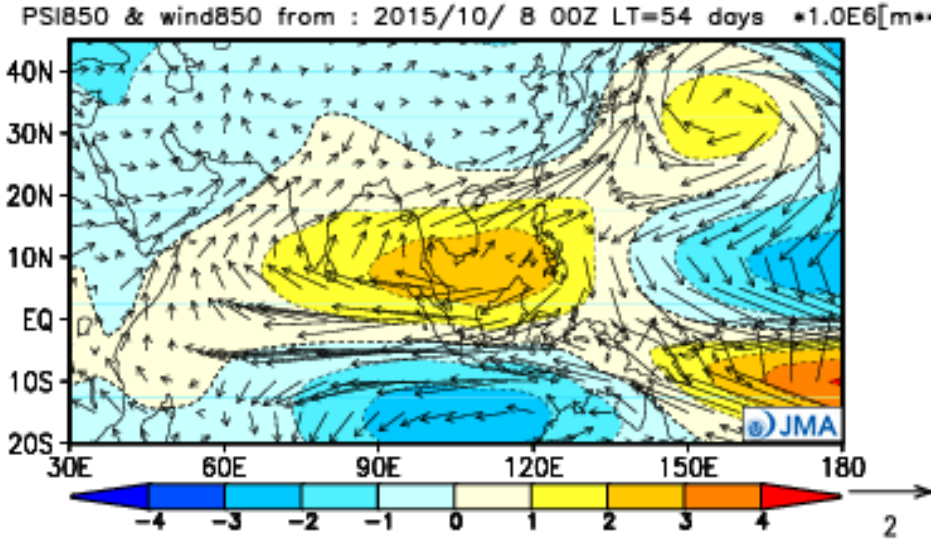

Precipitation

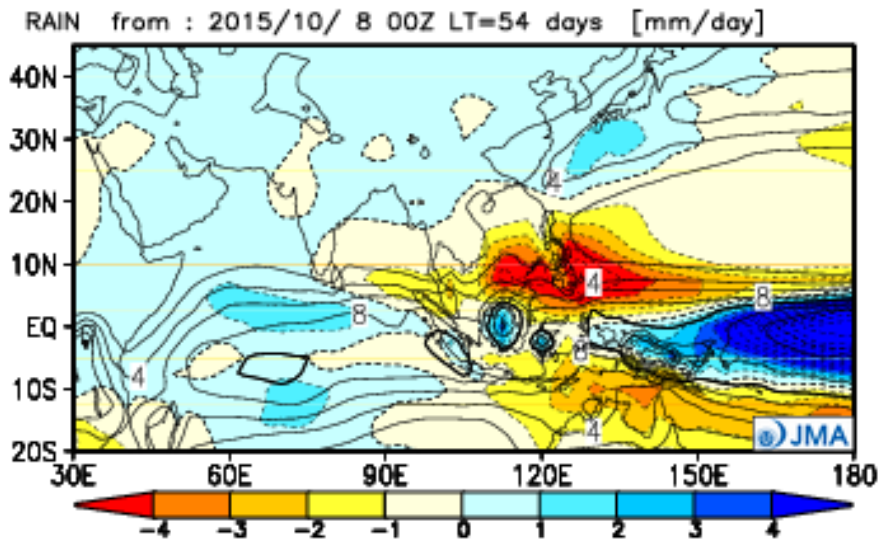

El Niño Modoki & CP El Niño

Nature,2009

The El Niño with a difference

Karumuri Ashok and Toshio Yamagata

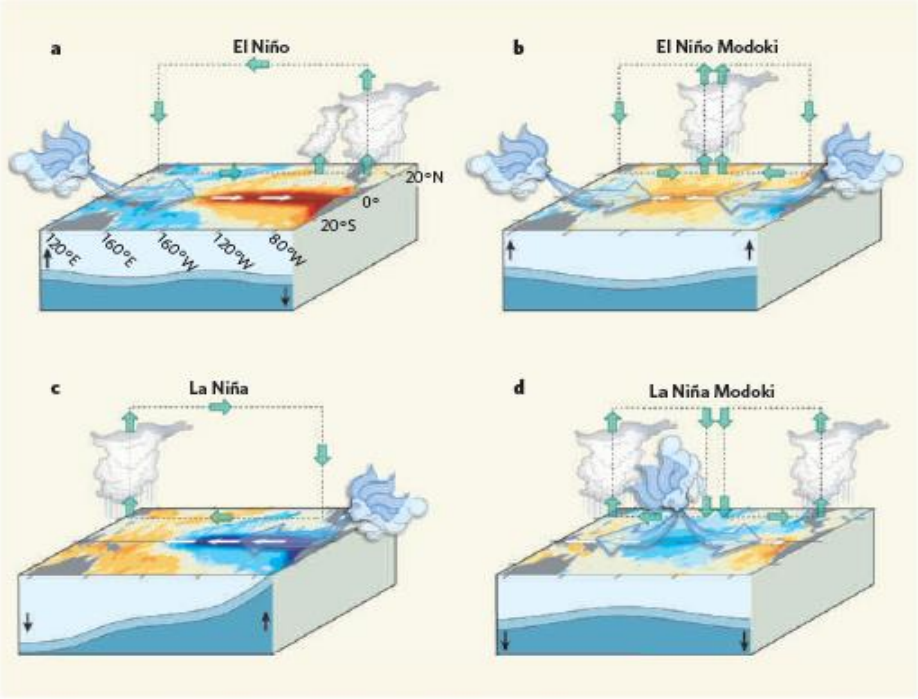

Figure 2 | Anomalous conditions in the tropical Pacific. **a**, An El Niño event is produced when the easterly winds weaken; sometimes, in the west, westerlies prevail. This condition is categorized by warmer than normal sea surface temperatures (SSTs) in the east of the ocean, and is associated with alterations in the thermocline and in the atmospheric circulation that make the east wetter and the west drier. **b**, An El Niño Modoki event is an anomalous condition of a distinctly different kind. The warmest SSTs occur in the central Pacific, flanked by colder waters to the east and west, and are associated with distinct patterns of atmospheric convection. **c**, **d**, The opposite (La Niña) phases of the El Niño and El Niño Modoki respectively. Yeh *et al.*[3] argue that the increasing frequency of the Modoki condition is due to anthropogenic warming, and that these events in the central Pacific will occur more frequently if global warming increases.

Nature,2009

El Niño in a changing climate

Sang-Wook Yeh[1], Jong-Seong Kug[1], Boris Dewitte[2], Min-Ho Kwon[3], Ben P. Kirtman[4] & Fei-Fei Jin

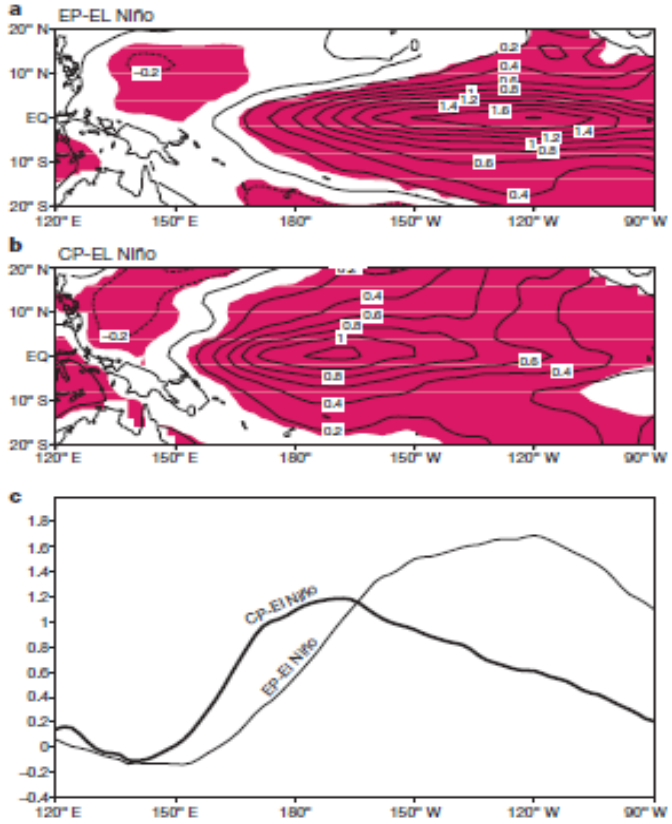

Figure 1 | Deviations of mean SST for the two characteristics of El Niño from the 1854–2006 climatology. **a**, The EP-El Niño; **b**, the CP-El Niño. The contour interval is 0.2 °C and shading denotes a statistical confidence at 95% confidence level based on a Student's *t*-test. **c**, The zonal structure for the composite EP-El Niño (thin line) and CP-El Niño (thick line) averaged over 2 °N to 2 °S.

ENSO-Monsoon relation

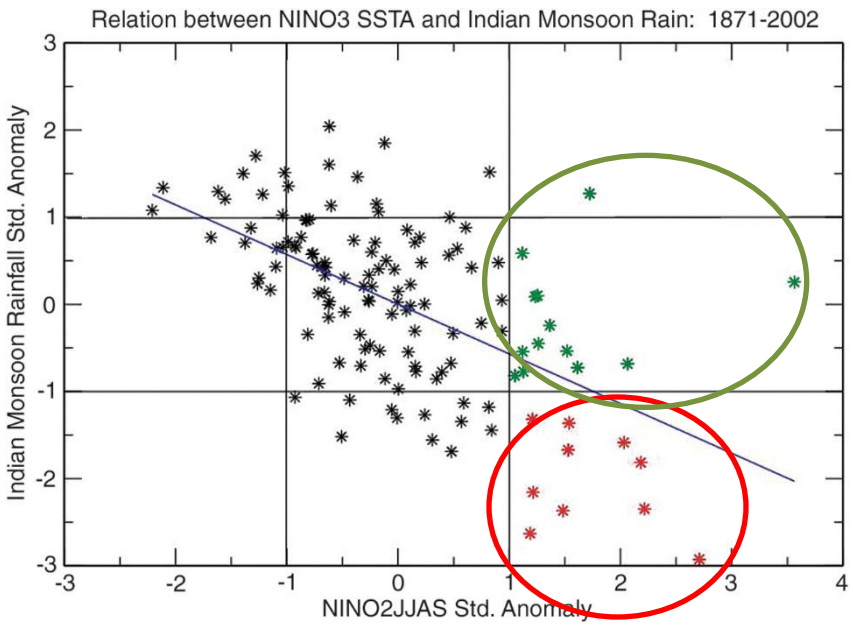

Plot of standardized, all-India summer [June to September (JJAS)] monsoon rainfall and summer NINO3 anomaly index. Severe drought and drought-free years during El Niño events (standardized NINO3 anomalies > 1) are shown in red and green, respectively.

From Kumar et al.(2006)

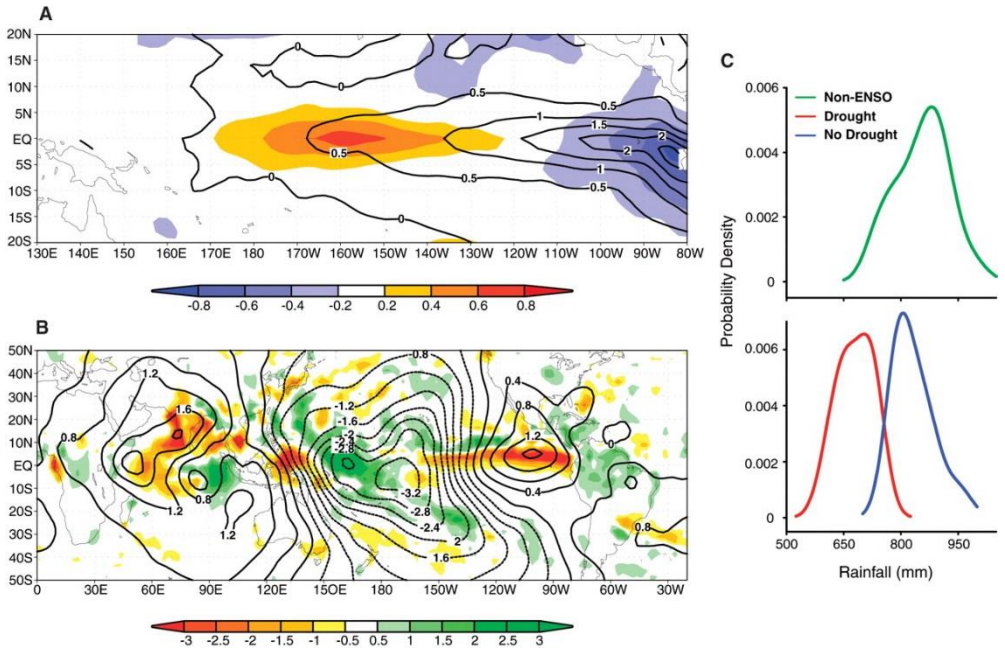

(**A**) Composite SST difference pattern between severe drought (shaded) and drought-free El Niño years. Composite SST anomaly patterns of drought-free years are shown as contours. (**B**) Composite difference pattern between severe drought and drought-free years of velocity potential (contours) and rainfall (shaded). (**C**) PDF of all-India summer monsoon rainfall from severe-drought (red curve) and drought-free (blue curve) years associated with El Nino occurrence and from the non-ENSO years (green curve). SST and velocity potential composite differences are based on 1950 to 2004, rainfall composites are based on 1979 to 2004, and PDFs are based on 1873 to 2004.

A dipole mode in the tropical Indian Ocean

N. H. Saji*, B. N. Goswami†, P. N. Vinayachandran* & T. Yamagata*‡

Saji et al., Nature 1999

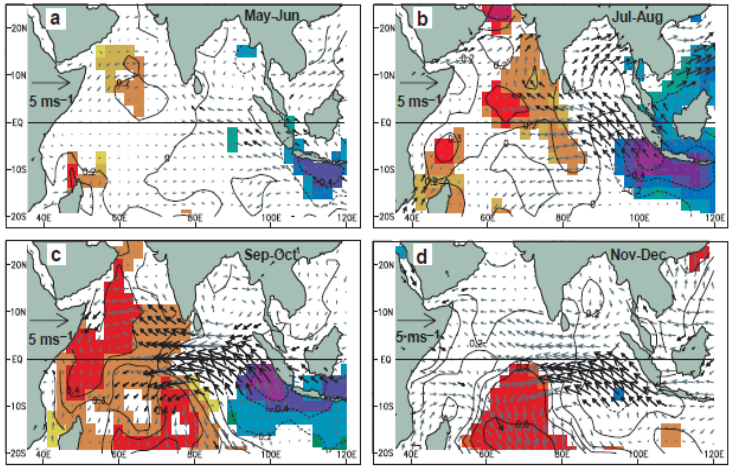

Figure 2 A composite dipole mode event. **a**–**d**, Evolution of composite SST and surface wind anomalies from May–June (**a**) to Nov–Dec (**d**). The statistical significance of the analysed anomalies were estimated by the two-tailed *t*-test. Anomalies of SSTs and winds exceeding 90% significance are indicated by shading and bold arrows, respectively.

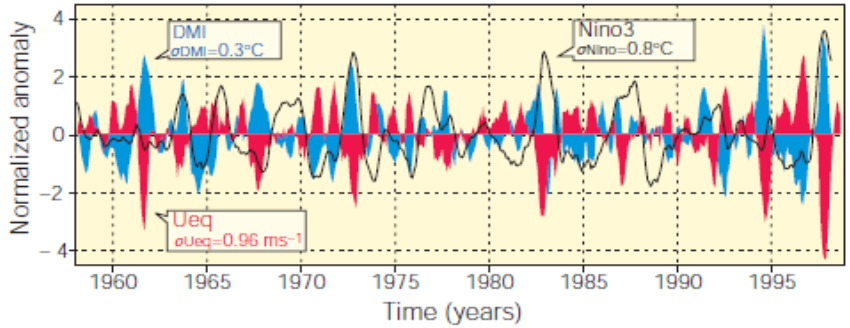

Figure 1 Dipole mode and El Niño events since 1958. Plotted in blue, the dipole mode index (DMI) exhibits a pattern of evolution distinctly different from that of the El Niño, which is represented by the Nino3 sea surface temperature (SST) anomalies (black line). On the other hand, equatorial zonal wind anomalies U_{eq} (plotted in red) coevolves with the DMI. All the three time series have been normalized by their respective standard deviations. We have removed variability with periods of 7 years or longer, based on harmonic analysis, from all the data sets used in this analysis. In addition, we have smoothed the time series using a 5-month running mean.

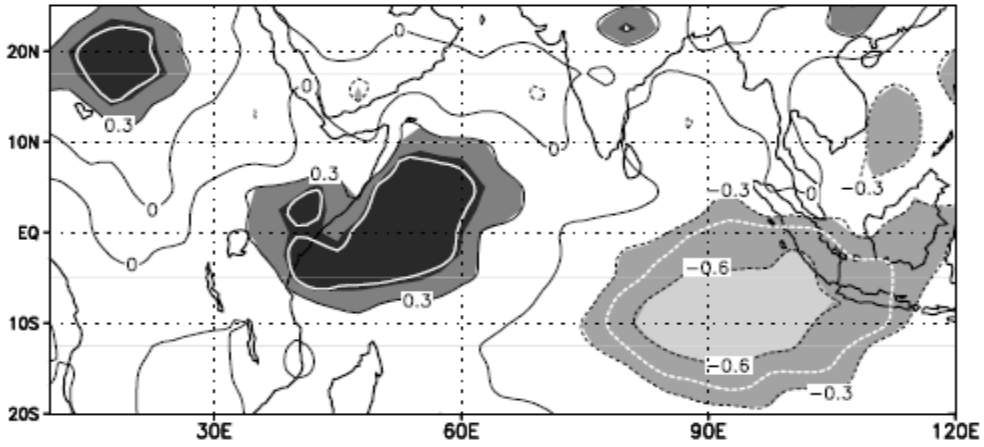

Figure 4 Rainfall shifts northwest of the OTCZ during dipole mode events. The map correlates the DMI and rainfall to illustrate these shifts. The areas within the white curve exceed the 90% level of confidence for non-zero correlation (using a two-tailed *t*-test).

Vol. 25: 151–169, 2003 | CLIMATE RESEARCH Clim Res | Published December 5

Possible impacts of Indian Ocean Dipole mode events on global climate

N. H. Saji[1,3,*], T. Yamagata[1,2]

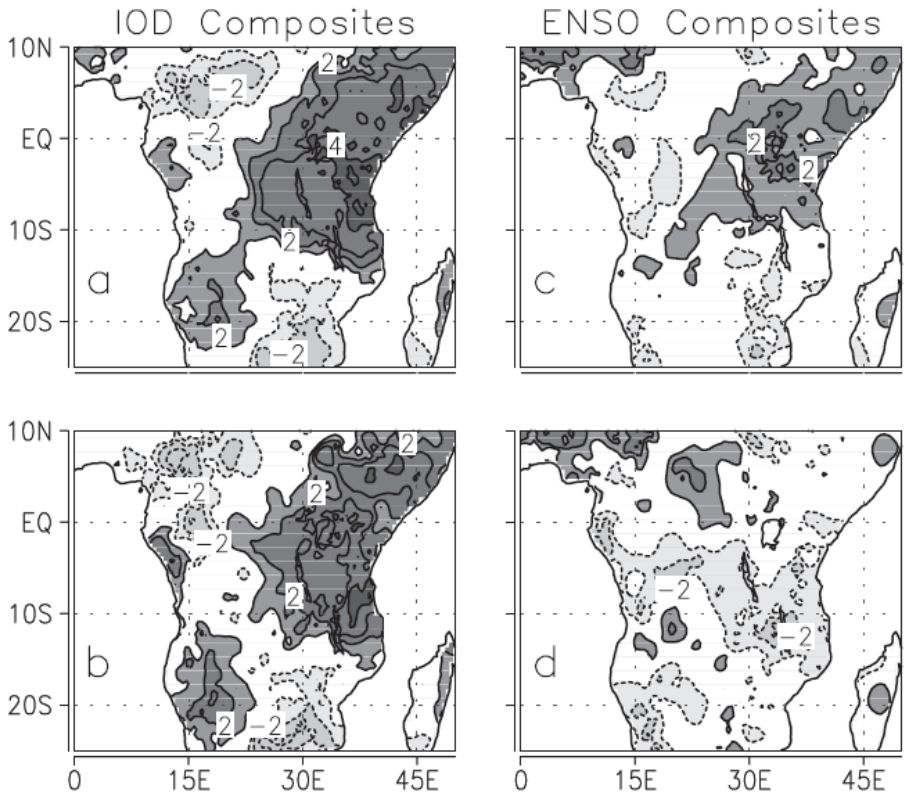

Fig. 1. Composite OND rain anomaly over Africa for (a) 19 IOD events, (b) 11 ENSO-independent IOD events, (c) 20 ENSO events and (d) 12 IOD-independent ENSO events. The composite anomaly was normalized by the standard deviation of rain during OND. Contours given at ±1, ±2, etc.

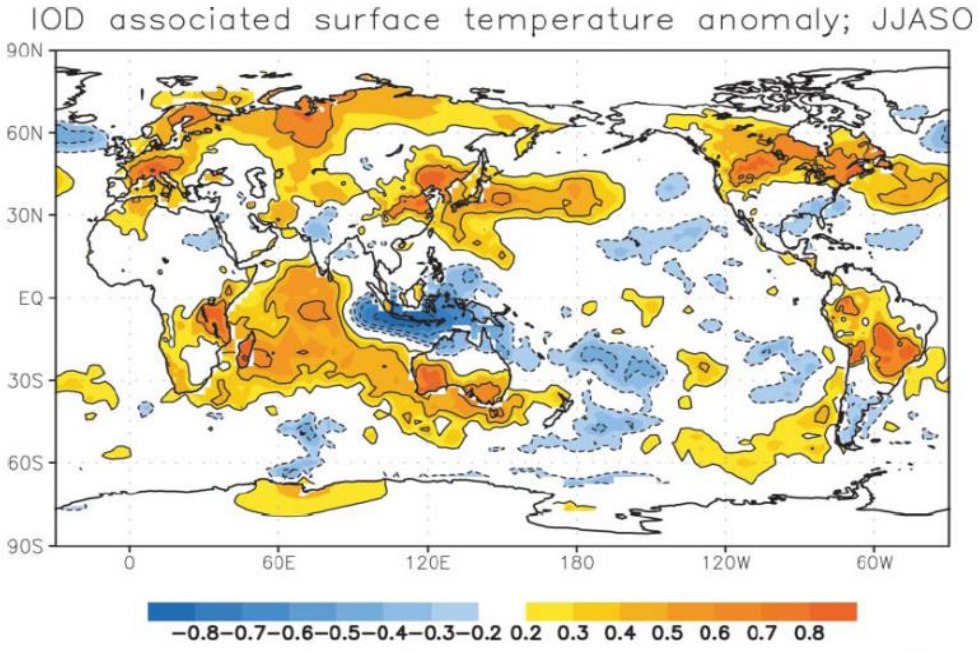

Fig. 21. Partial correlation of land and sea-surface temperature on DMI independent of Nino3 during JJASO

Indian Ocean Capacitor Effect on Indo–Western Pacific Climate during the Summer following El Niño

SHANG-PING XIE,*,+ KAIMING HU,# JAN HAFNER,* HIROKI TOKINAGA,* YAN DU,*,@
GANG HUANG,# AND TAKEAKI SAMPE*

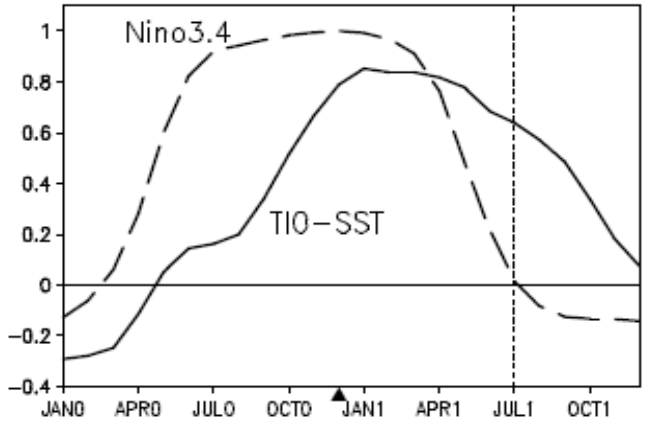

Fig. 1. Correlation of tropical Indian Ocean (40-100°E, 20°S-20°N) SST (solid) with the Nino3.4 (170°W-120°W, 5°S-5°N) SST index for Nov(0)-Dec(0)-Jan(1). Numerals in parentheses denote years relative to El Nino: 0 for its developing and 1 for decay year. The dashed curve is the Nino3.4 SST auto-correlation as a function of lag. The black triangle denotes Dec(0), the peak phase of ENSO.

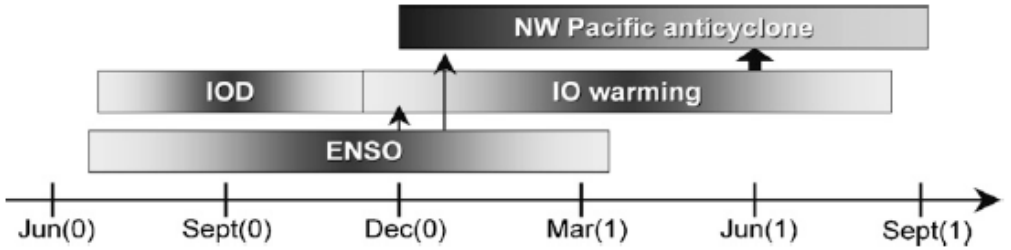

FIG. 13. Seasonality of major modes of Indo–western Pacific climate variability. Vertical arrows indicate causality, and the block arrow emphasizes the TIO capacitor effect, the major finding of the present study.

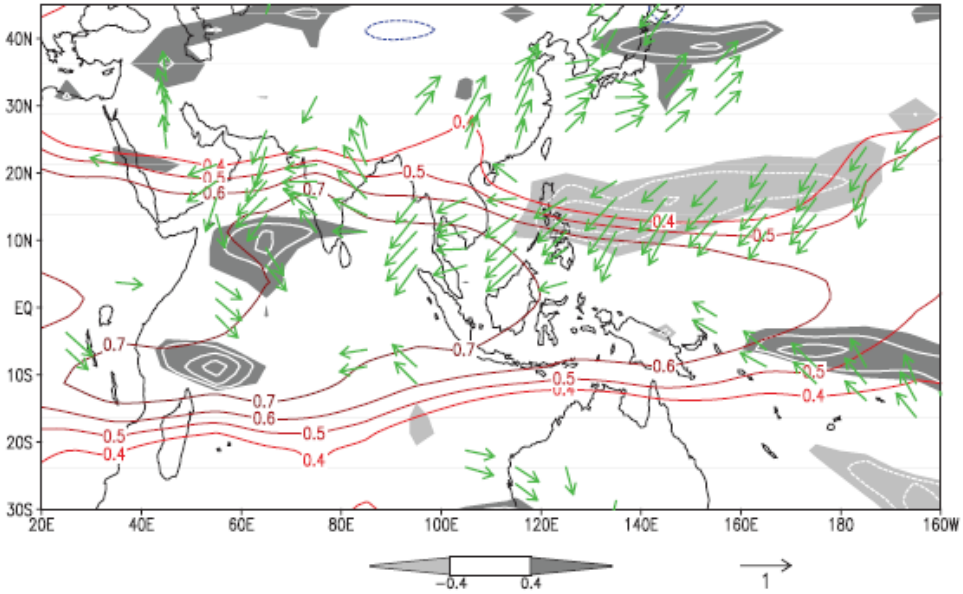

FIG. 6. JJA(1) correlation with the NDJ(0) Niño-3.4 SST index: tropospheric (850–250 hPa) temperature (contours), precipitation (white contours at intervals of 0.1; dark shade > 0.4; light < −0.4), and surface wind velocity (vectors).

2.4 Decadal Variability:
PDO, AMO,ENSO-Monsoon relation

Pacific Decadal Oscillation

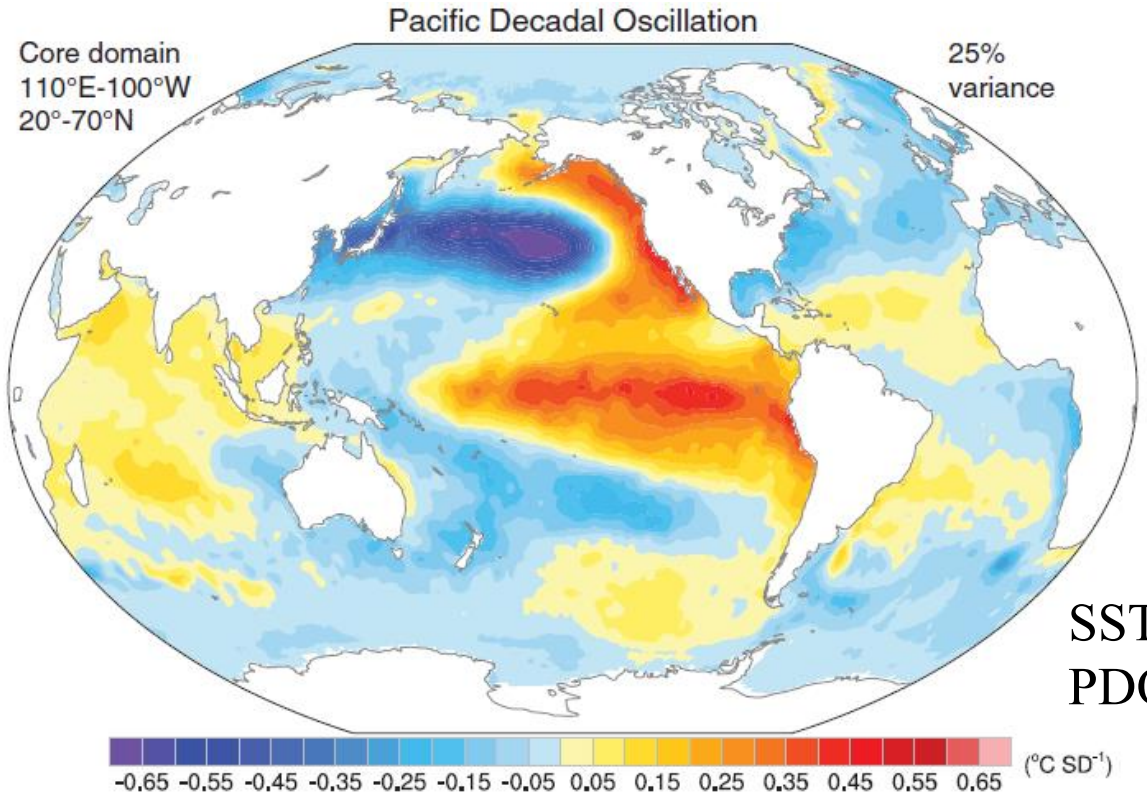

Trenberth and Fasullo (2013)

SST pattern regressed on PDO index

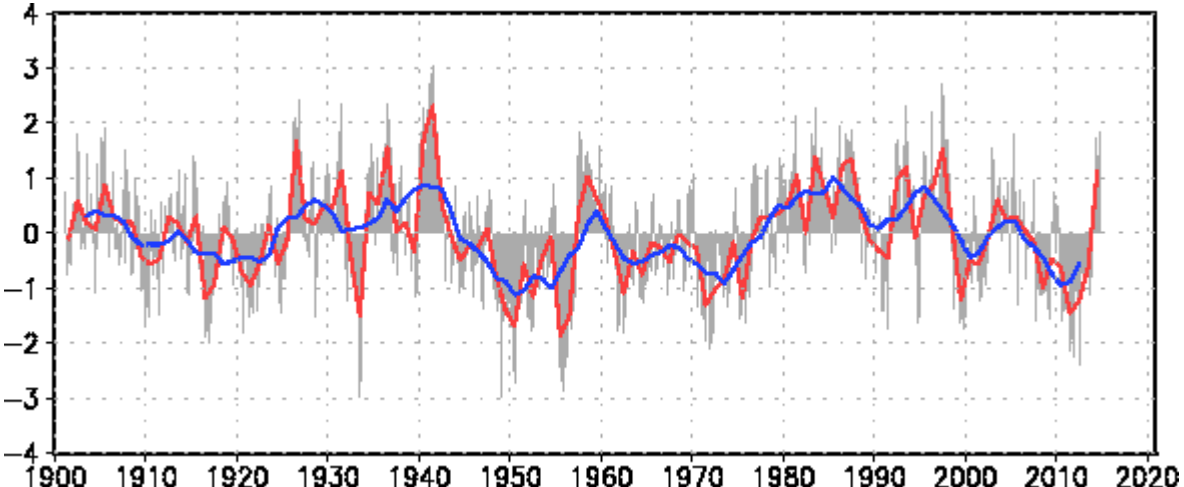

PDO index (From JMA HP)

Global warming slowdown and PDO/IPO

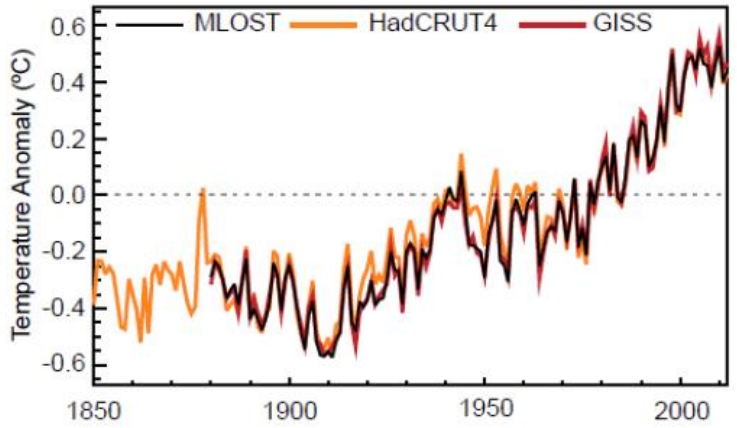

Annual Global Mean Surface Tem
anomalies relative to a 1961–19
the latest version of the three co
Surface Air Temperature (LSAT) a
Temperature (SST)
datasets (HadCRUT4, GISS and N

IPCC AR5 (2014)

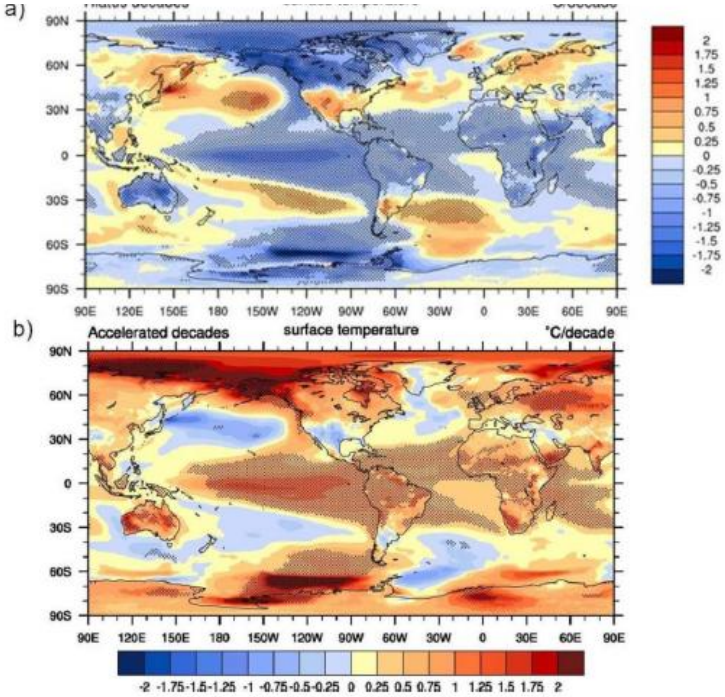

Five CCSM4 21st century simulations with RCP4.5
(uniform increase in GHGs, no volcanoes):
Composites of decades with near-zero warming trend (hiatus decades) and decades with rapid global warming (accelerated warming decades) show opposite phases of the IPO in the Pacific
(hiatus=linear trend of global T <-0.10K/decade; 8 hiatus decades
Accelerated=linear trend of global T>+0.41K/decade; 7 accelerated warming decades)

Meehl et al. (2013)

- IPO in positive phase → Accelerated warming decades
- IPO in negative phase → Hiatus decades

6

PDO/IPO and local climate

Temperature anomalies in Japan

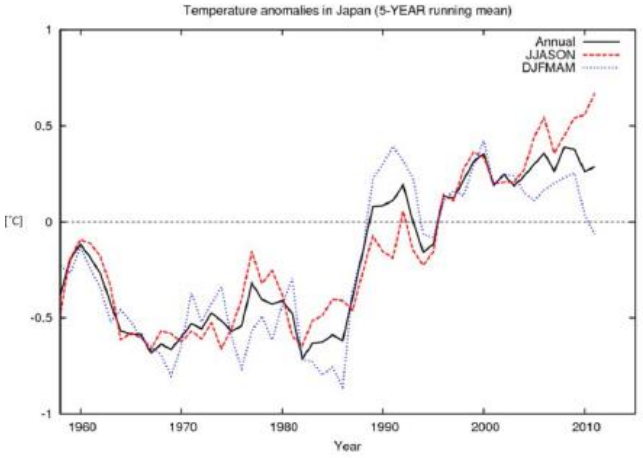

Urabe and Maeda (2014)

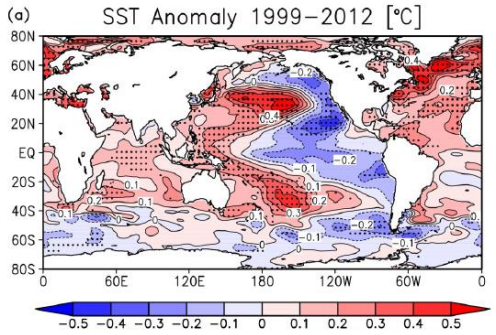

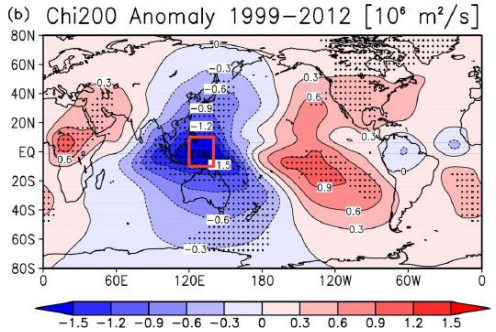

200 hPa height (Z200) Anomaly

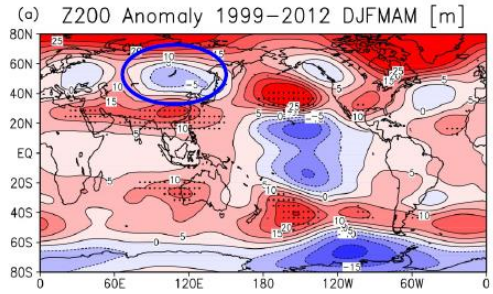

Winter – Spring

Far-Eastern trough (Takaya and Nakamura, 2013) is enhanced.

→ Monsoon is Enhanced, consistent with colder Japan's winter.

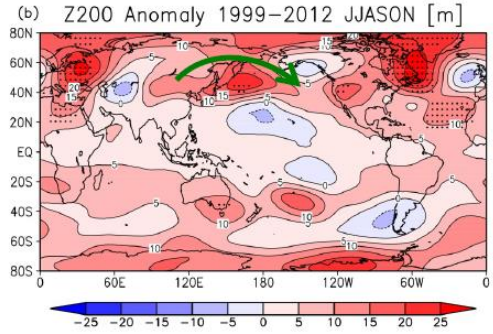

Summer – Autumn

Positive height anomalies near Japan.

→Westerly Jet shifts northward, consistent with higher temperature anomalies in Japan.

Consistent with enhanced seasonal contrast

Atlantic Multidecadal Oscillation (AMO)

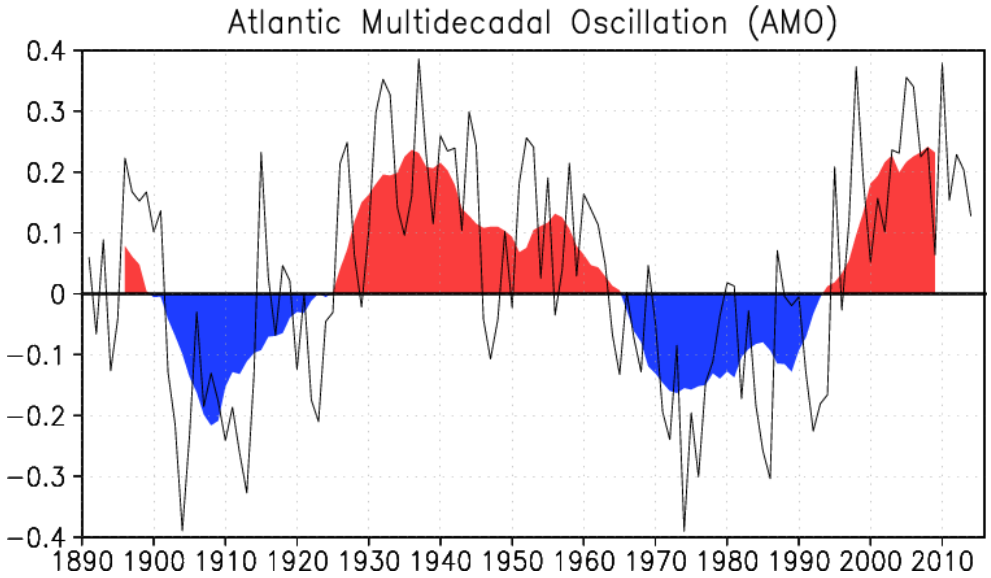

SST anomalies averaged in North Atalntic after removed linear trend. From JMA-HP

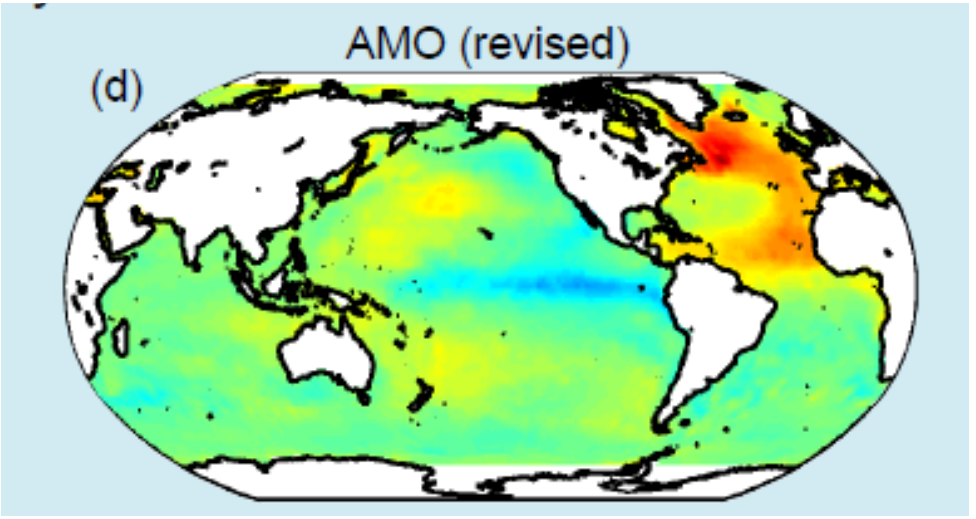

Decadal variability of ENSO/ Monsoon and their relationship

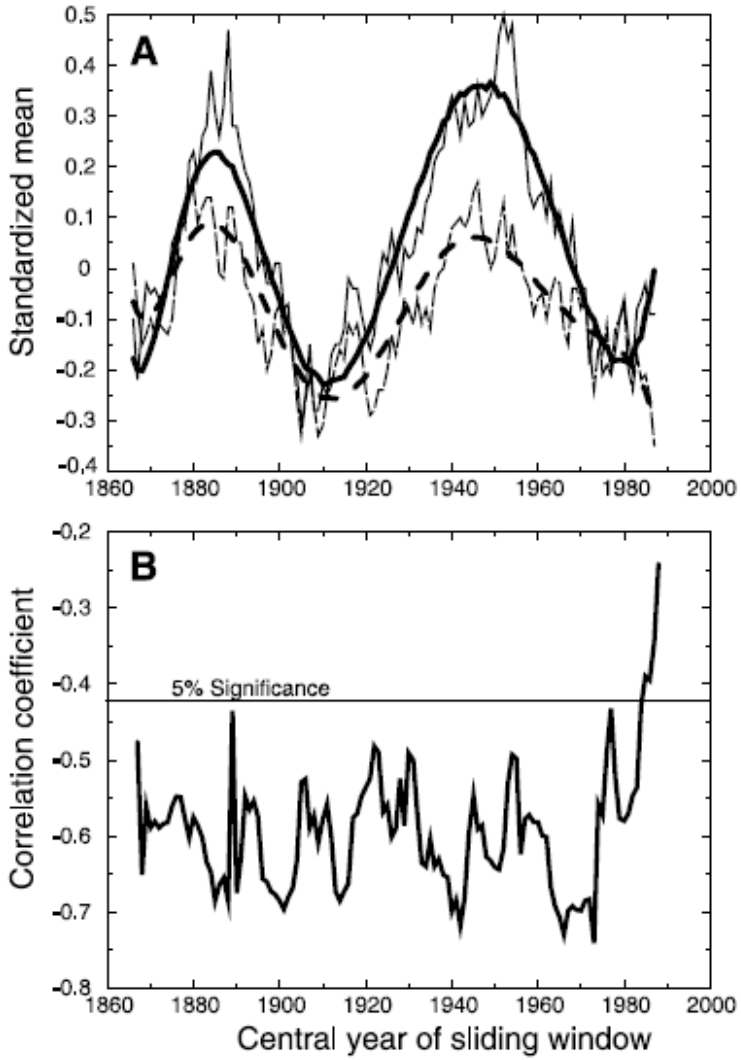

Fig. 1. (**A**) Shown are 21-year sliding standardized means of Indian summer monsoon rainfall (thin line) and June to August (JJA) NINO3 SST anomalies (thin dashed line) during 1856–1997. The corresponding solid lines represent the smoothed values (smoothing is done by fitting a polynomial). The sign of NINO3 SST is reversed to facilitate direct comparison. (**B**) Shown are 21-year sliding correlations between Indian summer monsoon rainfall and NINO3 SST anomalies (JJA) during 1856–1997. The horizontal line shows the 5% significance level.

On the Weakening Relationship Between the Indian Monsoon and ENSO

K. Krishna Kumar,[1]*† Balaji Rajagopalan,[2] Mark A. Cane[2]

1999

3. JMA’s latest one-month prediciton

JMA's latest one-month prediction

initial: 2015.11.11, valid:11.21-27(2nd week)

Stream function at 200hPa
(contour) and anomaly (shade)

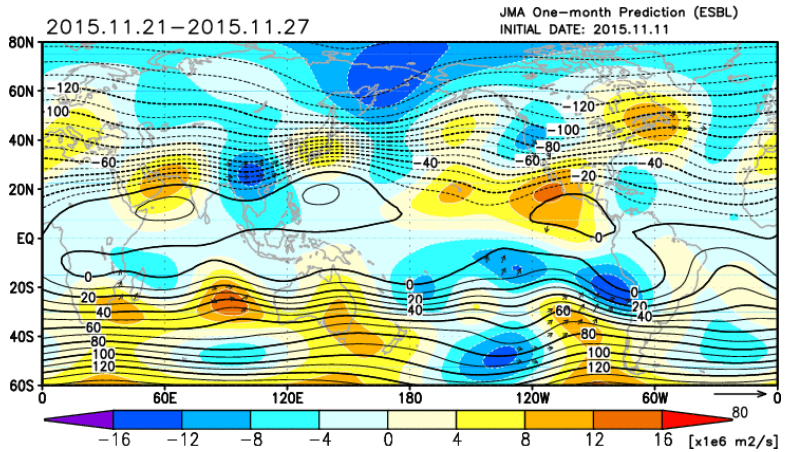

Stream function at 850hPa
(contour) and anomaly (shade)

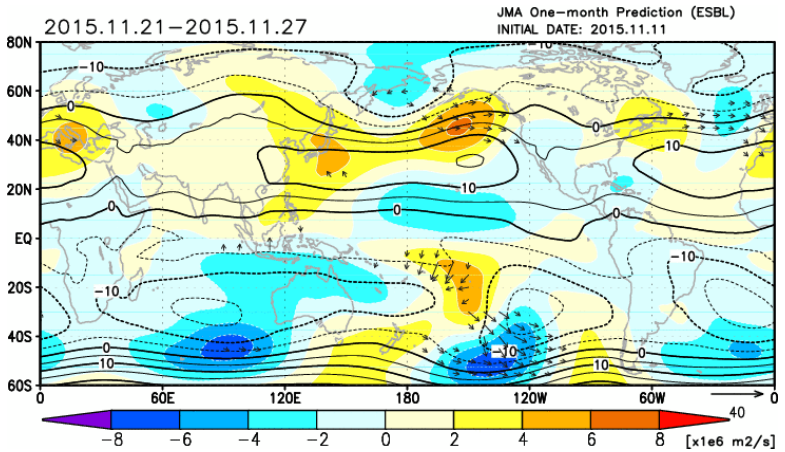

Stream function anomaly at 200hPa (contour)
and precipitation anomaly (shade)

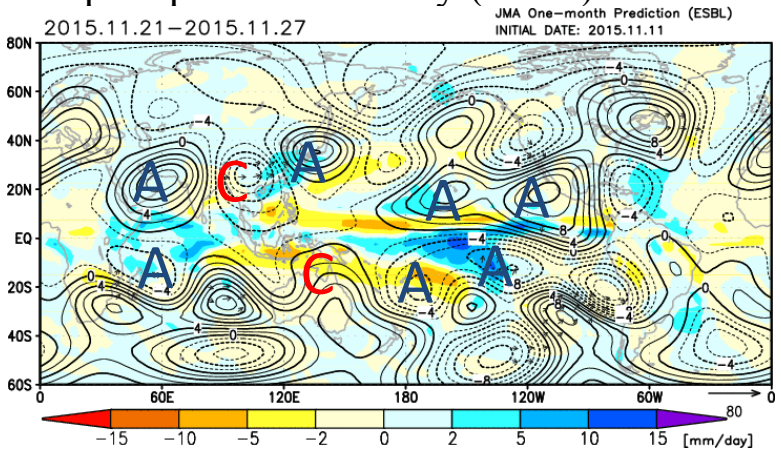

Stream function anomaly at 850hPa (contour)
and precipitation anomaly (shade)

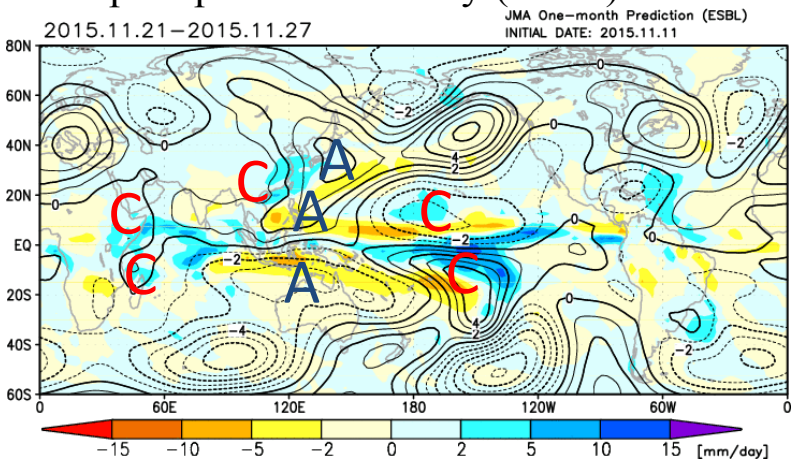

*Ensemble mean

JMA's latest one-month prediction

initial: 2015.11.11, valid:11.21-27(2nd week)

Velocity potential anomaly at 200hPa (shade)
and divergent flow anomaly (arrow)

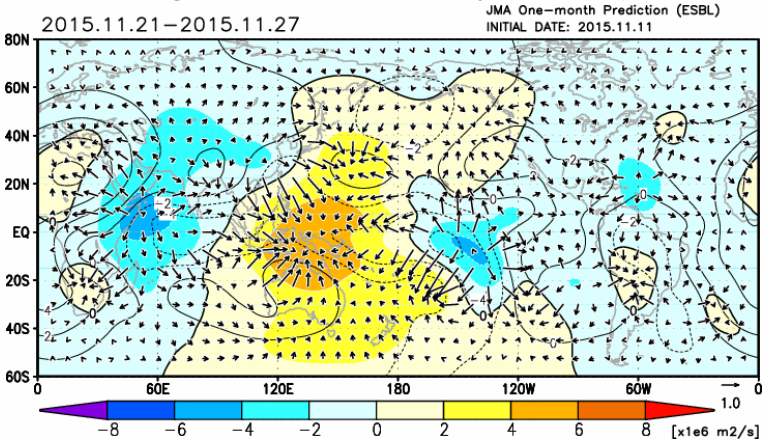

SST(contour) anomaly (shade)

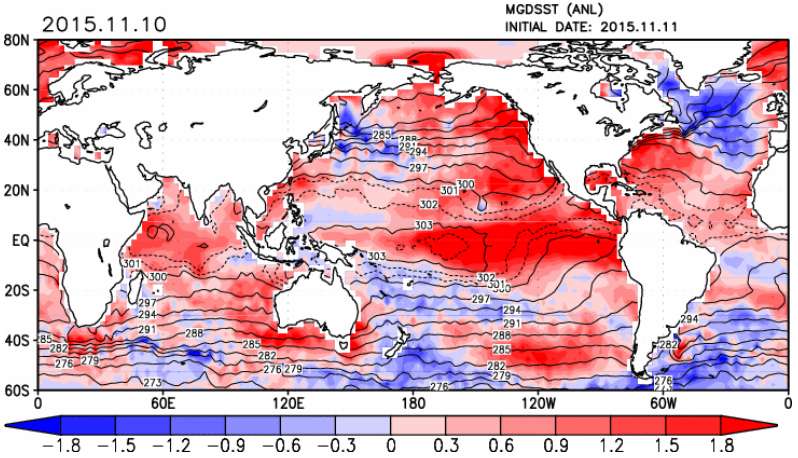

Stream function anomaly at 200hPa (contour)
and precipitation anomaly (shade)

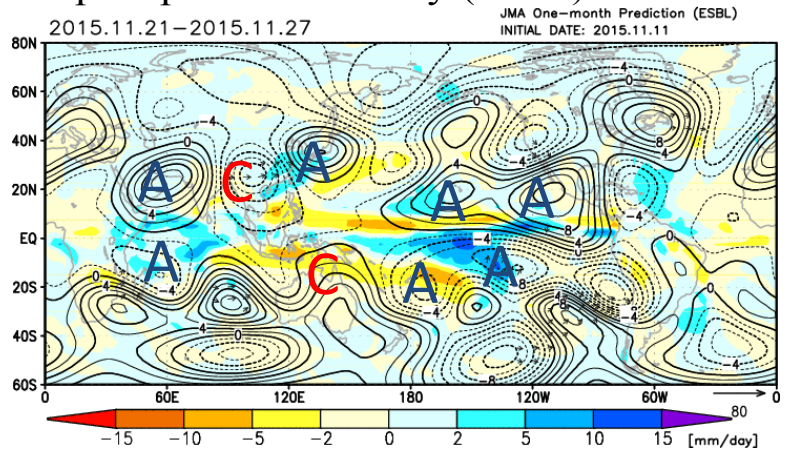

Stream function anomaly at 850hPa (contour)
and precipitation anomaly (shade)

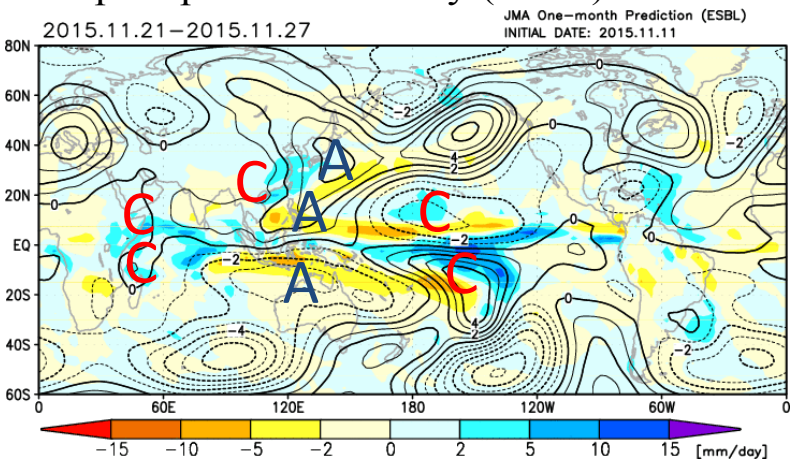

*Ensemble mean

JMA's latest one month prediction

initial: 2015.11.11, valid:12.05-11(4th week)

Velocity potential anomaly at 200hPa (shade) and divergent flow anomaly (arrow)

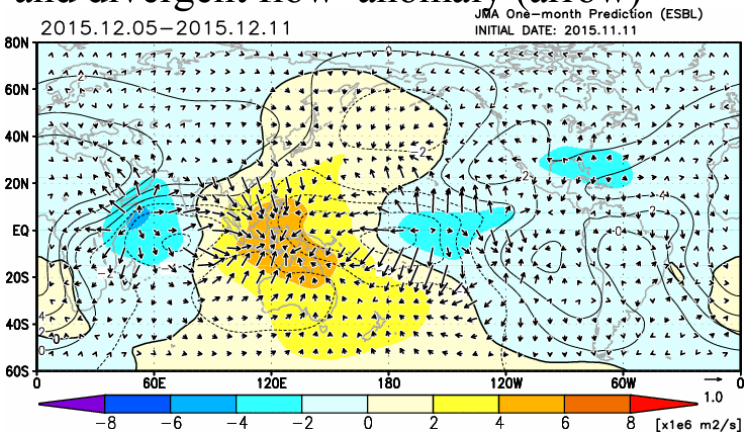

SST(contour) anomaly (shade)

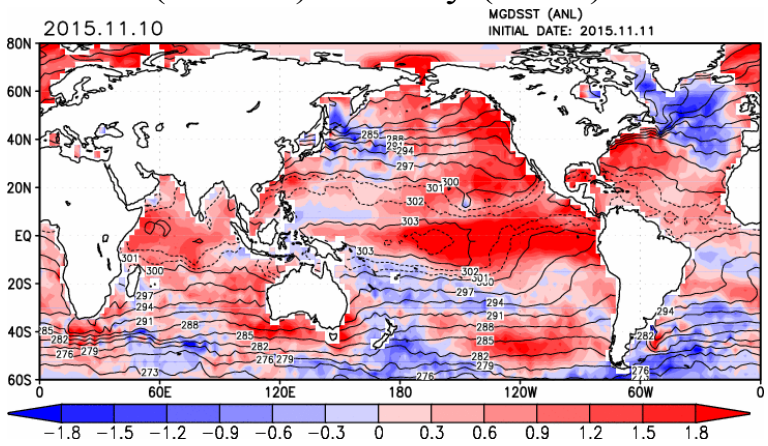

Stream function anomaly at 200hPa (contour) and precipitation anomaly (shade)

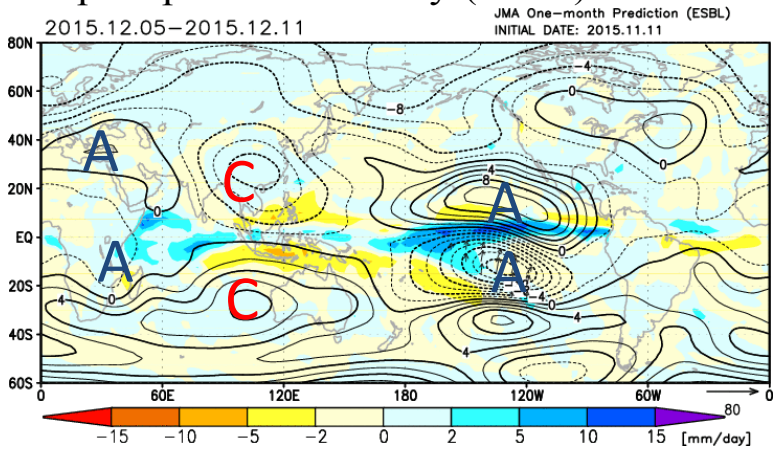

Stream function anomaly at 850hPa (contour) and precipitation anomaly (shade)

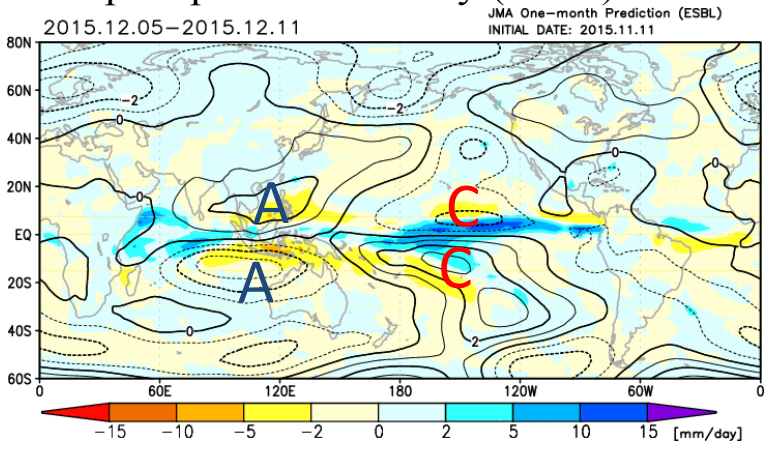

*Ensemble mean

Concluding remarks

- The global climate system consists of atmosphere including its composition and circulation, the ocean, hydrosphere, land surface, biosphere, snow and ice, solar and volcanic activities.
- These components interact on various spatial and temporal scales through the exchanges of heat, momentum, radiation, water and other materials.
- Climate variability refers to variations in the mean state and other statistics of the climate on all spatial and temporal scales beyond that of individual weather events.
- Climate variability may be due to natural internal processes within the climate system (internal variability), or to variations in natural or anthropogenic external forcing.
- Seasonal forecasters must learn climate variability, causes, impacts, and predicatbility of climate variability in various spatial and temporal scales.